Journal Pre-proof

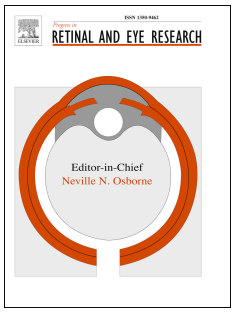

Structural photoreceptor evaluation in age-related macular degeneration. A comprehensive review of methods and clinical significance.

Lourdes Vidal-Oliver, Davide Garzone, Lukas Schloesser, Sarah Thiele, Maximilian Pfau, Wolf M. Harmening, Julius Ameln, Rosa Dolz-Marco, Nicolas Cuenca, Isabel Ortuño-Lizaran, Zhichao Wu, Robyn H. Guymer, Robert P. Finger

PII: S1350-9462(26)00013-3

DOI: https://doi.org/10.1016/j.preteyeres.2026.101447

Reference: JPRR 101447

To appear in: *Progress in Retinal and Eye Research*

Received Date: 26 September 2025

Revised Date: 30 January 2026

Accepted Date: 12 February 2026

Please cite this article as: Vidal-Oliver, L., Garzone, D., Schloesser, L., Thiele, S., Pfau, M., Harmening, W.M, Ameln, J., Dolz-Marco, R., Cuenca, N., Ortuño-Lizaran, I., Wu, Z., Guymer, R.H, Finger, R.P, Structural photoreceptor evaluation in age-related macular degeneration. A comprehensive review of methods and clinical significance., *Progress in Retinal and Eye Research*, https://doi.org/10.1016/j.preteyeres.2026.101447.

Title: Structural photoreceptor evaluation in age-related macular degeneration. A comprehensive review of methods and clinical significance.

Authors & Affiliations:

Lourdes Vidal-Oliver[a,b,], Davide Garzone[a], Lukas Schloesser[a], Sarah Thiele[c,d], Maximilian Pfau[d,e,f], Wolf M Harmening[d], Julius Ameln[d], Rosa Dolz-Marco[g], Nicolas Cuenca[h,i], Isabel Ortuño-Lizaran[h], Zhichao Wu[j,k], Robyn H Guymer[j,k], Robert P Finger[a]

[a] Department of Ophthalmology & Medical Faculty Mannheim, University Hospital Mannheim, University of Heidelberg, Mannheim, Germany.
Address: Theodor-Kutzer-Ufer 1-3, 68167 Mannheim, Germany

[b] Vitreoretinal Unit, Fundación Oftalmología Médica Comunidad Valenciana, Valencia, Spain.
Address: Pio Baroja 12, 46015 Valencia, Spain

[c] Department of Ophthalmology, University Medical Center Hamburg-Eppendorf, Hamburg, Germany
Address: Martinistraße 52, 20251 Hamburg, Germany

[d] Department of Ophthalmology & Medical Faculty Bonn, University Hospital Bonn, Bonn, Germany
Address: Ernst-Abbe-Straße 2, 53127 Bonn, Germany

[e] Department of Ophthalmology, University of Basel, Basel, Switzerland
Address: Mittlere Strasse 91, 4031 Basel, Switzerland

[f] Roche Pharmaceutical Research and Early Development, Roche Innovation Center Basel, Basel, Switzerland
Address: Grenzacherstrasse 124, CH-4070 Basel, Switzerland

[g] Oftalvist Clinic, Valencia, Spain
Address: C/ Ruzafa 19, 46004 Valencia, Spain

[h] Department of Physiology, Genetics and Microbiology, University of Alicante, Alicante, Spain

Address: Ctra. San Vicente del Raspeig s/n, 03690 San Vicente del Raspeig, Alicante, Spain

[i] Alicante Institute for Health and Biomedical Research (ISABIAL), Alicante, Spain

Address: Av. Pintor Baeza 12, 03010 Alicante, Spain

[j] Centre for Eye Research Australia, Royal Victorian Eye and Ear Hospital, East Melbourne, Australia

Address: 200 Victoria Parade, East Melbourne VIC 3002, Australia

[k] Ophthalmology, Department of Surgery, The University of Melbourne, Melbourne, Australia

Address: Grattan Street, Parkville, Victoria, 3010, Australia

ORCID ID Authors:

Lourdes Vidal-Oliver: 0000-0002-6225-1521

Maximilian Pfau: 0000-0001-9761-9640

Wolf M Harmening: 0000-0001-7053-1198

Julius Ameln: 0000-0002-0486-870X

Rosa Dolz-Marco: 0000-0002-2963-2541

Nicolás Cuenca: 0000-0002-6767-5710

Isabel Ortuño-Lizaran: 0000-0003-1083-9259

Robyn H Guymer: 0000-0002-9441-4356

Robert P Finger: 0000-0003-4253-7597

Corresponding Author:

Lourdes Vidal-Oliver

E-mail address: lourvioli@gmail.com

Address: Av. Pio Baroja 12, 46015 Valencia, Spain

Declaration of Interest Statement:

Lourdes Vidal-Oliver declares speaking and lecture fees from Roche and Alcon and travel reimbursement from Bayer and Roche. Sarah Thiele declares receiving financial support from Roche, Bayer and Heidelberg Engineering and Novartis, and receiving research money from Heidelberg Engineering, Novartis, Allergan, Bayer, Dorc. Wolf M Harmening reports receiving consultancy fees from RhyGaze. Rosa Dolz-Marco reports consultancy fees from Roche and Heidelberg Engineering; research support from Regeneron, Annexon, IvericBIO, Roche, Janssen and EyePoint; Speaker fees from Heidelberg Engineering, Roche and Abbvie. Robert P Finger reports receiving sponsorship or research funding from Biogen and Bayer; and honoraria or other financial compensation from Biogen, Apellis, Alimera, Astellas, Allergan, Caterna, Böhringer-Ingelheim, Novartis, Ophthea, ODOS, ProGenerika, Roche/Genentech, Stada Pharm. Maximilian Pfau reports employment from Roche. Other authors declare that they have no known competing financial interests or personal relationships that could have appeared to influence the work reported in this paper.

Funding Sources: This study was supported by the SERV (Spanish Society of Retina and Vitreous, scholarship to LVO).

Structural photoreceptor evaluation in age-related macular degeneration. A comprehensive review of methods and clinical significance.

ABSTRACT

Age-related macular degeneration (AMD) is a disease that primarily affects the outer retina, with progressive photoreceptor degeneration and atrophy of the retinal pigment epithelium (RPE). Advances in imaging now enable photoreceptor changes to be detected and quantified with unprecedented sensitivity, whereas comparable biomarkers of RPE dysfunction remain less developed. As such, photoreceptor-based biomarkers are increasingly considered potential surrogates for current clinical trial endpoints. This review examines the current imaging modalities—particularly optical coherence tomography (OCT) and modalities enhanced by adaptive optics (AO) — used to evaluate photoreceptor structure in AMD. We explore the intrinsic value of parameters such as outer nuclear layer thickness, external limiting membrane integrity, photoreceptor inner and outer segment thickness, ellipsoid zone (EZ) integrity, and EZ reflectivity on OCT, and cone density and regularity on AO imaging, highlighting their potential and limitations. While OCT-based metrics are the most accessible in clinical settings, their clinical utility is hampered by inconsistent segmentation protocols and methodological heterogeneity. AO imaging offers unmatched resolution but faces practical barriers to widespread adoption. The field is moving in a promising direction with emerging computational tools and artificial intelligence improving accuracy and scalability. However, progress is contingent on establishing consensus definitions, standardized acquisition and analysis protocols, and normative datasets. Future efforts should focus on translating high-resolution imaging into robust, reproducible biomarkers that can be widely adopted in both clinical practice and therapeutic development.

Structural photoreceptor evaluation in age-related macular degeneration. A comprehensive review of methods and clinical significance

1. Introduction

Age-related macular degeneration (AMD) is one of the most common causes of severe, irreversible vision loss worldwide, and its prevalence is expected to rise significantly in the coming decades.(Li et al., 2020) In AMD, the structural and functional integrity of the photoreceptor–retinal pigment epithelium (RPE)–Bruch's membrane–choriocapillaris complex decreases with disease progression including both neovascular and non-neovascular forms, ultimately affecting all components. (Bhutto & Lutty, 2012; M. Edwards & Lutty, 2021) Although RPE dysfunction typically precedes photoreceptor degeneration in both forms of late-stage AMD, it remains more challenging to quantify with current clinical imaging techniques, especially with optical coherence tomography (OCT). In contrast, photoreceptor alterations, such as those affecting the ellipsoid zone (EZ), can be detected and measured more reliably in vivo than RPE changes. (Schmidt-Erfurth et al., 2025) Of note, the Classification of Atrophy Meetings (CAM) Report 6 showed significantly lower inter-rater agreement in assessing RPE disruption compared with photoreceptor-based parameters such as EZ and external limiting membrane (ELM) disruption and outer nuclear layer (ONL) thinning.(Wu et al., 2022). The ability to measure photoreceptor integrity may offer a more sensitive and reproducible way to capture early retinal damage. In this context, photoreceptor integrity refers to the structural preservation of photoreceptors, typically assessed in vivo by the continuity and reflectivity of the EZ and, to a lesser extent, by the continuity of the ELM and interdigitation zone (IZ), as well as by thinning of the ONL.

As such, photoreceptor-based parameters may show promise in different clinical contexts within the AMD spectrum. Although the prognosis of patients with advanced AMD has improved over the past two decades -primarily due to the introduction of anti-VEGF and, more recently, complement-

inhibitor agents- no specific interventions have been established to prevent or delay late AMD onset, and as such dietary supplements and lifestyle modification are currently the only options available. (Chew et al., 2022; Knudtson et al., 2006; McGuinness et al., 2016) In intermediate AMD (iAMD), several interventional clinical trials have already been conducted using high-contrast best-corrected visual acuity (BCVA) or time to develop multimodal imaging-defined late AMD as primary outcomes. The LEAD Study, for example, investigated subthreshold nanosecond laser with a 36-month follow-up. (Boyer et al., 2024; Guymer et al., 2019) While several well-conducted randomized controlled trials have sought to intervene at earlier disease stages to slow progression, such as LEAD, these studies are inherently challenging to perform because very large sample sizes and long follow-up periods are required to reach currently regulator-accepted clinical endpoints. To enable earlier interventions, outcome measures that detect retinal damage before clinically relevant vision loss or the onset of atrophy are urgently needed. In this regard, photoreceptor structure assessments are particularly attractive, as they may serve as clinically meaningful endpoints with shorter readout times and potentially smaller sample size requirements compared to traditional functional or atrophy-based outcomes. (Wu et al., 2025a)

Importantly, the clinical utility of photoreceptor-based endpoints extends beyond early stages and is increasingly recognized in late AMD as well. In late AMD, BCVA has traditionally been the main outcome measure in clinical trials, especially in neovascular AMD (nAMD). (Lanzetta et al., 2024; Sahni et al., 2020) Furthermore, structural parameters, such as GA progression measured via fundus autofluorescence (FAF), have been employed in trials targeting GA. (Khanani et al., 2023; Patel et al., 2023) However, some clinical gaps still exist. For instance, when lesions do not yet involve the fovea, BCVA often remains unaffected despite extensive parafoveal damage. This highlights a limitation in using the total GA area as an outcome measure, if functional changes are required, particularly since foveal sparing is common even in advanced stages of GA. Furthermore**,** because detectable photoreceptor loss often precedes or extends beyond visible RPE atrophy, their evaluation (for

example, reduction in EZ integrity) provides an earlier and more sensitive marker of disease progression. (Pfau et al., 2020a)

A good example is the clinical trials evaluating elamipretide, a mitochondria-targeting drug in patients with non-exudative AMD. While the phase II study did not meet the primary outcomes (BCVA and GA growth area), the significantly smaller changes in EZ loss in treated patients compared to control patients represented a paradigm shift. (Ehlers et al., 2025) This demonstrated that photoreceptor-based parameters can capture treatment effects that conventional endpoints may miss, which is particularly relevant given the limited duration of most clinical trials (approximately 2 years). The rate of change of EZ loss has recently been recognized by the Food and Drug Administration (FDA) as a valid endpoint for clinical trials and now serves as the main structural outcome in the ongoing phase III trial. (BioTherapeutics, 2025; ISCRCTN, 2024). Notably, the rate of change of EZ loss was the primary endpoint used in the recently approved treatment for macular telangiectasia type 2 (MacTel2) (Hoy, 2025), further supporting its broader applicability in retinal disease trials.

To realize this potential, robust and standardized methods for photoreceptor assessment are essential. Yet, in the current literature, these metrics are addressed with considerable heterogeneity due to differences in imaging modalities and analytical definitions. Several photoreceptor assessment and quantification methods using different imaging modalities have been described in the literature and have emerged in parallel with technological advances. Current systems allow differentiating the outer retinal bands, enabling quantification of both thickness and reflectivity. Improved resolution in OCT, alongside novel computational approaches capable of handling large datasets, has opened the door to more refined structural assessment of the outer retina. This may enhance early detection of photoreceptor compromise and lead to the identification of more sensitive and specific biomarkers of outer retinal health. (Schmidt-Erfurth et al., 2025; Thiele et al., 2020, 2022)

In addition, the advent of adaptive optics (AO) technology applied to various imaging modalities has made it possible to study the cone mosaic at the cellular level, analyzing cone density, intercellular spacing, and regularity. (Burns et al., 2019) Recently, various AO imaging systems have been commercialized, potentially facilitating more widespread use. Finally, an alternative to AO, using a high-magnification lens in confocal scanning laser ophthalmoscopy can provide single-cell visualization and is also available commercially. (Gujar et al., 2022)

The purpose of this review is providing a comprehensive and systematic evaluation of the diverse methods and imaging modalities employed for photoreceptor assessment, highlighting the critical role of quantification and the significant clinical implications in AMD.

2. Anatomy of the human fovea

Ramón y Cajal described the retina's cellular structure as consisting of ten distinct layers, named from the innermost to the outermost as the inner limiting membrane (ILM), retinal nerve fiber layer (RNFL), ganglion cell layer (GCL), inner plexiform layer (IPL), inner nuclear layer (INL), outer plexiform layer (OPL), ONL, ELM, photoreceptor inner and outer segments (IS/OS), and RPE (Figure 1A,B)(Ramón y Cajal, 1892). In humans, other primates, and some birds, the central retina contains a specialized region known as the fovea, where many of these layers are absent. This area is responsible for high-acuity vision and exhibits a remarkable structural adaptation that allows light to directly reach the cone photoreceptors (Kolb et al., 2020).

The fovea is located at the center of the macula, a wider area at the central retina that also includes the perifovea and the parafovea. The location and size of these structures are illustrated schematically in Figure 1C-D. The fovea is approximately 1.5 mm in diameter and located 4–5 mm temporal to the optic nerve. It can be identified in vivo by its reddish-yellow coloration and the absence of blood vessels (Figure 1C).

Within the fovea, three key structures can be distinguished: the foveal avascular zone, the foveola, and the umbo (Figure 1C,D). The center of the foveal pit, known as the umbo, is composed exclusively of several rows of densely packed cone photoreceptors. The pit-shaped depression of the fovea is created by the lateral displacement of inner retinal neurons, allowing photons to reach the photoreceptors directly with minimal scattering. As a result, only the ILM, the ONL, the ELM, the outer segments (OS) of the photoreceptors, and the RPE remain in this central region (Cuenca et al., 2014, 2018; Kolb et al., 2020). These adaptations are responsible for the high visual acuity of this region.

Because of this layer displacement and high cone density within the fovea, the cone morphology varies significantly based on retinal location. Figure 2A outlines the typical cone structure: the outer segment, which contains membranous discs packed with photopigments; the inner segment, which includes the mitochondria-rich ellipsoid (responsible for energy production) and the myoid, where endoplasmic reticulum and Golgi apparatus are located; the cell body, housing the nucleus within the ONL; the axon; and finally the pedicle at the OPL, where synaptic interactions mainly occur. The morphology of these structural elements differs across retinal eccentricities. (Figure 2C-F). At the umbo, cones feature extremely thin (1-1.5μm) and elongated outer segments (40-50 μm), and their short axons typically connect with a single midget bipolar cell (Figure 2C, F). At the foveola, cone segments remain thin but slightly thicker than those at the umbo, while their axons are much longer and travel obliquely, sometimes spanning hundreds of microns. As cones extend further from the fovea (Figure 2D, F), their outer segments shorten (30-35 μm) and thicken (1.8-2 μm), and their axons reach their maximum length at the parafovea and then become shorter. In the peripheral retina (Figure 2E, F), their axons run vertical rather than obliquely, directly connecting photoreceptors to their secondary neurons. Figure 2F schematically depicts these progressive changes in cone morphology.

The fovea is composed of densely packed, elongated cone photoreceptors, which account for more than half of all retinal cones. In contrast, rod photoreceptors are predominant in the peripheral (non-central) retina. Foveal cones need to establish synaptic contacts with bipolar and horizontal cells in the OPL. Because of the high cone density at the fovea and the displacement of inner layers to form the foveal pit, the cones' postsynaptic cells (bipolar and horizontal cells) are usually located far from them. Thus, axons of foveal cones must extend considerable distances, histological measurements in human retina show that Henfe fibers (cone axons) reach lengths of approximately 400-700 μm, with a mean of about 560μ, peaking near ~1 μm eccentricity from the foveal center and declining toward zero beyond the central macula.(Drasdo et al., 2007).

The bundle of elongated cone axons in this region, arranged laterally, runs parallel to Müller cell long processes and, together, makes up a thick layer known as the Henle fiber layer (HFL), only present within the macula (Figure 2B; 3A,B). Progressing outwards from the foveola, the first rod photoreceptors appear, and their long axons also contribute to the HFL located between the ONL and the OPL. As the retina transitions from the fovea toward the periphery, the HFL gradually thins and and decreases progressively until becoming negligible, where the fibers cease to be obliquely oriented at about 4.5mm temporal to the foveal center.(Drasdo et al., 2007) This occurs because the axons of cone photoreceptors become progressively shorter, establishing synaptic connections with bipolar and horizontal cells located directly adjacent to their cell bodies.

Advancements in imaging technologies, particularly OCT, have significantly increased interest in studying the fovea and macula in relation to retinal diseases. OCT enables detailed, in vivo visualization of all retinal layers in the central retina. Understanding the microscopic structure at the cellular level of the fovea is crucial for interpreting OCT scans, as histological layers can be directly correlated with the hypo- and hyperreflective bands seen in OCT images. For example, improvements on histological resolution and optical imaging have allowed for the distinction between OPL and HFL as two distinct anatomical structures, that were named together as OPL in

Ramón y Cajal's original histological descriptions (Ramón y Cajal, 1892). As shown in Figure 3, there is a strong resemblance between histological sections and OCT images at the fovea, where the HFL distinction from OPL can also be seen and should be considered. In Figure 3A, a retinal cross-section stained with cytochrome C (in blue) highlights mitochondria, and its pattern closely matches the OCT bands in Figure 3 C-E, suggesting the potential role of mitochondria in generating these hyperreflective signals.

Since OCT became widely used, numerous studies have attempted to interpret the reflectivity bands according to retinal histological layers. While some correlations are generally agreed upon, others remain debated. Figure 3 present the most widely accepted associations between histology and OCT. The definition of the outer retinal bands and their anatomical correspondence are detailed in their corresponding sections.

3. Optical coherence tomography biomarkers

3.1. Anatomy and general considerations

Optical coherence tomography enables noninvasive, in vivo visualization of retinal architecture at near-cellular resolution through low-coherence light interference. (Huang et al., 1991) With the capabilities of current commercial spectral domain-OCT (SD-OCT) and swept source-OCT (SS-OCT) systems, typically offering axial resolutions of 3–7 µm, it is possible to evaluate distinct components of photoreceptor anatomy, including the ONL, ELM, EZ and IZ. These structures serve as surrogate biomarkers in both clinical and research settings to assess photoreceptor integrity, disease progression, and treatment response in conditions such as AMD.

Recent advancements in high-resolution OCT (axial resolution <3 µm), have significantly enhanced visualization of the outer retina. (Lee et al., 2020; Reche et al., 2023) As recently demonstrated by Goerdt et al using the research prototype developed by Heidelberg Engineering, (Goerdt et al., 2024), this technology allows finer delineation of subcellular structures that are not resolvable with conventional OCT systems, offering valuable insights into the microanatomy of photoreceptor–RPE

interactions. However, it is important to note that this technology remains limited to research settings and is not yet part of routine clinical imaging. As such, the present review focuses on biomarkers derived from conventional OCT systems, which currently form the basis for most clinical trial data and real-world studies in AMD.

In this section, we review photoreceptor-based OCT parameters in cohorts of AMD patients, emphasizing those used in studies that provide insights into AMD progression and treatment outcomes using large sample sizes. However, there is considerable variability in how these parameters are defined, measured, and reported. We summarize the different approaches researchers use to determine these biomarkers (e.g., thickness, integrity, reflectivity), the methods employed to obtain them (manual or computational), and the segmentation criteria applied, while providing expert contextualization of the available evidence throughout.

3.2. Outer nuclear layer thickness

3.2.1. Definition and boundaries

The ONL appears as a hyporeflective band on OCT, located between the HFL and the ELM, and anatomically corresponds to the photoreceptor cell nuclei. (Staurenghi et al., 2014) Consequently, there is extensive literature examining the tomographic characteristics of this layer as a means of investigating photoreceptor function, expressed as visual acuity or retinal sensitivity, suggesting the thinning of the ONL as a sign of photoreceptor degeneration. Quantifying the ONL thickness provides a highly interpretable readout, since ONL thinning (for a specific location) can be related to cone and photoreceptor loss based on the known photoreceptor distribution. (Cideciyan et al., 2020; Whitmore et al., 2023)

However, accurate ONL measurement critically depends on how the HFL is handled, as this layer may or may not be included in ONL thickness. While most retinal layers imaged with current OCT systems closely resemble histologic anatomy, the HFL is an exception due to its highly orientation-dependent reflectivity. (Lujan et al., 2011; Otani et al., 2011) Composed of obliquely oriented axons extending

198 from photoreceptor cell bodies in the ONL to their synapses in the inner retina, the HFL is most
199 prominent in the parafovea due to the displacement of inner retinal layers from the foveal center
200 (Figure 2). (Curcio et al., 1993) At the foveal pit, the high cone density—up to 5–6 rows—creates a
201 triangular ONL shape, which quickly reduces to 2–3 rows of mixed cones and rods (Figure 3A,B). In
202 the pit's triangular region, all hyporeflectivity comes from cone nuclei (ONL), but elsewhere, part of it
203 includes Henle fibers (Figure 3A,B).

204 ONL thickness measurement can be extracted directly using the automated segmentation algorithms
205 built into commercial OCT platforms that can provide this measurement from OCT volume scans,
206 being one of the photoreceptor-based parameters easiest to obtain. (Chua et al., 2019; Etheridge et
207 al., 2021; Farinha et al., 2021) An overview of the different methods and definitions to study ONL
208 thickness in AMD is shown in Table S1.

209 **3.2.2. Acquisition and analysis pitfalls**

210 **3.2.2.1.** Beam angle and directional reflectivity artifacts

211 Due to its orientation, HFL reflectivity is highly sensitive to the angle of incident OCT light. (Lujan et
212 al., 2011; Otani et al., 2011) Variations in beam alignment relative to the pupil, such as those
213 introduced by slight tilting of the scan, can cause the HFL to appear either hyperreflective (merging
214 with the OPL) or hyporeflective (contributing to the ONL). Such directional reflectivity artifacts
215 complicate boundary identification and introduce variability in ONL thickness measurements. In
216 contrast, foveal ONL thickness is less affected because the HFL is absent at the foveal center. (Cuenca
217 et al., 2018, 2020; Lujan et al., 2015)

218 **3.2.2.2.** Inclusion of HFL in ONL segmentation

219 Despite these known confounders, it remains unresolved whether including or excluding the HFL
220 from ONL measurements offers better correlation with functional outcomes. Commercial OCT
221 platforms typically provide automated ONL thickness outputs from macular volume scans, making

this one of the most accessible photoreceptor-based metrics. (Chua et al., 2019; Etheridge et al., 2021; Farinha et al., 2021) Most automated algorithms, both research and clinical, segment the HFL together with the ONL, thereby increasing thickness values relative to histologic definitions. (Pfau et al., 2021, 2022; Pfau et al., 2020a; Pfau, von der Emde, Dysli, et al., 2020; Saßmannshausen et al., 2021; Trinh, Kalloniatis, et al., 2022)

Establishing standardized segmentation protocols that explicitly address whether and where the HFL should be included is therefore essential for improving comparability across studies and for refining ONL-based biomarker strategies. An overview of the different methods and definitions used to quantify ONL thickness in AMD is provided in Table S1.

3.2.2.3. Structural distortions in the presence of drusen

Another major challenge arises in areas overlying drusen. Local deformation may cause displacement or compression of outer retinal layers, making it difficult to distinguish between structural crowding of intact photoreceptors and true photoreceptor loss. (Hartmann et al., 2012) One potential solution is the use of software capable of segmenting sub-RPE deposits, thereby excluding drusen-affected regions from ONL quantification. (Garzone et al., 2022; Thiele et al., 2022) However, regions with reticular pseudodrusen (RPD) remain particularly challenging to identify and accurately account for, limiting the reliability of ONL-based metrics in these areas.

3.2.2.4. Retinal eccentricity and age-related variability

Finally, retinal eccentricity and patient age influence outer retinal architecture and should be incorporated into both qualitative and quantitative analyses of the ONL**,** especially when comparing patients or longitudinal changes. (Chui et al., 2012; Trinh et al., 2022)

3.2.3. Clinical significance

The ONL, reflecting the density of photoreceptor cell bodies, undergoes measurable thinning in association with both healthy aging and the severity of AMD. Although photoreceptor nuclei are

more resilient than their inner and outer segments, progressive ONL loss still occurs and serves as a surrogate for photoreceptor degeneration. (Etheridge et al., 2021; Larsen et al., 2025)

3.2.3.1. Age-related and AMD-associated thinning

Population-based and clinical cohort studies demonstrate measurable ONL thinning in both aging and across stages of AMD. In the Coimbra Eye Study, mean ONL thickness decreased progressively across Rotterdam stages 2a, 2b, and 3, measuring 95.6, 92.8, and 87.4 µm, respectively. (Farinha et al., 2021) These stages are defined as follows: stage 2a includes eyes with soft indistinct drusen ≥125 µm or reticular drusen only; stage 2b includes soft distinct drusen ≥63 µm in combination with pigmentary abnormalities; and stage 3 includes soft indistinct drusen ≥125 µm or reticular drusen with pigmentary abnormalities. (van Leeuwen et al., 2003) Similarly, Saßmannshausen et al. demonstrated reduced ONL thickness in eyes with large drusen (–4.94 µm vs controls) and an annual decline of –0.03 SD, particularly in paracentral and superior macular regions. (Saßmannshausen et al., 2021; Trinh et al., 2022)

ONL thinning is particularly pronounced in eyes with RPD, consistent with the accelerated chorioretinal dysfunction characteristic of this phenotype. (Cozzi et al., 2024; Farinha et al., 2021; Trinh et al., 2022) All these studies included the HFL within the ONL boundary (Cozzi et al., 2024; Etheridge et al., 2021; Farinha et al., 2021; Larsen et al., 2025; Saßmannshausen et al., 2021), and Trinh et al. defined a combined OPL/HFL/ONL complex for their analyses. (Trinh et al., 2022)

3.2.4. Trial utility

Given its direct correspondence to photoreceptor nuclei, the ONL provides a structurally grounded and quantifiable biomarker with potential utility in interventional AMD trials, especially in GA. Its value spans monitoring of disease progression, detection of therapeutic effect, and development of surrogate functional endpoints.

3.2.4.1. Sensitive to progression beyond visible atrophy

In GA, ONL integrity provides insight into disease activity beyond clinically visible lesions. Photoreceptor thinning in perilesional areas correlates strongly with subsequent GA enlargement, suggesting that ONL loss may serve as an early structural marker of progression. (Pfau et al., 2020a) A mean thinning rate of –0.16 µm/year (adjusted for age and eccentricity, and including the HFL in the ONL measurements) highlights its sensitivity to subclinical change and potential use in progression modeling.(Pfau et al., 2020a)

3.2.4.2. Treatment-responsive structural endpoint

ONL metrics have demonstrated responsiveness to therapy. In the FILLY study, monthly pegcetacoplan treatment resulted in significantly less ONL thinning outside the atrophic lesion compared to sham, together with preservation of inner segment thickness. (Pfau et al., 2022) These findings demonstrate that ONL metrics can capture therapeutic effects, complementing established atrophy-based endpoints.

3.2.4.3. Functional surrogate through AI-based models

Further quantitative insight has been provided by studies employing AI-based layer segmentation. In particular, ONL thinning (including HFL) has emerged as the most robust predictor of sensitivity loss across varying eccentricities outside the GA area, including mesopic, dark-adapted cyan, and dark-adapted red sensitivities. (Pfau et al., 2020b) In the same study, the authors introduced the concept of *inferred sensitivity*, which estimates retinal sensitivity directly from structural OCT data. These models offer an objective alternative to conventional fundus-controlled microperimetry, with the potential to streamline functional assessment and improve reproducibility in both research and clinical settings. The relatively lower contribution of inner and outer segment metrics in this study was attributed to multicollinearity and segmentation challenges, which will need to be validated in future studies. The ability of these models to translate structural information into predicted functional outcomes could make them particularly valuable for early-phase studies, where functional testing may be limited by patient performance variability.

3.2.4.4. Requirements for broader adoption

To enable the widespread adoption of ONL as a clinical trial endpoint, standardization is essential. This includes the development of harmonized segmentation protocols, particularly with clear definitions for the inclusion or exclusion of the HFL; the application of adjustments for eccentricity and age to account for physiological variability; and the use of strategies to exclude areas with drusen or RPD. When these methodological advances are in place, ONL thickness holds promise as a sensitive secondary or exploratory structural endpoint, one that could capture neurodegenerative progression beyond the boundaries of GA.

3.3. First outer retinal band: external limiting membrane (ELM) integrity

3.3.1. Definition and boundaries

In the outer retina, we can distinguish four hyperreflective layers of varying intensity, corresponding to different compartments of cone and rod photoreceptors and retinal pigment epithelium (Figure 3). The ELM is the thinnest and least reflective of the outer hyperreflective retinal bands seen on OCT (Figure 3D). Histologically, the ELM is formed by a line of heterotypic adherens and tight junctions between the apical processes of Müller glia and the photoreceptor inner segments at the junction between the myoid region and the photoreceptor nuclei (Figure 3C,D). (Cuenca et al., 2020) Although the ELM is not traditionally classified as part of the blood–retinal barrier, it plays a critical role in maintaining retinal structural integrity, metabolic exchange, and homeostasis. (Edwards et al., 2017) Spaide and Curcio (Spaide & Curcio, 2011) identified it as the first hyperreflective outer retinal band in OCT images, a view supported in subsequent anatomical correlation studies. (Cuenca et al., 2018, 2020)

Evaluations of the ELM generally demonstrate higher reproducibility, attributed to its clearer delineation on OCT in the context of AMD. (Borrelli et al., 2023; Schmitz-Valckenberg et al., 2023).

As with the other hyperreflective outer retinal bands, assessment has traditionally been performed manually by investigators and is mostly defined as an interruption to the continuity of the first outer retinal band (see Table S2). However, AI-based segmentation software is available which can automatically quantify the integrity of the ELM. However, they do not define “ELM loss” as interruption of only the first hyperreflective outer retinal band. For example, the Discovery platform notably segments ELM loss from the upper boundary of the ELM to the upper boundary of the EZ, applying also a threshold of ≤5 µm thickness for ELM loss. (Wu et al., 2025a) It is important to note that the ELM itself anatomically corresponds to the junctions between Müller cells and photoreceptors and is therefore strictly a hyperreflective line. As such, when “ELM thickness” is reported—particularly by platforms like Discovery—it inherently encompasses adjacent structures, including the myoid zone. This contrasts with other manual or CNN-based delineations, which may target the ELM line alone without incorporating neighboring layers. (Coulibaly et al., 2023; Song et al., 2022)

3.3.2. Acquisition and analysis pitfalls

The assessment of the ELM is subject to the same OCT-related acquisition and analysis limitations described for EZ, including point spread function (PSF)-related blurring, logarithmic signal compression, beam-angle dependence, and pathology-induced shadowing (detailed in 3.4.2). Given the ELM’s thinness and relatively low intrinsic reflectivity, these factors may have an even greater impact on its apparent continuity and detectability.

3.3.3. Clinical significance

The integrity of Band 1 is strongly associated with functional prognosis: recovery of the ELM after treatment often correlates with improved BCVA, whereas extensive disruption predicts poorer recovery. (Muftuoglu et al., 2017; Padrón-Pérez et al., 2018) However, structural recovery of this band does not always equate to full functional restoration, possibly because of lingering Müller cell

dysfunction affecting photoreceptor metabolism, neurotransmitter uptake, or the cone-specific visual cycle, or due to partial photoreceptor loss despite intact Müller cells. (Bringmann et al., 2006; Landa et al., 2012)

The ELM is also a relevant anatomical biomarker in GA. Loss of the ELM demarcates the anatomical boundary of cRORA and may be used to monitor disease progression. (Dolz-Marco et al., 2018; Sayegh et al., 2011; Simader et al., 2014) In one study, ELM loss progressed more slowly in newly developed cRORA lesions than in long-standing atrophic areas (Coulibaly et al., 2023), suggesting that ELM loss may act as a stage-dependent marker of atrophic remodeling, with progression rates that vary over the natural course of cRORA development**.** Table S1 details studies addressing the integrity of the ELM and their main findings.

3.3.4. Trial utility

While not often selected as a primary outcome, the ELM is gaining attention as a supportive or exploratory endpoint in AMD interventional trials.

In clinical trials for GA, ELM loss often co-localizes with regions of photoreceptor degeneration, and its tracking may improve delineation of expanding atrophic zones alongside EZ and RPE thinning. (Arrigo et al., 2021) In the LEAD study, ELM thinning was tracked alongside EZ and RPE to assess subthreshold nanosecond laser effects in iAMD. While EZ loss showed the strongest association with progression, ELM changes also correlated with visual sensitivity decline (Wu et al., 2025a)

As segmentation tools become more refined and layer-specific biomarkers gain regulatory interest, ELM integrity could play a larger role in composite endpoints that combine photoreceptor structure and glial health.

3.4. Ellipsoid zone (EZ) integrity / “EZ-RPE” thickness/volume

3.4.1. Definition and boundaries

The ellipsoid zone (EZ), historically termed "IS/OS junction," (inner and outer segments junction) was formally named by the IN•OCT consensus panel in 2014 as the second outer retinal hyperreflective band, following the RPE. (Staurenghi et al., 2014) In this review, we adopt the term EZ for consistency with current nomenclature.

The assessment of OCT biomarkers, especially the EZ, has progressively shifted from manual, subjective grading by human experts to automated, software-based approaches. (Table S3) In many cases, this transition has improved scalability, efficiency, and reproducibility, particularly for analyzing large datasets, with automated methods often demonstrating agreement comparable to that of expert graders.

3.4.1.1. Anatomical ambiguity of the EZ band

The anatomical origin of this band has been debated. Adaptive optics OCT data support its correspondence to the junction between the inner and outer segments (IS/OS) of photoreceptors (Jonnal et al., 2014). In contrast, alternative interpretations based on anatomical studies identify this band as the photoreceptor inner segment ellipsoid zone (Spaide & Curcio, 2011), a region densely packed with mitochondria, which is known to be a major source of light scatter in the retina (Cuenca et al., 2018; Wilson et al., 2007) (Figure 3). Pathological evidence also supports this view: in AMD, outer segments may be lost while Band 2 remains visible, suggesting that the structure responsible lies within the inner segments rather than at the IS/OS interface. (Litts et al., 2018)

Given that the reflectivity of the ellipsoid zone arises from the dense mitochondrial population in the photoreceptor inner segments and that this reflectivity changes with mitochondrial dysfunction, changes in EZ integrity and reflectivity (see section 3.7) may serve as indicators of cellular metabolic health. (Kleerekooper et al., 2024)

3.4.1.2. EZ vs. EZ-to-RPE: definition variability

Automated segmentation platforms have greatly expanded EZ analyses, but their definitions and thresholds for EZ loss vary considerably, limiting standardization. Most widely used algorithms define the quantifiable region (defined as "EZ" or "photoreceptor layer") not by the second hyperreflective band alone but by the composite "EZ–RPE" slab, which inherently incorporates the IZ (Figure 4). However, the exact boundaries of this slab and the criteria for defining EZ disruption differ across platforms, complicating comparisons across studies (Table *1*).

Table 1. Overview of automated methods for ellipsoid zone (EZ) loss quantification: boundaries, thresholds, and key study findings

Platform	**Definition**	**Threshold for EZ loss**	**Studies and main findings**
RetinSight GA Monitor (Medical University of Vienna) (Mai et al., 2024; Riedl et al., 2022; Schmidt-Erfurth et al., 2025).	*upper* EZ boundary - *upper* RPE boundary	≤4 µm thickness	<u>Post-hoc analysis of OAKS and DERBY:</u> - More reduction of EZ loss than RPE loss with pegcetacoplan. (Schmidt-Erfurth et al., 2025) - GA area in FAF correlates with RPE loss area in OCT, but larger extent of PR damage. (Mai et al., 2024)
Discovery platform (AIWS AG, Bern, Switzerland) (Blair et al., 2025; Wu et al., 2025a)	*upper* EZ boundary - *upper* RPE boundary	≤5 µm thickness, or ≤1 pixel	<u>Post-hoc analysis of the LEAD Study</u> - EZ highest performance at detecting longitudinal changes in eyes with large drusen at baseline. (Wu et al., 2025a) - Subthreshold nanosecond laser treatment slows the progression of outer retinal band loss in eyes without RPD.(Guymer et al., 2025a)
Cleveland Clinic's machine learning-	*middle* of the EZ -	Multiple: 0 µm = total loss; <20:	<u>Post-hoc analysis of OSPREY trial:</u> - Lower EZ-RPE thickness associated with lower VA at

augmented segmentation and feature extraction platform (Abraham et al., 2022; Bell et al., 2024; Ehlers et al., 2021, 2022, 2024; Yordi et al., 2022; Yordi et al., 2024a; Yordi et al., et al., 2024b)	*middle* of the RPE	partial loss; <10 µm = EZ at-risk area; volume & area output	baseline and over time(Yordi et al., 2024a) - Lower volatility of IRF, SRF and SHRM volumes associated with improvement in EZ integrity and BCVA(Ehlers et al., 2024) - Lower volatility of SRF volume associated with improvement in EZ attenuation and smaller SHRM. (Ehlers et al., 2022) - EZ-RPE volume and EZ-RPE thickness correlate better with VA than EZ integrity. All EZ parameters improved 4 weeks after treatment (Ehlers et al., 2021) <u>Post-hoc analysis of the HAWK trial:</u> - Total EZ attenuation greater in eyes with bacillary detachment, but improved after treatment. (Yordi et al., 2024b) <u>Post-hoc analysis of the NTC03626636 trial:</u> - Baseline EZ integrity associated with better BCVA in the treated group. (Abraham et al., 2022) <u>ReCLAIM-2: Phase II Clinical Trial</u> - Treatment with elamipretide slows EZ damage. (Ehlers et al., 2025) <u>Independent dataset:</u> - EZ at risk area predicts GA progression (Kalra et al., 2023)

Legend: EZ: ellipsoid zone, RPE: retinal pigment epithelium, GA: geographic atrophy, VA: visual acuity, SRF: subretinal fluid, SHRM: subretinal hyperreflective material, IRF: intraretinal fluid, BCVA: best-corrected visual acuity, RPD: reticular pseudodrusen, FAF: fundus autofluorescence.

Because EZ loss metrics rely on platform-specific boundary definitions and loss thresholds (see Table 1), they are not directly interchangeable across studies, and cross-study or meta-analytic comparisons should therefore be interpreted with caution.

3.4.2. Acquisition and analysis pitfalls

Several fundamental optical and signal-processing characteristics of OCT influence the appearance and measurable thickness of the EZ and other outer retinal bands.

3.4.2.1. Optical limitations: point spread function and signal compression

OCT signal is subject to blurring due to the axial point-spread function (PSF), which describes how a point reflector is represented in depth. Because OCT records the convolution of the true retinal structure with the axial PSF, even very thin layers appear broadened, and closely spaced bands may partially overlap. This results in small but systematic biases in thickness measurements. (Drexler, 2004) The true in vivo PSF is rarely measured**,** as it depends strongly on each eye's optical aberrations and cannot be calibrated with a test object placed inside the eye; thus its effect is typically inferred rather than directly quantified. (Spaide & Curcio, 2011)

A second, related factor is the logarithmic compression applied to the OCT signal prior to display. This transformation condenses the large dynamic range of retinal backscatter into a visible grayscale but broaden highly reflective layers, thereby affecting measured thickness.(Drexler & Fujimoto, 2008; Huang et al., 1991; Spaide & Curcio, 2011)

Together, PSF-related blurring and log-scaled display represent inherent sources of measurement bias that affect all OCT-derived outer retinal metrics, especially thinner structures such as EZ.

3.4.2.2. Beam angle and directional reflectivity artifacts

The visibility and apparent thickness of the EZ band depend strongly on the angle of incidence between the OCT beam and the photoreceptors. This directional reflectivity, related to the Stiles–Crawford effect, causes backscattered light to vary with beam entry position. (Gao et al., 2008) As a result, small deviations in beam alignment can alter the reflectivity and contour of the outer retinal bands, affecting both cross-sectional interpretation and longitudinal comparisons. Such effects are particularly pronounced in eyes with drusen or other structural irregularities. (Griffin et al., 2021; Lee et al., 2021) To help identify scans affected by off-axis illumination, Park and Lujan proposed practical indicators: excessive asymmetry of the HFL on either side of the fovea or the presence of a dark triangular region at the superior part of the image suggests an oblique beam entry, and such scans should be excluded from quantitative analysis. (Park & Lujan, 2017)

More broadly, directional reflectivity also affects EZ (and ONL and IZ) measurements, and inconsistent acquisition strategies are therefore likely to limit their comparability, even when using large datasets or AI-based analyses. Section 3.10 provides recommendations and a quality control checklist for image acquisition.

3.4.2.3. Pathology-related reflectivity loss

Pathology-related factors may further confound the interpretation of EZ integrity. It remains difficult to distinguish between true photoreceptor loss and mere orientation changes that affect their reflectance properties in areas where typical retinal architecture is compromised, such as over drusen or near geographic atrophy. (Reumueller et al., 2019) For example, the EZ band can appear attenuated over drusen due to shadowing or altered reflectivity, yet it may re-emerge after drusen regression, highlighting the need to distinguish true EZ loss from instances in which the band is simply not visible. (Gao et al., 2008; Lujan et al., 2024) As with ONL assessment, automated detection and exclusion of RPD and drusen-affected regions may offer a practical means to minimize this source of measurement bias.

3.4.2.4. Quantification variability across methods

Historically, EZ integrity has been assessed using manual or semi-quantitative approaches, including dichotomous grading (present/absent) (Ferrara et al., 2017; Lindenberg et al., 2024; Mathew et al., 2013), categorical scales within fixed regions such as the central 1 mm (Cedro et al., 2023; Ryu et al., 2016; Wu et al., 2014a), and continuous caliper-based measurements of disruption width (Coscas et al., 2015; Mahmoudi et al., 2024) (Tables S2-S3).

These methods remain widely used but are limited by high intergrader variability, with particularly low agreement for EZ assessments (Müller et al., 2021; Schmitz-Valckenberg et al., 2023)

Modern CNN-based tools now allow scalable, reproducible segmentation and en face EZ maps when applied to volumetric OCT acquisitions (Itoh et al., 2016; Pfau et al., 2020b; Yoshida et al., 2025), but boundary definitions and required sampling density still vary across devices and analysis pipelines (see Table *1*).

Notably, the relationship between EZ reflectivity and automated measurements of EZ thickness has not been systematically investigated. The extent to which reflectivity loss biases thickness measurements therefore remains an important, yet unresolved, methodological limitation of current EZ-based metrics.

3.4.3. Clinical significance

3.4.3.1. Disease progression and early detection

Histology shows that photoreceptor degeneration begins with outer segment shortening, preceding inner segment loss and ELM disruption (Litts et al., 2015). On OCT, this implies that IZ alterations may be the earliest detectable change. Because composite EZ-to-RPE thickness metrics inherently span the IZ, early photoreceptor changes can still be captured even without explicit segmentation.

However, studies without composite metrics have relied predominantly on the EZ band, which has historically served as the principal early OCT biomarker of photoreceptor compromise, being more consistently identifiable than IZ alone. Large-scale population data reinforce the clinical relevance of these early structural changes: in the UK Biobank (>44,000 participants (OCT data segmenting EZ alone)(Keane et al., 2016), reduced photoreceptor thickness significantly increased the risk of incident AMD (HR 1.35), particularly among genetically predisposed individuals. (Zekavat et al., 2022)

Longitudinal analyses using composite metrics (EZ-to-RPE) further highlight the sensitivity of EZ-based biomarkers. In the sham treatment arm of the LEAD study (randomized, sham-controlled study of the use of subthreshold nanosecond laser (SNL) intervention in participants with bilateral large drusen and without signs of nGA; analyzing EZ-to-RPE, upper boundaries, loss = segmented layer ≤5 µm) (Lek et al., 2017), Wu et al. described EZ loss as the most sensitive structural indicator of progression, showing 0.05mm/year increase in its square root en face extent of loss, and outperforming RPE and ELM loss. (Wu et al., 2025a) These findings emphasize the ability of EZ-derived metrics to capture early photoreceptor deterioration in iAMD.

3.4.3.2. Photoreceptor alterations in GA

Several studies have documented substantial photoreceptor damage beyond the borders of visible GA, presented as: EZ loss or disruption (Amarasekera et al., 2022; Giocanti-Auregan et al., 2015; Takahashi et al., 2016), EZ–RPE thinning (Kalra et al., 2023; Mai et al., 2024) and thinning of the photoreceptor inner and outer segments. (Pfau et al., 2020a)
Likewise, a study based on ancillary SD-OCT data from the AREDS2 cohort, showed that thinning of the photoreceptor zone (from the inner plexiform layer to the RPE-drusen complex) and disruption of the IZ can precede the onset of GA by up to four years, highlighting the potential of photoreceptor alterations as early markers of atrophy. (Pasricha et al., 2021)

3.4.3.3. Photoreceptor integrity in exudative AMD

In exudative AMD, EZ has also been studied as a structural marker of photoreceptor health, although in a lesser extent than in GA, with mixed findings regarding the prediction of neovascular conversion. (Amarasekera et al., 2022; Ferrara et al., 2017; J. Lee et al., 2022; Vogl et al., 2021) Amarasekera et al. found that while loss of EZ integrity predicted iRORA and cRORA development, it was a not reliable predictor of neovascular conversion. (Amarasekera et al., 2022) Conversely, Ferrara et al. reported that EZ disruption (EZ band only, manual assessment) was associated with subsequent neovascularization (Ferrara et al., 2017), and Vogl et al., analyzing data from the HARBOR trial, observed that outer retinal changes often preceded GA, whereas accelerated choroidal thinning more often anticipated neovascular onset in fellow eyes of unilateral nAMD. (Vogl et al., 2021)

Beyond risk prediction, photoreceptor metrics also reflect treatment-related structural dynamics. Post hoc analyses of the OSPREY trial (EZ-RPE, middle boundaries) showed that increased fluid and hyperreflective material volatility during treatment increased EZ attenuation (total attenuation: 0 µm EZ-RPE thickness) and poorer BCVA, in both groups of eyes treated with brolucizumab and aflibercept. (Ehlers et al., 2022) Although subretinal fluid has been discussed as a possible protective factor for the outer retina,(Sharma et al., 2016; Zarbin et al., 2022) automated analyses suggest that it is the shift in fluid volume that causes cell damage. (Ehlers et al., 2021, 2022, 2024) In addition, they showed that better EZ recovery rates 4 weeks after treatment can predict visual acuity outcomes at week 52, suggesting % EZ attenuation as an early biomarker in eyes with exudative AMD. (Ehlers et al., 2021) Similarly, faster restoration of overall retinal architecture, including the EZ band, aligns with better visual results. (Yordi et al., 2022; Yordi et al., 2024b)

In more severe presentations such as submacular hemorrhage, baseline EZ integrity has also been shown to predict treatment success, with better-preserved EZ at presentation correlating with improved outcomes following vitrectomy, subretinal recombinant tissue plasminogen activator (rTPA) injection, and anti-VEGF treatment. (Ogata et al., 2022; Ueda-Arakawa et al., 2012)

3.4.3.4. Structure-function relationship

Data from the sham arm of the LEAD study demonstrated that in univariable analyses, changes in the *en face* extent of ELM (upper boundaries of ELM and EZ), EZ (upper boundaries of EZ and RPE), and RPE (upper boundaries of RPE and Bruch's membrane) loss (defined by thickness ≤5 μm) were all significantly associated with changes over time in mean sensitivity and the number of locations with deep visual sensitivity losses (≤10 dB) measured by microperimetry. However, multivariable analyses showed that only changes in the extent of EZ and ELM loss remained independently associated with changes in mean retinal sensitivity, whereas changes in RPE loss did not. However, changes in the number of locations with deep sensitivity loss (≤10 dB) were independently associated with changes of both the extent of EZ and RPE loss. (Wu et al., 2025a) Data from another cross-sectional study using targeted, high-density microperimetry testing of regions with at least iRORA showed that in univariable analyses, EZ and ELM disruption (loss of the visibility of these bands, based on manual grading, along with other components of photoreceptor and RPE loss) were both significantly associated with the presence of a deep visual sensitivity defect (≤10 dB) at specific test locations (Saeed et al., 2025) However, multivariable analysis showed that ELM disruption remained significantly associated with pointwise deep visual sensitivity defects, but not EZ disruption. These findings emphasize the nuanced relationship between structural changes and functional outcomes in non-neovascular AMD, highlighting the value of layer-specific metrics in monitoring progression.

Although BCVA is widely used in clinical practice, it often lacks sensitivity to subtle or localized photoreceptor injury, particularly outside the fovea. Nonetheless, several studies have demonstrated significant associations between BCVA and specific EZ-derived metrics - including EZ reflectivity (Yordi et al., 2024a), EZ disruption (Chhablani et al., 2013; Landa et al., 2011; Savastano et al., 2022), EZ band thickness (Oishi et al., 2013), and the combined EZ-to-RPE thickness (Ehlers et al., 2021; Yordi et al., 2024b), especially in eyes with foveal involvement. For broader or perifoveal dysfunction, however, microperimetry has consistently proven more sensitive than BCVA. (Birner et al., 2024, 2025; Landa et al., 2011; Pilotto et al., 2013; Querques et al., 2012; Wu et al., 2014a) This limitation

becomes particularly relevant as AMD progresses to GA, where central vision may remain relatively preserved despite marked parafoveal functional loss (Lindner et al., 2017) Microperimetry can detect the resultant scotomas and localized sensitivity deficits along GA borders, where residual cone-mediated function can persist even in the absence of a visible EZ band, provided the ONL remains intact. (Pfau et al., 2019b) These observations align with histological evidence demonstrating preferential rod loss (compared to cone loss), near GA margins, (Curcio et al., 1996) and are further supported by clinical studies showing delayed dark adaptation - a hallmark of impaired rod function – in association with photoreceptor structural changes, especially in eyes with RPD. (Fasih-Ahmad et al., 2024; Laíns et al., 2017)

3.4.3.5. Systemic correlates of photoreceptor disruption

Photoreceptor disruption may also be reflected in systemic biomarkers. In preliminary work, Laíns and colleagues recently demonstrated that 3 different plasma metabolites (N-acetylasparagine, a-CMBHC glucuronide, and linoleoyl-docosahexaenoylglycerol (18:2/22:6)) were significantly associated with the presence of EZ disruption.(Lains et al., 2024) This work will need validation in other studies, and if repeatable, may offer insights into disease pathology.

3.4.4. Trial utility

3.4.4.1. Early disease detection and iAMD trials

Although the LEAD trial's primary endpoint was time to development of multimodal imaging-defined late AMD, (Lek et al., 2017), post-hoc analyses of layer-specific structural biomarkers provided additional insights. In eyes without RPD and in retinal areas without drusen, subthreshold nanosecond laser treatment slowed progression of outer retinal band loss by approximately 85%, based on quantitative measurements using the Discovery platform (upper boundaries EZ-RPE; loss= $\leq$5 µm). (Guymer et al., 2025a) These results highlight the sensitivity of EZ-based measures for detecting subtle biological effects in intermediate AMD, even when the primary clinical endpoint (time to late AMD) shows no significant difference, and merit consideration for future interventional iAMD trial planning.

3.4.4.2. GA progression and predictive value

In clinical trials for GA, the primary outcome measure has traditionally been the change in lesion size as determined on fundus autofluoresence (FAF) imaging.(Heier et al., 2023) While RPE dysfunction is often considered the primary driver of photoreceptor death in GA, OCT can reveal photoreceptor degeneration earlier than visible RPE atrophy. (Mai et al., 2025; Schmidt-Erfurth et al., 2025) However, accurate photoreceptor damage beyond areas of RPE atrophy is poorly captured using FAF. (Mai et al., 2025; Schmidt-Erfurth et al., 2025) Photoreceptor OCT surrogate biomarkers could therefore add prognostic value in terms of disease progression and potential therapeutic response. (Mai et al., 2025; Riedl et al., 2022)

Post hoc analysis of the sham arms of the OAKS and DERBY trials showed that eyes with more extensive EZ than RPE damage at baseline exhibited faster GA enlargement, suggesting the EZ/RPE loss ratio (upper boundaries; loss= $\leq$4 µm) as a potential biomarker of rapidly progressing atrophy. (Schmidt-Erfurth et al., 2025) This metric may help identify high-risk patients more likely to benefit from complement-inhibiting therapies. Importantly, the EZ–RPE difference can now be quantified automatically using AI-based tools, although further work is needed to clarify whether this biomarker provides information beyond conventional predictors, such as baseline lesion size or shape-descriptive factors.(Pfau et al., 2019a) Of note, this interpretation must be considered in light of the structural and segmentation limitations outlined in section 3.4.2.: outer retinal alterations overlying RPD may preferentially affect EZ-based measurements, potentially exaggerating apparent EZ-RPE dissociation in certain regions.

A recent study by Yoshida et al. suggests that the method used to extract EZ and RPE metrics is less relevant in the context of predicting GA progression. (Yoshida et al., 2025) They demonstrated that distinct OCT-based modeling approaches (SLIVER-net, 3D CNNs, and segmentation-derived EZ/RPE thickness maps) achieved comparable predictive performance, suggesting a plateau with current methods and emphasizing the informational weight of the EZ and RPE layers. However, further studies using other platforms are needed to validate this.

The EZ-at-risk area (defined as EZ-to-RPE thickness <10 µm outside established GA) has also shown potential as a sensitive biomarker for early photoreceptor compromise. This metric is thought to identify photoreceptors that are structurally thinned and under stress but not yet irreversibly lost, thereby capturing tissue that may still be amenable to intervention. In a deep learning-based study, Kalra et al. demonstrated that automated quantification of this area could predict progression to GA. (Kalra et al., 2023) Compared with binary EZ loss definitions, EZ-at-risk may offer greater sensitivity to early change. In this context, EZ-at-risk may complement EZR, which reflects photoreceptor metabolic activity, by providing an additional structurally grounded marker of impending degeneration. While these findings highlight the clinical promise of EZ-at-risk for risk stratification, further large-scale validation studies are needed. Particularly important will be direct comparisons with other definitions of EZ loss (e.g. EZ-to-RPE $\leq$ 4 µm or 0 µm) to establish its relative predictive value and clinical utility. (Kalra et al., 2023)

3.4.4.3. Sensitive treatment endpoints

Studies examining EZ-RPE thickness as a composite measure of photoreceptor integrity have demonstrated slower rates of EZ loss with monthly pegcetacoplan treatment compared to every-other-month and sham-treated groups.(Mai et al., 2022; Riedl et al., 2022) Moreover, Schmidt-Erfurth et al. reported that the treatment-associated reduction in EZ loss (upper boundaries EZ-RPE; loss= <4 µm) exceeded the reduction in RPE loss, reinforcing their potential as responsive efficacy endpoints. (Schmidt-Erfurth et al., 2025)

3.4.4.4. Regulatory recognition of EZ loss as a structural endpoint

A pivotal moment for photoreceptor-centered biomarkers came in the ReCLAIM-2 phase II elamipretide trial (in eyes with non-central GA), where treated eyes demonstrated a 43% reduction in the rate of macular EZ loss (middle of the EZ to the middle of the RPE, loss = 0 µm) from baseline. (Ehlers et al., 2025)

Although the primary endpoints of the study were BCVA and GA area, the magnitude and consistency of EZ preservation prompted the FDA to designate EZ loss (defined as EZ-to-RPE

thickness of 0 µm) as a key structural endpoint in the ongoing phase III ReNEW trial (NCT06373731).(ISCRCTN, 2024) This marks a substantial shift toward integrating photoreceptor-derived OCT metrics into regulatory frameworks for GA drug development.

3.5. Inner (IS) and outer segment (OS) thickness

3.5.1. Definition and boundaries

Beyond these combined measures of photoreceptor thickness detailed in section 3.4, more granular approaches have sought to separate photoreceptor sublayers. Pfau and colleagues developed a CNN-based pipeline to independently segment the inner segments (IS), defined from the ELM to the upper boundary of the EZ, and the outer segments (OS), defined from the EZ to the upper boundary of the RPE-drusen complex, allowing calculation of discrete IS and OS thickness values (Figure 5) (Pfau et al., 2021, 2022; Pfau et al., 2020a).

3.5.2. Acquisition and analysis pitfalls

The same acquisition and analysis limitations described for the EZ (section 3.4.2) apply here as well.

3.5.3. Clinical significance

To date, separate analyses of photoreceptor inner and outer segments have been studied predominantly in eyes with GA. Natural-history analyses indicate that photoreceptor sublayers exhibit differential clinical relevance in GA: while inner segments show the greatest rate of macula-wide thinning over time, outer segment thickness demonstrates greater inter-eye variability and stronger prognostic association with future GA progression. (Pfau et al., 2020a)

3.5.4. Trial utility

A post hoc analysis of the FILLY trial showed that treatment with pegcetacoplan was associated with reduced photoreceptor thinning beyond the GA boundary, with the most consistent and dose-

dependent preservation observed at the level of the ONL and inner segments, whereas effects on outer segment thickness were less consistent. These findings suggest that IS thickness may be particularly sensitive to treatment effects in interventional settings. (Pfau et al., 2022)

However, studies directly comparing IS and OS thickness changes with other commonly used photoreceptor measures, such as EZ loss or EZ-to-RPE thickness, are currently lacking. As a result, it is still unclear which structural approach is best suited to assess treatment response in interventional clinical trials.

3.6. Interdigitation zone (IZ) integrity

3.6.1. Definition and boundaries

The third hyperreflective band seen on conventional SD-OCT and SS-OCT, located between the EZ and the RPE, has been a subject of ongoing debate regarding its anatomical correspondence and nomenclature. Current interpretations can be organized into four complementary frameworks.

a) IN•OCT consensus: Interdigitation zone (IZ)

The 2014 IN•OCT consensus panel designated this structure as the IZ, the interface where the apical processes of the RPE extend between and around the distal tips of photoreceptor outer segments (Figure 3D). This close structural interaction creates a distinct optical boundary, generating strong reflectivity in standard OCT images. (Staurenghi et al., 2014)

b) Adaptive-optics OCT: cone and rod outer segment tips (COST and ROST)

Adaptive optics OCT studies have suggested that this band arises from the posterior tips of cone outer segments (COST), and in more peripheral regions, also includes rod outer segment tips (ROST). The COST/ROST interpretation emphasizes the role of precise photoreceptor geometry and refractive index changes at the outer segment terminus in producing OCT reflectivity. (Jonnal et al., 2014; Zhang et al., 2006)

c) Histologic interpretation: phagosomes within the RPE

An alternative viewpoint comes from immunohistochemical studies, such as those by Cuenca et al. (Cuenca et al., 2018), suggesting that Band 3 arises not at the photoreceptor-RPE interface per se, but rather within the RPE cytoplasm itself. Thus, the signal is thought to originate from phagosomes, organelles formed during the daily shedding of the tips of cone outer segment discs (Figure 3C). These phagosomes, rich in tightly packed membranes, are highly efficient light scatterers and align well with the reflectivity patterns observed in OCT. Furthermore, their number and position change throughout the day, which may explain the temporal variations in Band 3 intensity and continuity observed in time-resolved OCT imaging (Kocaoglu et al., 2016; Pircher et al., 2010). In this interpretation, band 3 reflects a dynamic intracellular process within the RPE, rather than a fixed anatomical boundary.

d) Ultrahigh-resolution OCT: subdivision into OSIZ-1 and OSIZ-2

The most recent refinement in IZ interpretation comes from Goerdt et al. (2024), using a ultrahigh-resolution (<3 µm axial) OCT system combined with histologic and electron microscopy correlation. (Goerdt et al., 2024) They proposed that what had previously been perceived as a single band between EZ and RPE with conventional OCT is better described as a complex of two distinct substructures: (Figure 3E)

- OSIZ-1: a hyporeflective band corresponding to the portion of photoreceptor outer segments not yet covered by RPE apical processes.
- OSIZ-2: a more hyperreflective band representing photoreceptor outer segment tips embedded among compacted apical RPE processes, containing melanosomes external to the RPE cell body.

This interpretation not only offers finer structural granularity but also supports the hypothesis that these subcomponents may exhibit differential vulnerability in aging and disease. (Goerdt et

al., 2024) However, these distinctions are not discernible on current clinical SS- and SD-OCT devices, which lack the axial resolution and signal-to-noise ratio to reliably separate OSIZ-1 and OSIZ-2. As a result, clinical OCT collapses these zones into a single apparent “IZ” band, potentially obscuring critical biological processes occurring at the photoreceptor-RPE interface.

3.6.2. Acquisition and analysis pitfalls

As detailed for the EZ, OCT-specific limitations also apply to the IZ, but with greater impact due to its low contrast and strong directional reflectivity, making separation from adjacent outer retinal bands particularly challenging on clinical systems.

3.6.2.1. OCT signal limitations and directional reflectivity

As with the EZ, the IZ signal is even strongly influenced by directional reflectivity and beam angle. Slight variations in the alignment of the OCT beam relative to the optical axis of photoreceptors can significantly alter IZ intensity. These effects are especially pronounced in the presence of drusen or uneven topography (Berlin et al., 2023; Gao et al., 2008; Lujan et al., 2024), where signal distortion further reduces variability.

Berlin et al. (2023) highlighted the variability in IZ detection on standard B-scans and proposed objective criteria for IZ identification: (Berlin et al., 2023)

1. The presence of a visually distinct band between EZ and RPE, and
2. A corresponding peak in the longitudinal reflectivity profile, as measured by signal intensity plots through A-scans.

3.6.2.2. Age and physiological effects on IZ visibility

Even in healthy eyes, IZ visibility is not guaranteed, particularly in the subfoveal region. The Beijing Eye Study introduced a two-type classification: (Shao et al., 2018)

- Type 1 IZ: discrete and distinguishable IZ band
- Type 2 IZ: IZ signal merges with or is indistinguishable from the RPE

Type 2 configurations increase in prevalence with age and may be mistaken for pathological IZ loss, complicating interpretation in aging populations or early AMD. (Shao et al., 2018)

3.6.2.3. Algorithmic and segmentation limitations

Because the IZ cannot be robustly and reproducibly segmented as an independent layer on current clinical OCT platforms, most automated and AI-based algorithms do not attempt explicit IZ delineation. Instead, the IZ signal is typically subsumed within a broader EZ-to-RPE zone, often operationally labeled as "EZ," defined as the space between the EZ boundary and the RPE boundary (see section 3.4.1.2 and Table 1) (Abraham et al., 2022; Ehlers et al., 2021, 2022, 2024; Kalra et al., 2023; Mai et al., 2024; Schmidt-Erfurth et al., 2025; Yordi et al., 2024a; Yordi et al., 2024b).

While this approach provides a robust and functionally relevant parameter, it limits the ability to separately track IZ-specific changes. Future improvements in OCT resolution and software segmentation, such as the implementation of high-resolution devices and algorithms capable of isolating the IZ band, may allow more precise characterization of early photoreceptor alterations and validate the hypothesis that IZ changes precede both EZ attenuation and ELM disruption.

Nonetheless, several studies have specifically examined IZ integrity using methods similar to those applied to the EZ, including dichotomous assessments of presence or absence (Berlin et al., 2023) and continuous measures of IZ band length or area (Gu et al., 2018; Tomita et al., 2016)

In summary, current acquisition and analysis limitations render isolated IZ quantification unreliable in most clinical contexts. Until advances in high-resolution OCT become widely available, the IZ is best interpreted as part of a composite outer retinal zone rather than as a standalone biomarker.

3.6.3. Clinical significance

From a clinical perspective, the presence and integrity of this third outer retinal band are increasingly recognized as potential biomarkers of photoreceptor-RPE complex health. Given the high metabolic demands of photoreceptors and their reliance on RPE phagocytosis for outer segment renewal, alterations in IZ continuity or reflectivity may signal early degenerative changes. (Berlin et al., 2023)

Recent ultrahigh-resolution OCT studies further suggest that this region is not biologically uniform: the OSIZ-2 component shows a preferential decline in visibility with aging and in early AMD compared to the OSIZ-1. This differential vulnerability supports that disruption at the photoreceptor-RPE interface may occur early in disease and may precede more overt photoreceptor loss. (Goerdt et al., 2024)

While high-resolution imaging holds promise for more precise assessment of this region, most clinical trial data currently rely on conventional OCT, where the IN•OCT designation of "IZ" remains the standard.(Staurenghi et al., 2014) As imaging technology evolves, the potential of this band as a surrogate for photoreceptor function and disease progression warrants further investigation.

3.6.4. Trial utility

To date, the IZ has not been used as a standalone endpoint in AMD clinical trials, primarily due to limited visibility on SD- and SS-OCT system and inconsistent or absent segmentation support in software platforms. Nonetheless, the IZ is routinely included in trial-relevant metrics via its incorporation into EZ-to-RPE composite thickness or volume measurements. These composite biomarkers are leveraged in: RetinSight GA Monitor, Discovery platform and Cleveland Clinic's segmentation and feature extraction platform. (Ehlers et al., 2021; Schmidt-Erfurth et al., 2025; Wu et al., 2025a)

As noted in section 3.4.4 (EZ trial utility), these composite metrics have demonstrated prognostic value, treatment responsiveness, and are increasingly used as secondary endpoints in interventional trials.

Should OCT resolution and segmentation capabilities evolve to reliably isolate the IZ, this band may emerge as a primary marker of RPE-photoreceptor interface health, enabling earlier detection of degeneration, functional risk stratification, and treatment-response modeling.

3.7. Ellipsoid zone reflectivity

3.7.1. Definition

Reflectivity in OCT is a fundamental property that quantifies the amount of signal generated by the interference between light reflected from tissue structures and the reference beam within the device and thus applies to all anatomical layers visualized on OCT scans. However, the brightness or intensity displayed on clinical OCT images is not a direct or absolute measure of tissue reflectivity**,** as it is influenced by ocular media, acquisition parameters, sensitivity roll-off, signal normalization, and vendor-specific post-processing. (Drexler & Fujimoto, 2008)

Within this context, the reflectivity of the outer retinal bands, particularly the EZ, often referred to as EZ reflectivity or EZR, has gained increasing attention as a potential biomarker of photoreceptor health. However, high-quality OCT images and reporting image settings are necessary to ensure comparable results (see section 3.10 for recommendations and quality control checklist). Table S4 shows an overview of the studies using EZR in cohorts of AMD patients.

EZ reflectivity is thought to be closely linked to the high mitochondrial density within the ellipsoid portion of the photoreceptor inner segments, and therefore to photoreceptor metabolic activity and energetic demand.(Litts et al., 2018)

Unlike structural thickness, EZR is not provided by standard OCT platforms and requires custom post-processing. Calculation is sensitive to acquisition parameters and signal processing, and several metrics have been proposed to capture EZR with varying levels of precision and generalizability (Table S4).

3.7.2. Methodological approaches to EZR quantification

The quantification of the EZR was initially described by Hood et al. in individuals with achromatopsia or cone dystrophy, and since then, other authors have employed a similar methodology, albeit with notable variations.(Hood et al., 2011) To avoid the introduction of confounding variables that are dependent on image brightness, reflectivity should be reported in relation to other retinal structures within the same image, thereby emphasizing relative rather than absolute signal intensity (Table S4). (Gunawan et al., 2022; Thiele et al., 2020; Toprak et al., 2017; Wu et al., 2013a)

3.7.2.1. Relative ellipsoid zone reflectivity (rEZR)

Thiele and colleagues first introduced the term "relative EZ reflectivity" (rEZR), which refers to the ratio of the reflectivity of the EZ to that of the ELM. (Thiele et al., 2020) The rationale for selecting the ELM as a reference is its demonstrated stability across subjects, pathologies, retinal locations and further underlines less age-dependent impact, especially when compared to the RPE as a reference. (Gin et al., 2017; Wu et al., 2013b, 2013a) Although the INL has also been used as a reference with comparable results, its physiological absence in the foveal center would hamper reliable assessment here. (Cuenca et al., 2020)

Figure 6 depicts how rEZR is obtained from an OCT B-scan. Manual rEZR is feasible for small datasets but not scalable. To overcome this, Thiele et al. developed a computational method that uses raw linear OCT data (i.e., representing the native, untransformed OCT signal with linear reflectivity values ranging from 0-1 arbitrary units) to assess rEZR across volume scans and preserve topographical specificity.(Thiele et al., 2020, 2022) This approach (by using OCT raw images) captures the full reflectivity range of the EZ and avoids signal compression effects introduced by logarithmic transformation. (Thiele et al., 2020, 2022)

3.7.2.2. Normalized EZ reflectivity

An alternative method, normalized EZR, uses en face reconstructions segmented at the EZ plane. Pixel intensities are averaged across a region of interest (ROI), and the signal is normalized using internal image landmarks.(Borrelli et al., 2017; Saleh et al., 2017)

Therefore, calculating the mean value of all pixels of the region of interest should provide the same information as the cross-sectional projection or each individual A-scan. En face projections segmented in the EZ plane (generally provided by the inbuilt software of OCT devices) need to be imported into external software for analysis (e.g. ImageJ (National Institutes of Health, Bethesda, MD, USA)).

Two normalization strategies have been proposed:

- RPE-based normalization: Saleh et al. used the mean pixel intensity from the RPE en face slab as the reference.(Saleh et al., 2017) However, variability in RPE reflectivity in AMD limits its reliability.(Gambril et al., 2019)
- Bright/dark normalization: Borrelli et al. proposed a method using the RNFL as the bright reference and the vitreous as the dark reference. They introduced the term *"normalized EZ reflectivity"* in a study using a Cirrus HD-OCT (Carl Zeiss Meditec Inc., Dublin, CA, USA) and ImageJ (Borrelli et al., 2017) Figure 7 indicates the formula and shows example pictures of the different segmentation boundaries used to calculate normalized EZR. (Borrelli et al., 2017)

While normalized EZR provides a pragmatic solution for cross-sectional analyses, its dependence on post-processed en face images may limit accuracy compared with rEZR derived from raw OCT volumes.

3.7.3. Acquisition and analysis pitfalls

Several technical and biological factors affect EZR quantification:

3.7.3.1. Topographical variability

Similarly to other photoreceptor parameters previously mentioned, EZR shows a systematic dependence on retinal eccentricity, with the lowest reflectivity values observed at the foveal center. Therefore, to ensure accurate within-subject comparisons, analyses should be restricted to equivalent retinal regions or incorporate the exact topographical location of each EZR measurement into the statistical model. (Thiele et al., 2020).

3.7.3.2. Beam angle and directional reflectivity

As with EZ integrity, EZR is affected by directional reflectivity, scan tilt, and post-processing issues such as logarithmic transformation of the OCT signal (see section 3.4.2). Logarithmic scaling, used for image display in most commercial OCT platforms, alters signal intensities non-linearly, compressing high reflectivity values and distorting the ratio between layers such as the EZ and ELM. This affects quantitative analysis of reflectivity. Thiele et al. showed that accurate rEZR computation requires raw, linear OCT data, as logarithmic transformation results in loss of signal fidelity and suppresses reflectivity differences.(Thiele et al., 2020)

3.7.3.3. Artifacts from pathology

Drusen and RPD can obscure or attenuate EZ signal. rEZR calculations may be artificially reduced if these lesions fall within the region of interest. Excluding these areas or correcting for reflectivity "gaps" is essential.

3.7.3.4. Reference band limitations

Although rEZR uses the ELM as a reference as it is more stable than RPE, ELM itself may be also altered in AMD**.** Nonetheless, rEZR remains sensitive to early disease, potentially detecting subtle EZ or ELM dysfunction before structural disruption is evident. (Liermann et al., 2025)

In summary, the recommendation is to use raw (linear) OCT data whenever possible, exclude regions affected by drusen or RPD, and apply computational methods capable of estimating EZR across the

entire OCT cube while preserving topographical information and enabling age- and location-specific adjustment.

3.7.4. Clinical significance

3.7.4.1. Functional relevance in non-advanced AMD

Even before outer retinal atrophy becomes apparent on structural OCT, functional deficits can occur. (Hess et al., 2022; Kodjikian et al., 2023; Wu et al., 2021) These changes manifest as prolonged dark adaptation, reduced contrast sensitivity, and localized sensitivity loss on microperimetry.

In this context, the rEZR has emerged as a promising surrogate biomarker.

Recent findings from the MACUSTAR study reported strong associations between rEZR and low-luminance visual acuity, Pelli-Robson contrast sensitivity, and fundus-controlled perimetry. Notably, rEZR was not associated with BCVA, indicating that it may capture visual dysfunction not reflected in high-contrast acuity testing. (Liermann et al., 2025)

However, further studies focusing specifically on patients with early AMD, particularly those excluding retinal areas unaffected by drusen, and incorporating longitudinal follow-up are needed to validate these findings and to better understand the temporal dynamics of rEZR changes in relation to functional decline.

3.7.4.2. Disease progression and staging

In eyes with iAMD, rEZR declines steadily over time, with an even more pronounced reduction observed in eyes with RPD.(Saßmannshausen et al., 2022; Thiele et al., 2022) Thiele et al. reported a longitudinal rEZR reduction of 2.1 arbitrary units (AU) per year and a cross-sectional decrease of 8.4 AU per decade in participants of the sham treatment arm of the LEAD study, which included participants with bilateral large drusen. (Thiele et al., 2022) Cross-sectional data from the MACUSTAR study confirmed that rEZR declines progressively with AMD stage, showing reductions of –2.29, –8.05, and –22.35 AU in early, intermediate, and late AMD, respectively, compared to age-matched controls. (Saßmannshausen et al., 2022)

879 However, it should be noted that rEZR measurements in these studies did not account for the impact
880 of RPD. Stage 3 lesions that disrupt the EZ can create apparent “gaps” in reflectivity, and rEZR
881 calculations may erroneously include RPD lesions, which are typically less reflective than the EZ.
882 Thus, the more pronounced reduction in rEZR observed in eyes with RPD may partly reflect an
883 artifact rather than a purely biological effect, and both interpretations should be considered.

884 #### 3.7.5. Trial utility

885 EZ reflectivity-based metrics, especially rEZR, have several features that would make them useful for
886 interventional trials:

887 • Sensitive to early change. In eyes with iAMD, Gunawan et al. reported a transient decrease in
888 rEZR at two weeks following subthreshold nanosecond laser treatment, followed by
889 normalization at three months and an associated improvement in BCVA. (Gunawan et al.,
890 2022)
891 • Functionally meaningful. Recent evidence from the MACUSTAR Study links rEZR to contrast
892 and sensitivity loss (including changes in mesopic fundus-controlled perimetry, low-
893 luminance visual acuity, Moorfields Acuity Test and Pelli-Robson contrast sensitivity), and
894 may detect early dysfunction before structural thinning. (Liermann et al., 2025)
895 • Early/intermediate AMD. Because conventional endpoints (GA area and BCVA) are often
896 insensitive at early stages, rEZR offers a quantitative, image-based alternative.
897 • Scalable with AI. rEZR can be automated using CNN pipelines on raw OCT data, enabling
898 high-throughput volume-wide topographic mapping for endpoint modelling.

899 The main limitation is that longitudinal rEZR data remain sparse. Ongoing studies like MACUSTAR and
900 HONU are expected to provide critical natural history data.(Finger et al., 2019; Guymer et al., 2023)

901 ### 3.8. Comparative synthesis of photoreceptor-based OCT biomarkers in AMD

In the CAM criteria using OCT, features such as EZ or ELM loss, ONL thinning, subsidence of the OPL and the presence of a hyporeflective wedge-shaped band are all considered indicators of photoreceptor degeneration in incomplete and complete retinal pigment epithelium and outer retinal atrophy (iRORA and cRORA) (Figure 8).(Guymer et al., 2020; Sadda et al., 2018) Despite their pathophysiological relevance, change over time in structural photoreceptor biomarkers have not yet been widely adopted as primary endpoints in interventional trials. However, growing recognition of their strong association with functional outcomes has led to increasing interest in their use for both clinical monitoring and regulatory endpoints.(Chew et al., 2025; Fasih-Ahmad et al., 2024; Yordi et al., 2024a)

Photoreceptor-based OCT biomarkers offer diverse, layer-specific insights into retinal integrity and function in AMD. Their comparative advantages lie in what each structure represents (nuclei, segments, interfaces, or metabolic status) and how readily each can be quantified in both routine imaging and trial pipelines. Automated methods currently exist to extract many of these parameters. Table S5 summarizes the main automated method used in clinical studies, the OCT device and scan patterns and code availability.

While each marker offers distinct value, certain trends emerge. ONL thickness stands out as one of the most structurally grounded and treatment-sensitive biomarkers, particularly in GA. It provides a direct measure of photoreceptor nuclei and is amenable to both manual and automated segmentation. (Pfau et al., 2020a) Importantly, ONL metrics are already in use across clinical trials and AI-driven functional prediction models. (Pfau et al., 2022)

The rEZR captures metabolic dysfunction, possibly preceding structural loss, and shows strong correlations with low-luminance acuity and contrast sensitivity. (Liermann et al., 2025) This positions rEZR as a promising candidate for early/intermediate AMD trials, especially in settings where photoreceptor structure appears intact but function is compromised. Its reliance on raw (linear) OCT

data, however, limits current clinical applicability, as this is not currently available to clinicians in commercial systems.

Meanwhile, EZ integrity/EZ–RPE thickness remain the most established structural endpoints, evaluated in large clinical trials, that has shown this parameter to be responsive to both disease progression and therapeutic effects. (Schmidt-Erfurth et al., 2025; Wu et al., 2025a) However, they typically contain multiple layers (e.g., IZ and OS), which may obscure more nuanced biological processes.

Layer-specific metrics such as IS/OS thickness offer additional granularity, with early data suggesting differential treatment response across sublayers. (Pfau et al., 2022) However, their wider application awaits further standardization and comparison with conventional biomarkers.

Though less studied, the IZ may reflect early photoreceptor–RPE interface alterations. High-resolution imaging suggests this region undergoes preferential loss early in AMD, but its poor visibility on clinical OCT limits standalone utility. (Goerdt et al., 2024) Currently, the IZ is typically embedded within broader EZ–RPE measurements.

Finally, the ELM, while often underappreciated, may serve as an early indicator of Müller cell-photoreceptor interface disruption. It also defines the anatomical border of cRORA and is already integrated into automated platforms like Discovery. (Wu et al., 2025a)

In summary, post hoc analyses from major trials such as OSPREY (Ehlers et al., 2021, 2022, 2024; Yordi et al., 2024a), HAWK (Yordi et al., 2024b), FILLY (Mai et al., 2022), OAKS and DERBY (Mai et al., 2024; Schmidt-Erfurth et al., 2025), ReCLAIM-2 (Ehlers et al., 2025) and LEAD (Guymer et al., 2025a) have incorporated photoreceptor measures in exploratory or post hoc analyses, as summarized in Table 1. Importantly, the first regulatory acceptance of EZ integrity as a structural endpoint occurred in trials for MacTel2, ultimately supporting the approval of the first treatment for this condition (Hoy,

949 2025; Pauleikhoff et al., 2022). This milestone paved the way for similar applications in AMD: EZ
950 integrity has now also been accepted by the FDA as a primary structural endpoint in a phase 3 trial of
951 elamipretide for eyes with non-central GA, marking a significant advance in clinical trial design for
952 AMD (BioTherapeutics, 2025; ISCRCTN, 2024). These developments underscore the growing
953 importance of photoreceptor structural metrics in both regulatory frameworks and therapeutic
954 development, particularly as automated segmentation tools facilitate reliable and scalable
955 quantification.

956 Taken together, these biomarkers are complementary. Their selection should be guided by trial
957 phase, patient cohort (early AMD vs GA), imaging data availability (raw vs processed), and desired
958 endpoints (structural vs functional). Table 2 shows an overview of the different OCT-based
959 photoreceptor metrics and their relevance in different AMD stages.

960 Table 2. AMD stage × biomarker matrix summarizing predictive value and trial relevance of
961 photoreceptor OCT metrics in AMD

	ONL thickness	**EZ loss (EZ-to-RPE)**	**PR thinning (IS and OS)**	**rEZR**	**EZ-at-risk**	**ELM integrity**
e/iAMD	Thinning with disease progression (Farinha et al., 2021)	Indicator of disease progression(Wu, De Zanet, et al., 2025) Require smaller sample size (Wu, De Zanet, et al., 2025)		Associated with LLVA and CS (Liermann et al., 2025) Early indicator (Thiele et al., 2022)		Associated with mean retinal sensitivity (Wu, De Zanet, et al., 2025)
nAMD	Better visual outcomes after treatment (S. Lee et al., 2023)	Early biomarker for treatment outcomes (Ehlers et al., 2021)				Better visual outcomes after treatment (Chandak

						et al., 2025)
GA	Sensitivity loss (mesopic, dark-adapted cyan, dark-adapted red sensitivities) (Pfau, von der Emde, Dysli, et al., 2020) Treatment response to pegcetacoplan (Pfau et al., 2022)	EZ/RPE loss ratio biomarker of faster GA growth (Schmidt-Erfurth et al., 2025) Treatment response to elamipretide (Ehlers et al., 2025)	Progressive thinning near GA border(Pfau, von der Emde, de Sisternes, et al., 2020) Treatment response to pegcetacoplan (IS) (Pfau et al., 2022)		Predicts GA progression (Kalra et al., 2023)	Anatomical boundary of RORA (Dolz-Marco et al., 2018)

Legend. ONL: outer nuclear layer, EZ: ellipsoid zone, RPE: retinal pigment epithelium, PR: photorreceptors, IS: inner segment, OS: outer segment, rEZR: relative ellipsoid zone reflectivity, EZ-at-risk (EZ-to-RPE with a thickness < 10 µm, ELM: external limiting membrane, eAMD: early AMD, iAMD: intermediate AMD, nAMD: neovascular AMD, GA: geographic atrophy, LLVA: low-luminance visual acuity, CS: contrast sensitivity, RORA: retinal pigment epithelium and outer retinal atrophy.

3.9. Therapeutic context and endpoint implications

Recent therapeutic advances in non-neovascular AMD highlight the need to clearly distinguish between structural endpoints used in trials and those that are regulator-accepted or clinically validated. For complement inhibitors, phase III studies relied primarily on GA growth rate measured in FAF as the main structural endpoint, with functional outcomes showing modest or inconsistent gains. (Heier et al., 2023) While two drugs targeting complement inhibition have received FDA approval in the United States and Australia (pegcetacoplan and avacincaptad pegol), they have not been authorized in the European Union, underscoring differents levels of evidence and risk benefit

assessments. Against this background, photoreceptor-specific structural metrics remain biologically compelling, yet no drug has been approved based on an endpoint using these outcomes.

In this evolving landscape, EZ loss metrics in AMD are gaining attention as potential structural endpoints and appear to be following a validation pathway similar to that of MacTel2. In MacTel2, change in EZ loss area was the primary endpoint in pivotal trials (NTMT-02, NTMT-03-A/B), ultimately supporting FDA approval of *revakinagene taroretcel* (ENCELTO™) in 2025—the first treatment for the disease. (Chew et al., 2025) A similar approach is now being pursued in AMD: EZ loss rate was used as an exploratory endpoint in earlier-phase studies (e.g. ReCLAIM-2) and currently serves as the primary structural endpoint in an ongoing phase III trial of elamipretide (ReNEW) (ISCRCTN, 2024; Ehlers et al., 2025). As summarized in Table 3, while EZ loss is a validated, regulator-accepted primary endpoint in MacTel2, no AMD drug approvals to date have relied on this outcome.

In summary, structural assessment of photoreceptors using OCT offers a biologically meaningful and increasingly sensitive approach to quantifying retinal degeneration in AMD. Although important technical and methodological limitations remain, continued refinement and validation of these metrics suggest that photoreceptor-based measures may become an important component of structural endpoints in future interventional AMD trials.

Table 3. Regulatory status and clinical trial use of photoreceptor structural OCT endpoints in Macular Telangiectasia type 2 and Age-related Macular Degeneration

Feature	**Macular Telangiectasia type 2 (MacTel2)** (Hoy, 2025)	**Age-related macular degeneration (AMD)**(Ehlers et al., 2025; ISCRCTN, 2024)
Disease context	Bilateral neurodegenerative macular disease with Müller cell dysfunction and	Heterogeneous, multifactorial degenerative disease in which

	progressive, spatially confined photoreceptor loss.	photoreceptor dysfunction follows RPE degeneration.
Exact metric definition	Longitudinal change (mm^2/year) in the area of EZ loss (rate of change in EZ loss)	Longitudinal change in EZ integrity, defined as complete EZ loss (EZ–RPE thickness = 0 µm)
Role in clinical trials	Primary endpoint in phase II and phase III randomized controlled trials (NTMT-02, NTMT-03-A, NTMT-03-B)	Exploratory endpoint in phase II trials (e.g. ReCLAIM-2); primary structural endpoint in ongoing phase III trials of elamipretide
Regulatory status	Validated and regulator-accepted primary structural endpoint; supported FDA approval of revakinagene taroretcel (ENCELTO™) in March 2025	Regulator-recognized structural endpoint in selected trial contexts, but not yet linked to an approved AMD therapy
Advantages	High reproducibility; low compliance dependence; strong structure–function coupling; spatially well-defined disease area	Addresses time-limited trial designs; mechanistically aligned with photoreceptor-targeted therapies
Key limitations	Disease-specific endpoint; applicability outside MacTel2 not established	Requires robust segmentation and masking; stage-dependent
Regulatory implication	Serves as a disease-specific surrogate structural endpoint sufficient for drug approval	Represents an emerging surrogate structural endpoint with contextual regulatory acceptance but ongoing validation

Legend. EZ: ellipsoid zone, RPE: retinal pigment epithelium. References used in the table: (Chew et al., 2025; Ehlers et al., 2025; ISCRCTN, 2024)

3.10. Author toolkit

Box 1. Minimum reporting set for OCT-based photoreceptor structural endpoints.

- OCT device and software version (include axial/lateral resolution)
- Scan protocol
- Signal-strength cutoff
- Segmentation boundaries (upper/middle/lower) and “photoreceptor loss or damage” definition (threshold values)
- Henle fiber layer inclusion in the outer nuclear layer
- Drusen / reticular pseudodrusen segmentation grid
- Reflectivity calculation method
- Raw vs. logarithmic data availability

Box 2. Practical interpretation of EZ/IZ over drusen

- Verify tilt/entry and shadowing
- Rescan criteria
- Classify attenuation vs. absence
- When drusen regress, document reconstitution using en face ellipsoid zone maps (to avoid mislabeling recovery as “new tissue”).

Box 3. Standard relative ellipsoid zone reflectivity recipe

- Preferred reference layer (e.g. external limiting membrane)
- Mask rules (foveal pit, drusen, reticular pseudodrusen)
- Raw-image availability or image normalization
- Longitudinal alignment

- Beam-entry notes
- Reporting of coefficient of repeatability

1000

1001 Box 4. Acquisition quality control checklist for longitudinal OCT studies

1. Acquisition consistency

- Same OCT device and software version across visits
- Identical scan protocol (scan pattern, density, averaging)
- Consistent scan centering (e.g., fovea-centered)

2. Image quality

- Minimum signal strength / quality index threshold
- Absence of motion artifacts or blink truncation
- Adequate layer contrast (outer retinal band visibility)

3. Beam alignment

- Near-coaxial beam entry
- No HFL asymmetry or triangular shadow suggesting off-axis illumination

4. Pathology-related exclusions

- Regions affected by drusen, reticular pseudodrusen, shadowing, or segmentation failure flagged or excluded
- Documentation of new lesions appearing between visits

5. Segmentation and analysis

- Same segmentation algorithm/version used longitudinally
- Manual correction policy predefined and masked
- Consistent definition of layer boundaries (e.g., EZ vs EZ–RPE)

6. Registration and follow-up alignment

- Accurate scan registration to baseline

- Verification of anatomical correspondence

1002

1003 Box 5. Harmonization and interoperability: minimum reporting standards for multi-center OCT trials

1. Signal domain

- Specify whether quantitative metrics are derived from raw linear OCT data or from log-compressed/display data.
- If display data are used, report the exact intensity transform (e.g., logarithmic compression) and the normalization strategy applied (e.g., reference tissue, global scaling, device-specific normalization).

2. Reference layer and masking strategy

- Pre-define the reference layer used for relative metrics (e.g., rEZR), including its anatomical definition and sampling approach.
- Define masking/exclusion rules for the foveal pit, drusen/RPD and low-signal or shadowed regions.

3. Segmentation surfaces and slab definitions

- Explicitly name the segmentation boundaries used to compute thickness or reflectivity metrics (e.g., EZ–RPE, IZ-related slabs).
- Report vendor software versions and any manual corrections or algorithmic overrides.

4. Cross-device mapping

- Report scan parameters (scan length, number of B-scans, averaging), and boundary definitions.
- Include quality assurance or calibration step when available.

5. Data exportability and audit

- State whether raw (linear) OCT volumes and segmentation overlays are exportable and suitable for central auditing.

Legend. rEZR: relative ellipsoid zone reflectivity, EZ: ellipsoid zone, IZ: interdigitation zone, RPE: retinal pigment epithelium.

3.11. OCT-based definitions of atrophy and the role of nascent geographic atrophy (nGA)

3.11.1. Definition and general considerations

The CAM group proposed high-resolution OCT as the reference imaging modality for defining and classifying atrophy in AMD, due to its widespread availability, non-invasive nature, ease of use, and high axial resolution. To standardize terminology, they introduced the terms iRORA and cRORA as the terms to define atrophy using OCT. (Figures 8 and 9) (Guymer et al., 2020; Sadda et al., 2018)

Although RPE atrophy is beyond the scope of this review, both iRORA and cRORA include photoreceptor degeneration as a defining component. Indicators of such degeneration include thinning of the ONL, disruption of the ELM and EZ, subsidence of the OPL and INL and the presence of a hyporeflective wedge within HFL. When these structural changes occur in conjunction with RPE disruption and choroidal hypertransmission, the criteria for iRORA and cRORA are fulfilled (Figure 8). (Guymer et al., 2020; Sadda et al., 2018)

Nascent GA (nGA) was a term previously defined on OCT by the subsidence of the inner nuclear and outer plexiform layers and/or presence of a hyporeflective wedge-shaped band within HFL- without requiring evidence of disruption of the outer retinal bands, including the RPE – and with longitudinal data supporting its potential role as a surrogate endpoint for GA. (Figure 9) (Wu et al., 2014b)

In CAM report 4 it was suggested that nGA could be used as synonymous with iRORA, but they are not the same in terms of predicting risk of progression to GA and as such the retention of the original nGA description has merit. (Guymer et al., 2020; Wu et al., 2024a). In fact, nGA was found to mediate the observed association between iRORA and subsequent development of GA in longitudinal studies. (Wu et al., 2023) Both iRORA and cRORA lesions can also meet definition of nGA and vice versa but

the subsidence of the OPL/INL and /or the wedge-shaped band in HFL are required for nGA and appear to increase the risk of progression to GA.

In summary, iRORA and cRORA are the preferred OCT-based definitions of atrophy, applicable across both neovascular and non-neovascular AMD. GA is a term that refers one of two late forms of AMD and can be defined on color fundus photography (CFP), FAF or OCT (as cRORA). nGA is a specific set of features seen in early atrophy that are highly associated with risk of progression to GA.(Wu et al., 2020, 2023; Wu et al., 2024b) Of note, nGA was also incorporated into the multimodal imaging definition of late AMD used in the LEAD Study. (Guymer et al., 2019)

3.11.2. Clinical significance

From a clinical perspective, the onset of iRORA, cRORA, nGA, or GA could be considered as an incident endpoint in clinical trials. Such endpoints could allow for shorter study durations compared to current trial designs that rely on demonstrating a change in the slope of lesion growth over time. The slope-based approach remains the preferred method for regulatory agencies such as the FDA. Nonetheless, nGA stands out as a strong surrogate endpoint for GA, supported by longitudinal data showing that its hallmark features reliably predict progression to GA. At the time iRORA and cRORA were introduced, such longitudinal data were not available, and their initial value lay in providing a structured terminology framework rather than proven predictive utility. (Guymer et al., 2020; Sadda et al., 2018)

Evidence from the LEAD Study demonstrated that OCT-defined nGA is associated with a 78-fold increased rate of progression to CFP-defined GA over three years, and that it can be detected a median of 13 months earlier than GA onset. (Wu et al., 2020) The same authors also showed while iRORA is also associated with increased risk of GA, this risk may be mediated by the presence of nGA. (Wu et al., 2023) nGA carries even a significantly higher hazard ratio for progression to GA compared to cRORA (65.7 vs. 76.8 respectively).(Wu et al., 2024b) Furthermore, functional assessments suggest that nGA represents a stage of the disease in which visual function is better preserved than in

established GA (Wu et al., 2024b) Of note, automatic algorithms can already detect nGA. (Yao et al., 2024)

To date, the primary outcome in most interventional clinical trials for GA is the rate of lesion enlargement assessed using FAF. However, identifying earlier biomarkers that precede GA onset is critical for designing future trials focused on early intervention. CAM Report 7 recently provided a consensus from the CAM group, that the onset of end-stage atrophy, would be an appropriate endpoint for such trials. (Wu et al., 2025b)

3.12. Limitations of OCT for photoreceptor quantification

Despite its central role in clinical trials and natural-history studies, OCT has inherent limitations when used to quantify photoreceptors at a structural level. Axial resolution is high, but lateral resolution remains insufficient to resolve individual photoreceptors, such that OCT-derived metrics necessarily represent ensemble properties rather than cellular counts. Apparent thickness, continuity, and reflectivity of outer retinal bands are further influenced by angle of incidence, local curvature, and waveguiding effects, leading to spatially heterogeneous signal independent of true biological change. In regions of pathology, particularly over drusen or RPD, retinal bands may partially merge, split, or attenuate, complicating segmentation and longitudinal interpretation. Additional confounds arise from the HFL, whose oblique orientation and reflectivity characteristics can contaminate measurements attributed to the ONL or adjacent outer retinal slabs, especially outside the foveal center.

These constraints limit the OCT's ability to directly measure photoreceptor cell loss, packing geometry, or mosaic disruption, and motivate complementary approaches that operate at a finer spatial scale.

Adaptive optics retinal imaging addresses several of these gaps by providing cellular-scale lateral resolution, enabling direct visualization of individual cone photoreceptors and their spatial organization. These methods are detailed in section 5.

4. Confocal scanning laser ophthalmoscopy (Spectralis High-magnification module)

4.1. General considerations

Confocal scanning laser ophthalmoscopy (cSLO) can be used to visualize parafoveal cones under favorable imaging conditions without adaptive optics, e.g. by using the Spectralis high-magnification module (Heidelberg Engineering, Heidelberg, Germany).(Heidelberg Engineering Inc, 2026) It consists of a magnification lens that can be attached to the camera head of any Spectralis device, providing an additional -8 diopters power. With this module, photoreceptor-resolved images can be obtained in selected eyes, with a field of view of 8x8º and a digital lateral resolution of 1.5 μm (Figures 10 and 11) (Table 4), provided tat fixation is stable, ocular media are clear, and optical aberrations are minimal. To minimize the effects of ocular aberrations, refractive errors should be corrected with spectacles or contact lenses, and the tear film should be preserved. (Heidelberg Engineering Inc, 2026)In selected patients, using the high-speed modality and lower ART frames to reduce eye movement artefacts may also improve the rate of usable, high quality images. (Wynne et al., 2022) However, it is still challenging to image eyes with any pathology,(Konstantinou et al., 2021) and to extract quantitative photoreceptor-based parameters, images must be imported into external software.

4.2. Methods to analyze photoreceptors

Mulders and colleagues describe a detailed and validated computational method for calculating various parameters using different functions and plugins in ImageJ (National Institutes of Health, Bethesda, MD, USA) improving repeatability and reliability compared to manual methods.(Mendonça et al., 2020) Cone cells were detected by using the *3D Maxima Finder* plugin, identifying only those structures larger than preset cut-offs based on degrees of eccentricity; Cone packing was calculated

using Voronoi analysis and counting the number of neighbor cells; cone regularity was determined using the *Biovoxxel* neighbor analysis and defined as the percentage of cells with 6 neighbors; cone inter-cell distance was obtained by Delaunay triangulation and nearest neighbor distance using the *Biovoxxel 2D* distribution analysis plugin. (Mulders et al., 2021) Although they did not compare these parameters with those obtained by adaptive optics, other authors report a -24% difference in cone density in images taken with the high magnification module compared to AO. They used custom software, *Mosaic Analytics* (Translational Imaging Innovations, Hickory, NC), and a custom *MATLAB* script to obtain the measurements in both imaging modalities. (Wynne et al., 2022)

4.3. Clinical significance

Although this technology is available in the clinical setting and only needs to be added to the widely used Spectralis HRA, the difficulty in obtaining good quality images and the heterogeneity of the described data quantification methods limit its use.

5. The role of adaptive optics (AO)

5.1. General considerations

The advent of OCT has enabled the acquisition of high-resolution images of the retina, allowing for an accurate differentiation of the retinal layers, as observed in histology.(Goerdt et al., 2024) Nevertheless, the visualization of individual cells is constrained by the lateral resolution, which is limited by the eye's optical aberrations. Retinal imaging devices can effectively mitigate many optical aberrations, but high-order aberrations that originate from minute irregularities within the eye (e.g., the cornea, lens, and vitreous) can only be addressed through the incorporation of AO technology.(Liang et al., 1997; Roorda et al., 2002) In other words, AO is not a standalone imaging modality; rather, it represents a technological enhancement of existing techniques to improve the transverse resolution by measuring and correcting these optical aberrations in real time. Most of

these systems are based on wavefront sensor technology, which requires both a wavefront sensor (most commonly a Shack-Hartmann wavefront sensor) and a wavefront corrector (deformable mirror). Other systems, designated as sensorless AO and computational AO, present a more computational challenging software-based wavefront correction approach. (Burns et al., 2019) Currently, only hardware-based AO technology incorporated into a flood-illumination retinal camera (rtx1, Imagine Eyes, Orsay, France), an AO-transscleral flood illumination camera (AO-TFI) (Cellularis Discovery, EyeSight, Geneva, Switzerland), and an AO-SLO system (MONA, Robotrak Technologies, Nanjing, China) are commercially available. Nevertheless, research prototypes, including refined AO-SLO and AO-OCT, already exist. (Bonnin et al., 2024; Chui et al., 2024; Heitkotter et al., 2023; Reumueller et al., 2019; Rossi et al., 2017; Sredar et al., 2021) Table 4 provides a comprehensive overview of the fundamental characteristics of each AO imaging modality. Only with AO-SLO it is possible to quantify photoreceptors under direct visualization up into the foveal center. (Ameln et al., 2025; Domdei et al., 2021; Reiniger et al., 2021)

Despite these advances, longer intrasession acquisition times remain a challenge in AO imaging. Due to the inherently small sampling window, multiple individual images must often be captured and montaged to cover a larger retinal area. This not only increases the total imaging duration but also heightens the risk of motion artifacts and subject cooperation bias. To mitigate these issues, many AO systems integrate high-speed eye-tracking to dynamically correct for microsaccades and involuntary eye movements during image acquisition.(Burns et al., 2019; Roorda et al., 2002)

Table 4. Technical specifications of the different imaging modalities available to image photoreceptors

	Acquisition time	Axial resolution (μm)	Lateral resolution (μm)	Field of view (single capture)
SS-OCT	Depends on scan settings	5	15	12mm
SD-OCT	Depends on scan settings	7	14	16.5mm

High-resolution OCT (Spectralis, Heidelberg Engineering)	Depends on scan settings	3	14	16.5mm
cSLO (Spectralis High-magnification module)	Seconds (undefined)	100	1,5μm/pixel (digital)	8x8º
AO-FIO	2-4 s	300	2	4x4º
AO-TFI	6 s	300	2-3	6.7x6.7º
AO-SLO	30-90 s	100	2	1/2ºx1/2º
AO-OCT	Not standardized	5	2	2x2º

Legend. SD-OCT specifications of the Spectralis-HRA OCT 3 (Heidelberg Engineering, Heidelberg, Germany) and SS-OCT of the Cirrus 6000, as the most used devices in the research setting. (Carl Zeiss Meditec Inc, n.d.) Acquisition time in OCT depends on scan settings (scan size, averaging real time, scan density, scan speed). AO-TFI and AO-FIO with the rtx1 (Imagine Eyes), acquisition times showed per video capture. AO-SLO specifications from the Paris and Pittsburg NIRAF AOSLO devices (Gofas-Salas et al., 2024) Axial and transverse resolution are in tissue unless indicated otherwise. OCT: optical coherence tomography, SS-OCT: swept-source OCT, SD-OCT: spectral-domain OCT, cSLO: confocal scanning laser ophthalmoscopy, AO: adaptive optics, FIO: flood-illumination ophthalmoscopy, TFI: transscleral flood illumination, SLO: scanning laser ophthalmoscopy.

5.2. Photoreceptor-based parameters

The most commonly used parameters include cell density, expressed either in metric (cells/mm^2) or angular units (cells/degree^2), obtained by dividing the number of cells by the total area of a region of interest; intercellular spacing (μm or minutes of arc), obtained by measuring the mean value of the distance between neighboring cells; and regularity, calculated as the % of cells that have 6 neighboring cells These parameters can be calculated using software with automatic cell recognition, with the possibility of manual correction of inaccuracies (Figure 12). (Gutnikov et al., 2025; Heisler et al., 2018; Liu et al., 2024; Soltanian-Zadeh et al., 2023) .

Axial length plays a critical role in interpreting retinal measurements, particularly when distinguishing between lateral (metric) and angular dimensions in photoreceptor imaging. (Li et al., 2010; Obata & Yanagi, 2014; Wang et al., 2019) Because metric units (e.g., cells/mm², µm spacing) are directly dependent on the physical scale of the retina, they vary substantially with axial length due to retinal stretching, especially in myopic eyes. Conversely, angular units (e.g., cells/deg²) remain relatively stable or even increase with axial elongation, as they are referenced to visual angle rather than physical distance.(Wang et al., 2019; Li et al., 2010) To avoid misleading conclusions in imaging or functional comparisons, one must report or adjust for axial length when using metric units. (Obata & Yanagi, 2014)

5.3. Clinical significance

The importance of cone cell quantification in a non-invasive and clinically feasible manner has already been highlighted by many researchers as a potential candidate biomarker for new therapeutic interventions. (Burns et al., 2019) In a recent report, Curcio et al. highlight AMD as a disease with an apparent fovea-center gradient photoreceptor loss. (Curcio et al., 2024) As a result, prevention and early detection of the disease are possible by obtaining individualized longitudinal photoreceptor maps. However, the available clinical studies of in vivo individual cone quantification are still limited to a small number of patients and/or short follow-up times (Table 5).

Table 5. Studies using an adaptive-optics flood illumination retinal camera (rtx1, Imagine Eyes, Orsay, France) in age-related macular degeneration.

study	type	eyes	Imaging protocol	parameter	finding
(Rossi et al., 2021)	longitudinal	182 eyes with AMD (early, intermediate and late)	Fovea-centered image and 8 additional images separated by 2º.	Detection of drusen	Reflectivity of drusen change with gaze direction and can be enhanced by combining overlapping AO images.
(Querques et al., 2016)	Cross-sectional	5 eyes with foveal sparring GA	Not defined	Cone density 3271 ± 1,109 cones/mm^2	Hypereflective clumps in the borders of GA Persistence of cone cells in foveal-sparring GA area.

(Borella et al., 2024)	Cross-sectional	8 patients	Not defined	Detection of hyporeflective clumps	Hyporeflective clumps are autofluorescent in NIRAF, suggesting melanin and melanolipofucsin origin.
(Murari et al., 2024)	Cross-sectional	16 patients with presymptomatic AMD	Fovea-centered image and 4 images separated by 1º.	Microsaccade amplitude	Small central drusen are associated with changes of fixational eye movements.
(Gocho et al., 2013)	Longitudinal	12 eyes with GA	Not defined	Hyporeflective clumps and GA growth	Hyporeflective clumps accompany and precede GA.
(Obata & Yanagi, 2014)	Cross-sectional	60 eyes > 50 years	2º superior and 5º temporal to the fovea	Cone density (cells/mm^2) Cone angular density (cells/deg^2) Cone spacing (μm) Regularity (%)	Cone density (in metrical units) depends on age and axial length.
(Mrejen et al., 2014)	Cross-sectional	22 eyes with SSDs and drusen	Areas with RPD and drusen between 1º and 8º from foveal center.	Cone density	Lower cone density in eyes with RPD.
(Hagag et al., 2025)	Prospective cohort study	Subset of eyes from the PINNACLE Study (iAMD)	5 horizontally overlapping captures by 2º	Cone mosaic visibility	Reduced cone mosaic visibility corresponds to areas of IZ loss seen in OCT

Legend. GA: geographic atrophy, AO: adaptive optics, NIRAF: near-infrarred autofluorescence, RPD: reticular pseudodrusen, IZ: interdigitation zone.

5.4. Limitations

Limitations of these techniques include limited availability, especially of AO-SLO and AO-OCT systems. The high cost, hardware complexity, small field of view and long intrasession times explain why these technologies are only available in research settings.(Pircher & Zawadzki, 2017) Furthermore, their research utility is further constrained by uncertain repeatability and reproducibility. (Miloudi et al., 2015)

5.5. AO Imaging modalities

5.5.1. Adaptive-optics flood illumination retinal camera (AO-FIO)

5.5.1.1. General considerations

The rtx1 retinal camera (Imagine Eyes, Orsay, France) is currently the most widely used clinical AO device. It is a hardware-based method with a Shack-Hartmann wavefront sensor and a wavefront

corrector, which includes a deformable mirror that can adjust its shape to correct for the eye's optical aberrations. It is incorporated on a flood-illumination retinal camera that uses an infrared light, providing en face images from the retina of a limited field of view (4 x 4º, approximately 1.2 x 1.2mm retinal area) within seconds, being less affected by eye movements than other imaging techniques that require longer exposure times, such as AO-SLO. The improved lateral resolution in tissue (2 μm) allows visualization of the cone mosaic from about 1 deg eccentricity. Cones of the foveal center and rods are not visible with this modality. (Akyol et al., 2021; Lombardo et al., 2012)

The final image displayed is the result of averaging 40 recorded frames, which improves contrast and image quality by reducing noise. (Cooper et al., 2011) The instrument also includes built-in software based on Voronoi analysis that provides parameters such as: cone density, spacing, regularity, and dispersion. This is calculated based on the automatic detection of cone cells within a selected region of interest, which can be assessed and manually modified by the operator. This method has shown good reproducibility and interobserver agreement, especially for cone density and spacing. (Bidaut Garnier et al., 2014; Obata & Yanagi, 2014) It should be noted that image quality can have a significant effect on quantitative parameters, so the sharpness of the photoreceptor mosaic should always be checked as a quality control. (Gale et al., 2019) An example of a fovea-centered rtx1 image with automatic cone cell recognition by the software is depicted in Figure 12.

5.5.1.2. Clinical significance

With age and disease, cone density decreases, and inter-cell spacing increases in a parallel manner, with greater affection in eyes with RPD than with only conventional drusen. (Mrejen et al., 2014) This reduced visibility of the cone mosaic may correspond to areas of IZ loss in the OCT, even when the EZ is intact, as recently shown in the PINNACLE study in eyes with iAMD. (Hagag et al., 2025) In GA, cone cells can still be quantified in foveal-sparring areas. (Querques et al., 2016)

In addition to cone quantification, other authors have focused on the visualization of small drusen to detect cases of AMD before the appearance of typical diagnostic clinical signs on color fundus

photography or OCT. Murari and colleagues describe 45% of elderly patients with apparent drusen on AO-FIO (adaptive optics flood-illumination ophthalmoscopy) who were misclassified as controls. (Murari et al., 2024) In addition, Rossi and colleagues proposed a method to further improve drusen visualization by combining overlapping AO-FIO images using a custom algorithm based on the reflectivity of drusen, which can change with the direction of gaze. (Rossi et al., 2021) In eyes with atrophy, hyporeflective clumps, probably corresponding to migrating RPE or macrophages containing RPE organelles, may precede and accompany areas of GA. (Borella et al., 2024; Gocho et al., 2013) Monthly changes in the enlargement of the GA border can also be objectified. (Gocho et al., 2013) However, the characterization of AMD biomarkers associated other than those associated with photoreceptors is beyond the scope of this review.

5.5.2. Adaptive optics transscleral flood illumination (AO-TFI)

A commercially available adaptive optics (AO) device has recently been introduced that uses transscleral flood illumination (TFI) instead of the traditional transpupillary approach (Cellularis Discovery, EyeSight, Geneva, Switzerland). (Eppenberger et al., 2022) Besides, AO-TFI is also available as an add-on to the rtx1 retinal camera (Imagine Eyes, Orsay, France). This technique is currently optimized for imaging the retinal pigment epithelium (RPE), as photoreceptor cells are more challenging to visualize with TFI, although also possible.(Mantel et al., 2022) In transpupillary illumination, light enters the eye perpendicularly to the photoreceptors, enhancing their reflectivity and often masking the underlying RPE signal. In contrast, TFI delivers light obliquely through the sclera, which reduces photoreceptor reflectance and improves the signal-to-noise ratio for visualizing the RPE beneath.(Laforest et al., 2020) Our literature search found no reports of studies analyzing photoreceptors in AMD using AO-TFI.

5.5.3. Adaptive optics scanning laser/light ophthalmoscopy (AO-SLO)

5.5.3.1. General considerations

AO-SLO uses a scanning beam of light to illuminate a small spot on the retina at a time. In its most common implementation, a confocal pinhole is used in the detection path, filtering the backscattered signal, so only the signals focused on a specific plane, covering a small field of view, are detected. Other promising imaging setups, including split detection, quadrant reflection or multi offset aperture do exist.(Kalitzeos et al., 2024; Mozaffari et al., 2018; Scoles et al., 2014) These approaches collect light laterally displaced from the optical axis and are therefore sensitive to multiply scattered light. Although confocal AO-SLO can provide better resolution images of the photoreceptor mosaic in healthy eyes, the interpretation is more challenging in the presence of pathology. This is largely because the waveguiding properties that generate confocal AO-SLO contrast vary in disease. (Chen et al., 2022; Scoles et al., 2014; Sredar et al., 2021)In these cases, split-detection may allow visualization of the inner segments usually still showing visible photoreceptors in cases where the confocal setup presents severe image deterioration due to outer segment misalignment, damage or loss.(Scoles et al., 2014)

Compared to AO-FIO, AO-SLO offers improved resolution but requires longer acquisition times. This is because multiple images must be merged to cover larger regions of interest, making the final image more susceptible to eye movements (e.g. 30 to 45 minutes have been reported to scan an area of 15°×15° to 20°×20° in both eyes). (Zhang et al., 2020) However, this approach also enables precise measurement of those movements. Currently, retinal tracking using SLO is the most accurate technique for quantifying fixational eye movements. (Reiniger et al., 2021)

5.5.3.2. Clinical significance

Rods and cones can be distinguished in vivo using AO-SLO based on their morphology, reflectance, and location. Cones are larger, exhibit directional reflectivity (waveguiding), and are densely packed in the fovea. (Scoles et al., 2014) Due to their lower reflectance and smaller size, rods are generally more difficult to visualize than cones, especially in standard confocal AO-SLO. Split-detection AO-SLO enables clear visualization of rod inner segments, even when their outer segments are not reflective,

by capturing multiply scattered light (Cunefare et al., 2016; Scoles et al., 2014) Quantitative analysis of cell spacing and packing geometry also helps differentiate rods from cones in mixed mosaics(Heitkotter et al., 2023).

In the context of AMD, changes in cone mosaic visibility seen with AO-SLO may be seen in genetically predisposed individuals before clinically visible changes.(Land et al., 2014) In early and iAMD, this technique has been used mainly to study photoreceptor and RPE changes in the presence of other biomarkers such as soft drusen, RPD and HRF. (Boretsky et al., 2012; Mrejen et al., 2014; Wang et al., 2025; Xu et al., 2017; Zhang et al., 2014a; Zhang et al., 2020) Particularly in eyes with RPD, which have lower cone density at baseline and a faster decline in the presence of both RPD and drusen compared to drusen alone, even in apparently unaffected areas. (XWang et al., 2023) Furthermore, the cone density differs with the different stages of RPD.(Xu et al., 2020) Whereas only changes in photoreceptor reflectivity were observed in Stages 1 and 2, photoreceptor loss became evident in Stage 3 RPD. (Zhang et al., 2014a) However, although less frequently, an apparent photoreceptor restoration after RPD regression has been observed, which is likely a product of a changed interaction of cone outer segments with the imaging light. An intact photoreceptor mosaic on AO-SLO and intact EZ on OCT were observed in 37% of RPD. (Zhang et al., 2020)

In GA, Shiri Zayit-Soudry et al. observed an irregular appearance of the photoreceptor mosaic and a reduced cone reflectivity, both over drusen and around areas of GA. They also noted cone spacing preservation until late in the course of GA progression.(Zayit-Soudry et al., 2013) Furthermore, Qin et al. observed an association between choriocapillaris hypoperfusion based on OCT-angiography and decreased cone density at GA borders; in their study, choriocapillaris hypoperfusion correlated more robustly than cone density with distance from GA border.(Qin et al., 2018)

Of note, many clinical AO-SLO studies to date have used confocal detection.(Wang et al., 2023; Zhang et al., 2014b) As outlined above, confocal AO-SLO relies on photoreceptor waveguiding, which can be

disrupted in disease by outer-segment misalignment or structural alteration. (Scoles et al., 2014) As a result, reduced cone visibility or apparent cone loss in confocal images may not necessarily reflect true photoreceptor cell loss, a limitation that is particularly relevant for longitudinal interpretation. Furthermore, evaluating rods could also be useful in early studies, especially in eyes with RPD, where preferential rod damage has been demonstrated.(Lim et al., 2025) Future studies incorporating alternative AO-SLO detection modes, such as split-detection or offset-aperture imaging, may help better distinguish photoreceptor dysfunction from cellular loss and improve the clinical interpretability of photoreceptor-level metrics. Accordingly, future clinical studies and trials should explicitly report the AO-SLO detection configuration used (e.g., confocal versus non-confocal), as this choice directly influences photoreceptor visibility and metrics.

5.5.3.3. Functional testing

AOSLO has also been combined with microperimetry to enable cell-resolved functional testing (Figure 13).(Harmening et al., 2014; Harmening & Sincich, 2019; Tuten et al., 2012) This approach allows for detection of visual sensitivity loss at a micron-scale resolution. Significant functional deficits were already observed in areas of cRORA and iRORA.(Ameln et al., 2024; Saßmannshausen et al., 2024) Saßmannshausen and colleagues have furthermore shown evidence of residual visual function at the margins of cRORA lesions. (Saßmannshausen et al., 2024) This may serve as a valuable biomarker in iAMD, particularly for future interventional clinical trials, addressing the clinical benefit of slowing the progression of cRORA.

5.5.4. Adaptive-optics optical coherence tomography (AO-OCT)

5.5.4.1. General considerations

Optical coherence tomography offers a distinct advantage in providing a three-dimensional representation of retinal structures with an exceptionally high axial resolution (as low as 3 µm in research prototypes) and an unparalleled sensitivity, surpassing that of all other in vivo imaging modalities in clinical settings. This sensitivity enables the detection of transparent cells, expanding

the dynamic range to detect even subtle variations in backscattered light. The enhanced axial resolution, coupled with the improved lateral resolution achieved through the incorporation of AO facilitates the investigation of the distinct parts of the photoreceptor cells. Furthermore, it is possible to differentiate between the three distinct cone types based on outer segment length dynamics with differential illumination. (Miller & Kurokawa, 2020) Additionally, the differentiation between planes, such as those located above or below drusen or RPD, can be achieved. (Meadway et al., 2014) However, it remains difficult to distinguish between true photoreceptor loss and mere orientation changes that affect their reflectance properties in areas where typical retinal architecture is compromised, such as over drusen or near geographic atrophy.(Reumueller et al., 2019)

5.5.4.2. Clinical significance

Although very promising in the research setting, the clinical applications of AO-OCT are still minimal due to the low availability of the technique and the long acquisition times that are still required, making acquisition difficult and very sensitive to eye movements, especially in AMD patients with fixation instability.(Pircher & Zawadzki, 2017) In the largest clinical study of AMD patients, Reumueller and colleagues report an exclusion rate of 35% of images, primarily due to artefacts associated with eye movements.(Reumueller et al., 2019)

5.5.4.3. Functional testing

Beyond visual psychophysics and electroretinography, retinal function can also be objectively assessed using the optoretinogram (ORG), a promising technique that detects light-evoked structural changes in photoreceptor outer segments.(Hillmann et al., 2016; Pandiyan et al., 2020) AO-OCT-based ORG enables functional assessment at the subcellular level. Although this technique is still in the experimental stage and no studies have been published in AMD to date, the accuracy and objectivity it provides could be of great value in the future.

The clinical applicability of AO-OCT-based ORG is currently limited by the small field of view and complexity inherent to AO systems. Recently, more accessible research prototypes – such as the so-called coarse-scale ORG systems – have been introduced.(Jiang et al., 2022) These systems operate without AO and offer improved usability while showing good agreement with AO-based measurements and may be useful in clinical trials in the near future.

6. Intrinsic value of the different photoreceptor parameters

Both nGA and cRORA reflect outer retinal damage and are among the strongest predictors of progression to late-stage GA. While they are event-based outcomes, this does not necessarily limit their utility. Recent data indicate that sample size requirements for detecting treatment effects using nGA may be comparable to those for continuous measures such as EZ loss (Wu et al., 2025a) Furthermore, CAM Report 7 demonstrated international consensus on the onset of end-stage atrophic AMD constitutes an acceptable clinical trial endpoint. Nevertheless, continuous outcome measures may still offer complementary advantages, including greater sensitivity for detecting subtle therapeutic effects, and could be especially valuable in interventional trials of earlier AMD stages. (Flores et al., 2023; Guymer et al., 2025b; Wu et al., 2023) They reflect different biological components such as photoreceptor nuclei (ONL), segments and interfaces (EZ, IZ, ELM), or metabolic status (rEZR). ONL thickness appears to be a structurally robust measure and has been adopted in clinical trials and predictive models, particularly in GA. (Pfau et al., 2022; Pfau et al., 2020a) EZ integrity and EZ–RPE thickness are currently the most established structural endpoints and have shown sensitivity to disease progression and treatment effects, although they incorporate multiple sublayers that may limit biological specificity. (Ehlers et al., 2025; Schmidt-Erfurth et al., 2025) In comparative analyses, EZ-based metrics have tended to demonstrate greater sensitivity and lower sample size requirements for detecting statistically significant change than ELM- or RPE-based loss measures. (Wu et al., 2025a) rEZR may also serve as an early indicator of photoreceptor dysfunction,

reflecting reductions and reorganization of the mitochondrial content and overall photoreceptor metabolism. (Thiele et al., 2020) However, its clinical applicability remains constrained by reliance on raw OCT data, and large longitudinal studies comparing reflectivity to thickness metrics are still lacking. More granular measures, including IS/OS thickness and IZ integrity, may offer additional insight into differential photoreceptor vulnerability, though further standardization and validation are needed.

Although AO imaging offers detailed insights into individual cone photoreceptors, its clinical use remains limited. Some studies have shown correlations between OCT-based metrics and cone density measured with AO, though primarily in healthy eyes. (Domdei et al., 2023; Li et al., 2023) Larger datasets that include pathologic eyes are needed to validate these findings for broader clinical application.

Reported repeatability and smallest detectable change values for photoreceptor-based metrics are summarized in Table S6; however, these estimates should be interpreted cautiously due to substantial heterogeneity in study populations, imaging protocols, analytic definitions, and statistical reporting.

7. Current limitations and future directions

Differences in imaging protocols, anatomical definitions, and methods to obtain photoreceptor-based parameters make comparisons between studies complex, limiting the extrapolation of results. Additionally, the staging of AMD varies across studies, and the distinction between pathological and normal aging changes is often not addressed in the literature.

The implementation of DL-based methods trained with large datasets of OCT scans can efficiently provide information mainly on continuous photoreceptor-based parameters from large datasets. This has recently become available in some OCT platforms for use in both research and clinical settings. However, cutoff points for baseline photoreceptor degeneration should be defined as inclusion

criteria in clinical trials. Additionally, EZ and ELM disruption maps should be adjusted for the presence of RPD and drusen as they can result in artifacts of the OCT image.

The success of DL approaches depends heavily on access to large, high-quality datasets. However, none of the existing open-access databases currently fulfill the FAIR (Findable, Accessible, Interoperable, Reusable) data principles, as highlighted in a recent report by the Ryan Initiative for Macular Research (RIMR) consortium.(Gim et al., 2025) To advance the field, researchers must build FAIR-compliant datasets following guidelines. This is crucial to support DL applications in image classification, feature segmentation, biomarker discovery, and prediction of treatment outcomes. The RIMR consortium is a promising initiative in this regard, bringing together global collaborators to contribute imaging data and facilitate consistent study design and validation across multiple datasets.

Improvements in lateral resolution can be efficiently achieved by incorporating AO into existing imaging modalities, allowing structural and functional information to be obtained from small clusters or even individual photoreceptor cells. This may allow small changes in sensitivity to be detected using stimuli that are considerably smaller with AOSLO-microperimetry than with conventional microperimetry. (Ameln et al., 2024; Domdei et al., 2019, 2021; Harmening et al., 2014; Harmening & Sincich, 2019; Saßmannshausen et al., 2024; Tuten et al., 2012)

Limitations of AO technology include its significant space requirements and cost, which pose a significant challenge in terms of its practical implementation in the clinical setting, especially for AO-OCT and AO-SLO.(Pircher & Zawadzki, 2017) Faster scanning protocols with a larger field of view, efficient eye-tracking systems, and less hardware-complicated, such as sensorless or computational AO devices, would overcome the current limitations.

A key future direction might be the development of a novel AMD classification system that incorporates photoreceptor-based structural metrics to enable more granular monitoring of disease progression. Current AMD classification systems (e.g., Beckman Classification (Ferris et al., 2013)) still

rely on the assessment of CFP, focusing largely on drusen—historically considered the hallmark of AMD. However, advances in imaging and image analysis now allow us to directly assess the actual site of disease impairment, such as photoreceptors, with greater sensitivity. This opens new opportunities to more accurately characterize disease progression and to evaluate treatment outcomes in clinical trials. A revised severity scale, ideally based on longitudinal multimodal imaging data, should be developed to better estimate the risk of vision loss. Importantly, there is a need for consensus on the retinal zones where measurements are most predictive of functional outcomes. For iAMD trials, regulatory bodies must agree to earlier structural endpoints, such as validated biomarkers of photoreceptor integrity, rather than requiring progression to GA followed by monitoring of lesion growth.

8. Conclusions

Photoreceptor characteristics are promising biomarkers for early damage in AMD and may help to detect minor changes in progression or treatment outcomes in every stage of the disease. OCT-based parameters are the most widely reported because of the high availability of this technology. However, there is still a lack of standardized protocols for measuring many of these photoreceptor-based parameters, resulting in high heterogeneity among studies. This heterogeneity stems not only from methodological differences but also from inconsistencies in definitions. Different studies may use the same terminology while measuring fundamentally different aspects of photoreceptor integrity.

Researchers have developed several custom, manual, semi-automated and fully automated methods to analyze the first (ELM), second (EZ) and third (IZ) outer retinal bands. The parameters integrity, thickness and reflectivity have been described using a variety of methods and segmentation boundaries, including computational methods that can analyze large datasets. These methods have

already been demonstrated to detect significant changes in the analysis of treatment outcomes of antiangiogenic and complement inhibitor therapy.

Furthermore, incorporating AO technology can enhance the lateral resolution of existing imaging modalities up to 2 μm, which is enough to detect individual photoreceptor cells. AO-FIO, AO-SLO, and AO-OCT provide an accurate image of the cone mosaic from which parameters such as cone density, inter-cell distance, or regularity can be extracted. This enables the detection of small changes at the cellular level, which may be of utmost importance when assessing results in clinical trials following cell-based interventions or gene therapy. Although AO-FIO and AO-TFI systems are now commercially available, clinical adoption remains limited.

Given the significant discrepancies in segmentation boundaries, nomenclature, methodologies, and imaging modalities described in the literature, there is an urgent need to establish consensus-based protocols and normative datasets. The CAM are a series of international expert meetings focused on standardizing the definition and classification of atrophy in AMD using multimodal imaging, particularly OCT. These efforts aim to establish precise definition and reading criteria that support consistent interpretation and the potential use of photoreceptor-based biomarkers as surrogate endpoints in early intervention trials. The RIMR initiative complements this by enabling researchers to upload and access shared datasets, facilitating the application of standardized analysis methods across diverse populations. In parallel, ongoing large-scale natural history studies—such as MACUSTAR, HONU, PINNACLE, and ALSTAR—are expected to generate critical longitudinal data that will further support the development of robust, reproducible, and clinically meaningful photoreceptor metrics for both research and regulatory use.

REFERENCES

1463 Abraham, J.R., Jaffe, G.J., Kaiser, P.K., Chiu, S.J., Loo, J., Farsiu, S., Bouckaert, L., Karageozian, V.,
1464 Sarayba, M., Srivastava, S.K. and Ehlers, J.P., 2022. Impact of baseline quantitative OCT features on
1465 response to risuteganib for the treatment of dry age-related macular degeneration: the importance
1466 of outer retinal integrity. Ophthalmology Retina, 6(11), pp.1019–1027.
1467 https://doi.org/10.1016/j.oret.2022.05.002

1468 Akyol, E., Hagag, A.M., Sivaprasad, S. and Lotery, A.J., 2021. Adaptive optics: principles and
1469 applications in ophthalmology. Eye, 35(1), pp.244–264. https://doi.org/10.1038/s41433-020-01286-z

1470 Amarasekera, S., Samanta, A., Jhingan, M., Arora, S., Singh, S. and Tucci, D., 2022. Optical coherence
1471 tomography predictors of progression of non-exudative age-related macular degeneration to
1472 advanced atrophic and exudative disease. Graefe's Archive for Clinical and Experimental
1473 Ophthalmology, 260(3), pp.737–746. https://doi.org/10.1007/s00417-021-05419-2

1474 Ameln, J., Saßmannshausen, M., von der Emde, L., Carmichael-Martins, A., Holz, F.G., Ach, T. and
1475 Harmening, W.M., 2024. Assessment of local sensitivity in incomplete retinal pigment epithelium and
1476 outer retinal atrophy (iRORA) lesions in intermediate age-related macular degeneration (iAMD). BMJ
1477 Open Ophthalmology, 9(1), p.e001638. https://doi.org/10.1136/bmjophth-2024-001638

1478 Ameln, J., Witten, J.L., Gutnikov, A., Lukyanova, V., Holz, F.G. and Harmening, W.M., 2025. In vivo
1479 cone photoreceptor topography of the human foveola. Investigative Ophthalmology & Visual
1480 Science, 66(11), p.13. https://doi.org/10.1167/iovs.66.11.13

1481 Arrigo, A., Aragona, E., Battaglia, O., Saladino, A., Amato, A., Borghesan, F., Pina, A., Calcagno, F.,
1482 Hassan Farah, R., Bandello, F. and Battaglia Parodi, M., 2021. Outer retinal tubulation formation and
1483 clinical course of advanced age-related macular degeneration. Scientific Reports, 11(1), pp.1–12.
1484 https://doi.org/10.1038/s41598-021-94310-5

1485 Bell, J., Whitney, J., Cetin, H., Le, T., Cardwell, N., Srivasatava, S.K. and Ehlers, J.P., 2024. Validation of
1486 inter-reader agreement and consistency for quantification of ellipsoid zone integrity and sub-RPE
1487 compartmental features across retinal diseases. Diagnostics, 14(21), p.2395.
1488 https://doi.org/10.3390/diagnostics14212395

1489 Berlin, A., Matney, E., Jones, S.G., Clark, M.E., Swain, T.A., McGwin, G., Martindale, R.M., Sloan, K.R.,
1490 Owsley, C. and Curcio, C.A., 2023. Discernibility of the interdigitation zone (IZ), a potential optical
1491 coherence tomography (OCT) biomarker for visual dysfunction in aging. Current Eye Research,
1492 48(11), pp.1050–1056. https://doi.org/10.1080/02713683.2023.2240547

1493 Bhutto, I. and Lutty, G., 2012. Understanding age-related macular degeneration (AMD): relationships
1494 between the photoreceptor/retinal pigment epithelium/Bruch's membrane/choriocapillaris complex.
1495 Molecular Aspects of Medicine, 33(4), pp.295–317. https://doi.org/10.1016/j.mam.2012.04.005

1496 Bidaut Garnier, M., Flores, M., Debellemanière, G., Puyraveau, M., Tumahai, P., Meillat, M., Schwartz,
1497 C., Montard, M., Delbosc, B. and Saleh, M., 2014. Reliability of cone counts using an adaptive optics
1498 retinal camera. Clinical and Experimental Ophthalmology, 42(9), pp.833–840.
1499 https://doi.org/10.1111/ceo.12356

1500 BioTherapeutics, S., 2025. Stealth BioTherapeutics announces achievement of 50% enrollment target
1501 in Phase 3 ReNEW study of elamipretide in patients with dry age-related macular degeneration.
1502 Available at: https://stealthbt.com/stealth-biotherapeutics-announces-achievement-of-50-
1503 enrollment-target-in-phase-3-renew-study-of-elamipretide-in-patients-with-dry-age-related-macular-
1504 degeneration/ (Accessed: May 2025).

1505 Birner, K., Reiter, G.S., Steiner, I., Deák, G., Mohamed, H., Schürer-Waldheim, S., Gumpinger, M.,
1506 Bogunović, H. and Schmidt-Erfurth, U., 2024. Topographic and quantitative correlation of structure

and function using deep learning in subclinical biomarkers of intermediate age-related macular degeneration. Scientific Reports, 14(1), p.28165. https://doi.org/10.1038/s41598-024-72522-9

Birner, K., Reiter, G.S., Steiner, I., Zarghami, A., Sadeghipour, A., Schürer-Waldheim, S., Gumpinger, M., Bogunovic, H. and Schmidt-Erfurth, U., 2025. Structure-function correlation of deep-learning quantified ellipsoid zone and retinal pigment epithelium loss and microperimetry in geographic atrophy. Investigative Ophthalmology and Visual Science, 66(3), p.26. https://doi.org/10.1167/iovs.66.3.26

Blair, J.P.M., Guymer, R.H., Krzemińska-Ściga, A., De Zanet, S., Ciller, C., Apostolopoulos, S. and Wu, Z., 2025. Geographic atrophy structure-function relationships based on loss of OCT outer retinal bands and fundus autofluorescence. Ophthalmology Science, p.101035. https://doi.org/10.1016/j.xops.2025.101035

Bonnin, S., Gocho, K., Norberg, N., Gofas, E., Lejoyeux, R., Chaumette, C., Grieve, K., Couturier, A. and Paques, M., 2024. Spatially resolved imaging of human macular capillaries using adaptive optics-enhanced optical coherence tomography angiography. Scientific Reports, 14(1), p.15540. https://doi.org/10.1038/s41598-024-65534-y

Borella, Y., Danielsen, N., Markle, E.M., Snyder, V.C., Lee, D.M.W., Zhang, M., Eller, A.W., Chhablani, J., Paques, M. and Rossi, E.A., 2024. Are the hypo-reflective clumps associated with age-related macular degeneration in adaptive optics ophthalmoscopy autofluorescent? Investigative Ophthalmology and Visual Science, 65(10), p.28. https://doi.org/10.1167/iovs.65.10.28

Boretsky, A., Khan, F., Burnett, G., Hammer, D.X., Ferguson, R.D., van Kuijk, F. and Motamedi, M., 2012. In vivo imaging of photoreceptor disruption associated with age-related macular degeneration: a pilot study. Lasers in Surgery and Medicine, 44(8), pp.603–610. https://doi.org/10.1002/lsm.22070

Borrelli, E., Abdelfattah, N.S., Uji, A., Nittala, M.G., Boyer, D.S. and Sadda, S.V.R., 2017. Postreceptor neuronal loss in intermediate age-related macular degeneration. American Journal of Ophthalmology, 181, pp.1–11. https://doi.org/j.ajo.2017.06.005

Borrelli, E., Barresi, C., Lari, G., Berni, A., Battista, M., Reibaldi, M., Cascavilla, M.L. and Bandello, F., 2023. Capturing the transition from intermediate to neovascular AMD: longitudinal inner retinal thinning and factors associated with neuronal loss. Investigative Ophthalmology and Visual Science, 64(4). https://doi.org/10.1167/iovs.64.4.21

Boyer, D., Hu, A., Warrow, D., Xavier, S., Gonzalez, V., Lad, E., Rosen, R.B., Do, D., Schneiderman, T., Ho, A., Munk, M.R., Jaffe, G., Tedford, S.E., Croissant, C.L., Walker, M., Rückert, R. and Tedford, C.E., 2024. LIGHTSITE III: 13-month efficacy and safety evaluation of multiwavelength photobiomodulation in nonexudative (dry) age-related macular degeneration using the Lumithera Valeda light delivery system. Retina, 44(3), pp.487–497. https://doi.org/10.1097/IAE.0000000000003980

Bringmann, A., Pannicke, T., Grosche, J., Francke, M., Wiedemann, P., Skatchkov, S.N., Osborne, N.N. and Reichenbach, A., 2006. Müller cells in the healthy and diseased retina. Progress in Retinal and Eye Research, 25, pp.397–424. https://doi.org/10.1016/j.preteyeres.2006.05.003

Burns, S.A., Elsner, A.E., Sapoznik, K.A., Warner, R.L. and Gast, T.J., 2019. Adaptive optics imaging of the human retina. Progress in Retinal and Eye Research, 68, pp.1–30. https://doi.org/10.1016/j.preteyeres.2018.08.002

Carl Zeiss Meditec Inc., n.d. ZEISS Cirrus 6000. Technical specifications. https://www.zeiss.com/meditec/en/products/optical-coherence-tomography-devices/cirrus-6000-performance-oct/specifications.html

Cedro, L., Hoffmann, L., Hatz, K., 2023. Geographic atrophy in AMD: Prognostic factors based on long-term follow-up. Ophthalmic Res. 66, 791–800. https://doi.org/10.1159/000527786

1552 Chandak, S., Gurudas, S., Pakeer, R.M., Kazantzis, D., Ghanchi, F., Grabowska, A., Talks, S.J., Pearce, I.,
1553 McKibbin, M., Kotagiri, A., Menon, G., Burton, B.J., Gale, R., Sivaprasad, S., 2025. Factors associated
1554 with achieving various visual acuity outcomes during loading doses of aflibercept 2 mg for treatment
1555 naïve exudative age-related macular degeneration: PRECISE Study Report 7. Eye (Lond.).
1556 https://doi.org/10.1038/s41433-025-03687-4

1557 Chen, M., Jiang, Y.Y., Gee, J.C., Brainard, D.H., Morgan, J.I.W., 2022. Automated assessment of
1558 photoreceptor visibility in adaptive optics split-detection images using edge detection. Transl. Vis. Sci.
1559 Technol. 11, 25. https://doi.org/10.1167/tvst.11.5.25

1560 Chew, E.Y., Clemons, T.E., Agrón, E., Domalpally, A., Keenan, T.D.L., Vitale, S., Weber, C., Smith, D.C.,
1561 Christen, W., AREDS2 Research Group, 2022. Long-term outcomes of adding lutein/zeaxanthin and ω-
1562 3 fatty acids to the AREDS supplements on age-related macular degeneration progression: AREDS2
1563 Report 28. JAMA Ophthalmol. 140, 692–698. https://doi.org/10.1001/jamaophthalmol.2022.1849

1564 Chew, E.Y., Gillies, M., Jaffe, G.J., Gaudric, A., Egan, C., Constable, I., Clemons, T., Aaberg, T., Manning,
1565 D.C., Hohman, T.C., Bird, A., Friedlander, M., MacTel CNTF NTMT-03 Research Investigators, 2025.
1566 Cell-based ciliary neurotrophic factor therapy for macular telangiectasia type 2. NEJM Evid. 4,
1567 EVIDoa2400481. https://doi.org/10.1056/EVIDoa2400481

1568 Chhablani, J., Kim, J., Freeman, W., Kozak, I., Wang, H., Cheng, L., 2013. Predictors of visual outcome
1569 in eyes with choroidal neovascularization secondary to age-related macular degeneration treated
1570 with intravitreal bevacizumab monotherapy. Int. J. Ophthalmol. 6, 62–66.
1571 https://doi.org/10.3980/j.issn.2222-3959.2013.01.14

1572 Chua, S.Y.L., Dhillon, B., Aslam, T., Balaskas, K., Yang, Q., Keane, P.A., Tufail, A., Reisman, C., Foster, P.J.,
1573 Patel, P.J., UK Biobank Eye and Vision Consortium, 2019. Associations with photoreceptor thickness
1574 measures in the UK Biobank. Sci. Rep. 9, 19440. https://doi.org/10.1038/s41598-019-55937-9

1575 Chui, T.Y.P., Migacz, J.V., Muncharaz Duran, L., Haq, A., Otero-Marquez, O., Dubra, A., Rosen, R.B.,
1576 2024. Improving cone identification using merged non-confocal quadrant-detection adaptive optics
1577 scanning light ophthalmoscope images. Biomed. Opt. Express 15, 6117–6135.
1578 https://doi.org/10.1364/BOE.513787

1579 Chui, T.Y.P., Song, H., Clark, C.A., Papay, J.A., Burns, S.A., Elsner, A.E., 2012. Cone photoreceptor
1580 packing density and the outer nuclear layer thickness in healthy subjects. Invest. Ophthalmol. Vis.
1581 Sci. 53, 3545–3553. https://doi.org/10.1167/iovs.12-9592

1582 Cideciyan, A.V., Jacobson, S.G., Roman, A.J., Sumaroka, A., Wu, V., Charng, J., Lisi, B., Swider, M.,
1583 Aguirre, G.D., Beltran, W.A., 2020. Rod function deficit in retained photoreceptors of patients with
1584 class B Rhodopsin mutations. Sci. Rep. 10, 12552. https://doi.org/10.1038/s41598-020-69428-6

1585 Cooper, R.F., Dubis, A.M., Pavaskar, A., Rha, J., Dubra, A., Carroll, J., 2011. Spatial and temporal
1586 variation of rod photoreceptor reflectance in the human retina. Biomed. Opt. Express 2, 2577–2589.
1587 https://doi.org/10.1364/BOE.2.002577

1588 Coscas, F., Coscas, G., Lupidi, M., Dirani, A., Srour, M., Semoun, O., Français, C., Souied, E.H., 2015.
1589 Restoration of outer retinal layers after aflibercept therapy in exudative AMD: Prognostic value.
1590 Invest. Ophthalmol. Vis. Sci. 56, 4129–4134. https://doi.org/10.1167/iovs.15-16506

1591 Coulibaly, L.M., Reiter, G.S., Fuchs, P., Lachinov, D., Leingang, O., Vogl, W.D., Bogunovic, H., Schmidt-
1592 Erfurth, U., 2023. Progression dynamics of early versus later stage atrophic lesions in nonneovascular
1593 age-related macular degeneration using quantitative OCT biomarker segmentation. Ophthalmol.
1594 Retin. 7, 762–770. https://doi.org/10.1016/j.oret.2023.04.009

1595 Cozzi, M., Casaluci, M., Ruggi, G., Airaldi, M., Romano, F., Bertoni, A., Green-Gomez, M., Nolan, J.M.,
1596 Staurenghi, G., Invernizzi, A., 2024. In vivo correlation between macular pigment optical volume and
1597 retinal layers thickness. Invest. Ophthalmol. Vis. Sci. 65, 23. https://doi.org/10.1167/iovs.65.8.23

1598 Cuenca, N., Fernández-Sánchez, L., Sauvé, Y., Segura, F.J., Martínez-Navarrete, G., Tamarit, J.M.,
1599 Fuentes-Broto, L., Sanchez-Cano, A., Pinilla, I., 2014. Correlation between SD-OCT,
1600 immunocytochemistry and functional findings in an animal model of retinal degeneration. Front.
1601 Neuroanat. 8, 151. https://doi.org/10.3389/fnana.2014.00151

1602 Cuenca, N., Ortuño-Lizarán, I., Pinilla, I., 2018. Cellular characterization of OCT and outer retinal
1603 bands using specific immunohistochemistry markers and clinical implications. Ophthalmology 125,
1604 407–422. https://doi.org/10.1016/j.ophtha.2017.09.017

1605 Cuenca, N., Ortuño-Lizarán, I., Sánchez-Sáez, X., Kutsyr, O., Albertos-Arranz, H., Fernández-Sánchez,
1606 L., Martínez-Gil, N., Noailles, A., López-Garrido, J.A., López-Gálvez, M., Lax, P., Maneu, V., Pinilla, I.,
1607 2020. Interpretation of OCT and OCTA images from a histological approach: Clinical and experimental
1608 implications. Prog. Retin. Eye Res. 77, 100828. https://doi.org/10.1016/j.preteyeres.2020.100828

1609 Cunefare, D., Cooper, R.F., Higgins, B., Katz, D.F., Dubra, A., Carroll, J., Farsiu, S., 2016. Automatic
1610 detection of cone photoreceptors in split detector adaptive optics scanning light ophthalmoscope
1611 images. Biomed. Opt. Express 7, 2036–2050. https://doi.org/10.1364/BOE.7.002036

1612 Curcio, C.A., Kar, D., Owsley, C., Sloan, K.R., Ach, T., 2024. Age-related macular degeneration, a
1613 mathematically tractable disease. Invest. Ophthalmol. Vis. Sci. 65, 4.
1614 https://doi.org/10.1167/iovs.65.3.4

1615 Curcio, C.A., Medeiros, N.E., Millican, C.L., 1996. Photoreceptor loss in age-related macular
1616 degeneration. Invest. Ophthalmol. Vis. Sci. 37, 1236–1249.
1617 https://pubmed.ncbi.nlm.nih.gov/8641827

1618 Curcio, C.A., Millican, C.L., Allen, K.A., Kalina, R.E., 1993. Aging of the human photoreceptor mosaic:
1619 evidence for selective vulnerability of rods in central retina. Invest. Ophthalmol. Vis. Sci. 34, 3278–
1620 3296. https://pubmed.ncbi.nlm.nih.gov/8258514

1621 Dolz-Marco, R., Balaratnasingam, C., Messinger, J.D., Li, M., Ferrara, D., Freund, K.B., Curcio, C.A.,
1622 2018. The border of macular atrophy in age-related macular degeneration: a clinicopathologic
1623 correlation. Am. J. Ophthalmol. 193, 166–177. https://doi.org/10.1016/j.ajo.2018.06.009

1624 Domdei, N., Ameln, J., Gutnikov, A., Witten, J.L., Holz, F.G., Wahl, S., Harmening, W.M., 2023. Cone
1625 density is correlated to outer segment length and retinal thickness in the human foveola. Invest.
1626 Ophthalmol. Vis. Sci. 64, 11. https://doi.org/10.1167/iovs.64.15.11

1627 Domdei, N., Linden, M., Reiniger, J.L., Holz, F.G., Harmening, W.M., 2019. Eye tracking-based
1628 estimation and compensation of chromatic offsets for multi-wavelength retinal microstimulation with
1629 foveal cone precision. Biomed. Opt. Express 10, 4126–4142. https://doi.org/10.1364/BOE.10.004126

1630 Domdei, N., Reiniger, J.L., Holz, F.G., Harmening, W.M., 2021. The relationship between visual
1631 sensitivity and eccentricity, cone density and outer segment length in the human foveola. Invest.
1632 Ophthalmol. Vis. Sci. 62, 31. https://doi.org/10.1167/iovs.62.9.31

1633 Drasdo, N., Millican, C.L., Katholi, C.R., Curcio, C.A., 2007. The length of Henle fibers in the human
1634 retina and a model of ganglion receptive field density in the visual field. Invest. Ophthalmol. Vis. Sci.
1635 47, 2901–2911. https://doi.org/10.1167/iovs.06-1212

1636 Drexler, W., 2004. Ultrahigh-resolution optical coherence tomography. J. Biomed. Opt. 9, 47–74.
1637 https://doi.org/10.1117/1.1629677

1638 Drexler, W., Fujimoto, J., 2008. State-of-the-art retinal optical coherence tomography. Prog. Retin. Eye
1639 Res. 27, 45–88. https://doi.org/10.1016/j.preteyeres.2007.07.005

1640 Edwards, M., Lutty, G.A., 2021. Bruch's membrane and the choroid in age-related macular
1641 degeneration. Adv. Exp. Med. Biol. 1256, 89–119. https://doi.org/10.1007/978-3-030-59925-3_5

1642 Edwards, M.M., McLeod, D.S., Bhutto, I.A., Grebe, R., Duffy, M., Lutty, G.A., 2017. Subretinal glial
1643 membranes in eyes with geographic atrophy. Invest. Ophthalmol. Vis. Sci. 58, 1352–1367.
1644 https://doi.org/10.1167/iovs.17-21458

1645 Ehlers, J.P., Hu, A., Boyer, D., Cousins, S.W., Waheed, N.K., Rosenfeld, P.J., Brown, D., Kaiser, P.K.,
1646 Abbruscato, A., Gao, G., Heier, J., ReCLAIM-2 (SPIAM-202) Study Investigators, 2025. ReCLAIM-2: A
1647 randomized phase II clinical trial evaluating elamipretide in age-related macular degeneration,
1648 geographic atrophy growth, visual function, and ellipsoid zone preservation. Ophthalmol. Sci. 5,
1649 100628. https://doi.org/10.1016/j.xops.2024.100628

1650 Ehlers, J.P., Lunasco, L.M., Yordi, S., Cetin, H., Le, T.K., Sarici, K., Kaiser, P.K., Khanani, A.M., Talcott,
1651 K.E., Hu, J., Meng, X., Srivastava, S.K., 2024. Compartmental exudative dynamics in neovascular age-
1652 related macular degeneration: Volumetric outcomes and impact of volatility in a phase III clinical
1653 trial. Ophthalmol. Retin. 8, 765–777. https://doi.org/10.1016/j.oret.2023.03.009

1654 Ehlers, J.P., Patel, N., Kaiser, P.K., Heier, J.S., Brown, D.M., Meng, X., Reese, J., Lunasco, L., Le, T.K., Hu,
1655 M., Srivastava, S.K., 2022. The association of fluid volatility with subretinal hyperreflective material
1656 and ellipsoid zone integrity in neovascular AMD. Invest. Ophthalmol. Vis. Sci. 63, 17.
1657 https://doi.org/10.1167/iovs.63.6.17

1658 Ehlers, J.P., Zahid, R., Kaiser, P.K., Heier, J.S., Brown, D.M., Meng, X., Reese, J., Le, T.K., Lunasco, L., Hu,
1659 M., Srivastava, S.K., 2021. Longitudinal assessment of ellipsoid zone integrity, subretinal
1660 hyperreflective material, and subretinal pigment epithelium disease in neovascular age-related
1661 macular degeneration. Ophthalmol. Retin. 5, 1204–1213. https://doi.org/10.1016/j.oret.2021.05.010

1662 Eppenberger, L.S., Mohanna, S., Pfaeffli, O., Bachmann, L.M., Thiel, M.A., Schmid, M.K., 2022. First
1663 clinic experiences of transscleral optical imaging to study retinal pigment epithelium and

photoreceptor cells. *Invest. Ophthalmol. Vis. Sci.* 63, 4460 – F0139. https://iovs.arvojournals.org/article.aspx?articleid=2782589

Etheridge, T., Liu, Z., Nalbandyan, M., Cleland, S., Blodi, B.A., Mares, J.A., Bailey, S., Wallace, R., Gehrs, K., Tinker, L.F., Gangnon, R., Domalpally, A., CAREDS2 Research Study Group, 2021. Association of macular thickness with age and age-related macular degeneration in the Carotenoids in Age-Related Eye Disease Study 2 (CAREDS2), an ancillary study of the Women's Health Initiative. *Transl. Vis. Sci. Technol.* 10, 39. https://doi.org/10.1167/tvst.10.2.39

Farinha, C., Silva, A.L., Coimbra, R., Nunes, S., Cachulo, M.L., Marques, J.P., Pires, I., Cunha-Vaz, J., Silva, R., 2021. Retinal layer thicknesses and neurodegeneration in early age-related macular degeneration: insights from the Coimbra Eye Study. *Graefe's Arch. Clin. Exp. Ophthalmol.* 259, 2545–2557. https://doi.org/10.1007/s00417-021-05184-2

Fasih-Ahmad, S., Wang, Z., Mishra, Z., Vatanatham, C., Clark, M.E., Swain, T.A., Curcio, C.A., Owsley, C., Sadda, S.V.R., Hu, Z.J., 2024. Potential structural biomarkers in 3D images validated by the first functional biomarker for early age-related macular degeneration – ALSTAR2 baseline. *Invest. Ophthalmol. Vis. Sci.* 65. https://doi.org/10.1167/iovs.65.2.13

Ferrara, D., Silver, R.E., Louzada, R.N., Novais, E.A., Collins, G.K., Seddon, J.M., 2017. Optical coherence tomography features preceding the onset of advanced age-related macular degeneration. *Invest. Ophthalmol. Vis. Sci.* 58, 3519–3529. https://doi.org/10.1167/iovs.17-21699

Ferris, F.L., Wilkinson, C.P., Bird, A., Chakravarthy, U., Chew, E., Csaky, K., Sadda, S.R., 2013. Clinical classification of age-related macular degeneration. Ophthalmology 120, 844–851. https://doi.org/10.1016/j.ophtha.2012.10.036

Finger, R.P., Schmitz-Valckenberg, S., Schmid, M., Rubin, G.S., Dunbar, H., Tufail, A., Crabb, D.P., Binns, A., Sánchez, C.I., Margaron, P., Normand, G., Durbin, M.K., Luhmann, U.F.O., Zamiri, P., Cunha-Vaz, J.,

1687 Asmus, F., Holz, F.G., 2019. MACUSTAR: Development and clinical validation of functional, structural,
1688 and patient-reported endpoints in intermediate age-related macular degeneration. Ophthalmologica
1689 241, 61–72. https://doi.org/10.1159/000493980

1690 Flores, R., Fradinho, A.C., Pereira, R.S., Mendes, J.M., Seabra, M.C., Tenreiro, S., Carneiro, Â., 2023.
1691 Identifying imaging predictors of intermediate age-related macular degeneration progression. Transl.
1692 Vis. Sci. Technol. 12, 22. https://doi.org/10.1167/tvst.12.7.22

1693 Gale, M.J., Harman, G.A., Chen, J., Pennesi, M.E., 2019. Repeatability of adaptive optics automated
1694 cone measurements in subjects with retinitis pigmentosa and novel metrics for assessment of image
1695 quality. Transl. Vis. Sci. Technol. 8, 1–9. https://doi.org/10.1167/tvst.8.3.24

1696 Gambril, J.A., Sloan, K.R., Swain, T.A., Huisingh, C., Zarubina, A.V., Messinger, J.D., Ach, T., Curcio, C.A.,
1697 2019. Quantifying retinal pigment epithelium dysmorphia and loss of histologic autofluorescence in
1698 age-related macular degeneration. Invest. Ophthalmol. Vis. Sci. 60, 2481–2493.
1699 https://doi.org/10.1167/iovs.18-26044

1700 Gao, W., Cense, B., Zhang, Y., Jonnal, R.S., Miller, D.T., 2008. Measuring retinal contributions to the
1701 optical Stiles-Crawford effect with optical coherence tomography. Opt. Express 16, 6486–6501.
1702 https://doi.org/10.1364/OE.16.006486

1703 Garzone, D., Terheyden, J.H., Morelle, O., Wintergerst, M.W.M., Saßmannshausen, M., Schmitz-
1704 Valckenberg, S., Pfau, M., Thiele, S., Poor, S., Leal, S., Holz, F.G., Finger, R.P., Agostini, H., Altay, L., Atia,
1705 R., Bandello, F., Basile, P.G., Behning, C., Belmouhand, M., … Zakaria, N., 2022. Comparability of
1706 automated drusen volume measurements in age-related macular degeneration: a MACUSTAR study
1707 report. Sci. Rep. 12, 1–10. https://doi.org/10.1038/s41598-022-15757-6

1708 Gim, N., Ferguson, A., Blazes, M., Soundarajan, S., Gasimova, A., Jiang, Y., Sánchez, C.I., Zalunardo, L.,
1709 Corradetti, G., Elze, T., Honda, N., Waheed, N.K., Cairns, A.M., Canto-Soler, M.V., Domalpally, A.,

1710 Durbin, M., Ferrara, D., Hu, J., Nair, P., … Lee, C.S., 2025. Publicly available imaging datasets for age-
1711 related macular degeneration: Evaluation according to the Findable, Accessible, Interoperable,
1712 Reusable (FAIR) principles. Exp. Eye Res. 255, 110342. https://doi.org/10.1016/j.exer.2023.110342

1713 Gin, T.J., Wu, Z., Chew, S.K.H., Guymer, R.H., Luu, C.D., 2017. Quantitative analysis of the ellipsoid
1714 zone intensity in phenotypic variations of intermediate age-related macular degeneration. Invest.
1715 Ophthalmol. Vis. Sci. 58, 2079–2086. https://doi.org/10.1167/iovs.16-20913

1716 Giocanti-Auregan, A., Tadayoni, R., Fajnkuchen, F., Dourmad, P., Magazzeni, S., Cohen, S.Y., 2015.
1717 Predictive value of outer retina en face OCT imaging for geographic atrophy progression. Invest.
1718 Ophthalmol. Vis. Sci. 56, 8325. https://doi.org/10.1167/iovs.15-17638

1719 Gocho, K., Sarda, V., Falah, S., Sahel, J.-A., Sennlaub, F., Benchaboune, M., Ullern, M., Paques, M.,
1720 2013. Adaptive optics imaging of geographic atrophy. Invest. Ophthalmol. Vis. Sci. 54, 3673–3680.
1721 https://doi.org/10.1167/iovs.12-11273

1722 Goerdt, L., Swain, T.A., Kar, D., McGwin, G., Berlin, A., Clark, M.E., Owsley, C., Sloan, K.R., Curcio, C.A.,
1723 2024. Band visibility in high-resolution optical coherence tomography assessed with a custom review
1724 tool and updated, histology-derived nomenclature. Transl. Vis. Sci. Technol. 13, 19.
1725 https://doi.org/10.1167/tvst.13.12.19

1726 Gofas-Salas, E., Lee, D.M.W., Rondeau, C., Grieve, K., Rossi, E.A., Paques, M., Gocho, K., 2024.
1727 Comparison between two adaptive optics methods for imaging of individual retinal pigmented
1728 epithelial cells. Diagnostics (Basel) 14, 737. https://doi.org/10.3390/diagnostics14070737

1729 Griffin, S.M., Jia, Y., Johnson, A.J., Antony, B.J., McDonald, H.R., Johnson, R.N., Lujan, B.J., 2021.
1730 Directional reflectivity of the ellipsoid zone in dry age-related macular degeneration. Ophthalmic
1731 Surg. Lasers Imaging Retina 52, 145–152. https://doi.org/10.3928/23258160-20210304-11

1732 Gu, R., Deng, G., Jiang, Y., Jiang, C., Xu, G., 2018. Area of the cone interdigitation zone in healthy
1733 Chinese adults and its correlation with macular volume. BMC Ophthalmol. 18, 188.
1734 https://doi.org/10.1186/s12886-018-0862-3

1735 Gujar, R., Muzi, A., Cagini, C., Mariotti, C., Piccolino, F.C., Chhablani, J., Lupidi, M., 2022. In-vivo
1736 visualization of the photoreceptors using Spectralis High Magnification Module imaging in central
1737 serous chorioretinopathy. Am. J. Ophthalmol. Case Rep. 25, 101249.
1738 https://doi.org/10.1016/j.ajoc.2021.101249

1739 Gunawan, J.R., Thiele, S.H., Isselmann, B., Caruso, E., Guymer, R.H., Luu, C.D., 2022. Effect of
1740 subthreshold nanosecond laser on retinal structure and function in intermediate age-related macular
1741 degeneration. Clin. Exp. Ophthalmol. 50, 31–39. https://doi.org/10.1111/ceo.13956

1742 Gutnikov, A., Hähn-Schumacher, P., Ameln, J., Zadeh, S.G., Schultz, T., Harmening, W., 2025. Neural
1743 network assisted annotation and analysis tool to study in-vivo foveolar cone photoreceptor
1744 topography. Sci. Rep. 15, 23858. https://doi.org/10.1038/s41598-025-21591-7

1745 Guymer, R.H., Blair, J.P.M., De Zanet, S., Apostolopoulos, S., Ciller, C., Wu, Z., Al-Qureshi, S., Busija, L.,
1746 Constable, I., Louis, D., Harper, C., Wickremasinghe, S., Van Wijngaarden, P., Lim, L., Durkin, S.,
1747 Runciman, J., Gihotra, J., Muecke, J., Haywood, K., … Scullion, L., 2025. Effect of subthreshold
1748 nanosecond laser on loss of OCT outer retinal bands in age-related macular degeneration: A LEAD
1749 Study Report. Ophthalmol. Sci. 5, 100839. https://doi.org/10.1016/j.xops.2024.100839

1750 Guymer, R.H., Rosenfeld, P.J., Curcio, C.A., Holz, F.G., Staurenghi, G., Freund, K.B., Schmitz-
1751 Valckenberg, S., Sparrow, J., Spaide, R.F., Tufail, A., Chakravarthy, U., Jaffe, G.J., Csaky, K., Sarraf, D.,
1752 Monés, J.M., Tadayoni, R., Grunwald, J., Bottoni, F., Liakopoulos, S., … Sadda, S.R., 2020. Incomplete
1753 retinal pigment epithelial and outer retinal atrophy in age-related macular degeneration:

1754 Classification of Atrophy Meeting Report 4. Ophthalmology 127, 394–409.
1755 https://doi.org/10.1016/j.ophtha

1756 Guymer, R.H., Rosenfeld, P.J., Ehlers, J.P., Attar, M., Chen, H., Ferris, F., Fujimoto, J.G., Ip, M., Pfau, M.,
1757 Saßmannshausen, M., Shen, J., Zacks, D.N., van Zyl, T., Wu, Z., Jaffe, G.J., 2025. Designing the next
1758 generation of clinical trials in intermediate AMD—a consensus driven, pragmatic, proof of concept
1759 early intervention study. *Exp. Eye Res.* 255, 109661. https://doi.org/10.1016/j.exer.2024.109661

1760 Guymer, R.H., Wu, Z., Hodgson, L.A.B., Caruso, E., Brassington, K.H., Tindill, N., Aung, K.Z.,
1761 McGuinness, M.B., Fletcher, E.L., Chen, F.K., Chakravarthy, U., Arnold, J.J., Heriot, W.J., Durkin, S.R.,
1762 Lek, J.J., Harper, C.A., Wickremasinghe, S.S., Sandhu, S.S., Baglin, E.K., … LEAD Study Group, 2019.
1763 Subthreshold nanosecond laser intervention in age-related macular degeneration: The LEAD
1764 randomized controlled clinical trial. *Ophthalmology* 126(6), 829–838.
1765 https://doi.org/10.1016/j.ophtha.2019.01.013

1766 Guymer, R., Wu, Z., Gao, S., Zhang, M., Steffen, V., Litts, K., Chang, M., Elsrott, J., Chen, C., Zhang, J.,
1767 Liu, L., Chen, H., 2023. HONU: A multicenter, prospective, observational study of the progression of
1768 intermediate age-related macular degeneration. *Invest. Ophthalmol. Vis. Sci.* 64(8), 2754.
1769 https://iovs.arvojournals.org/article.aspx?articleid=2786016

1770 Hagag, A.M., Holmes, C., Raza, A., Riedl, S., Anders, P., Kaye, R., Prevost, T., Fritsche, L.G., Rueckert,
1771 D., Bogunović, H., Scholl, H.P.N., Schmidt-Erfurth, U., Lotery, A.J., Sivaprasad, S., 2025. Features of
1772 intermediate and late dry age-related macular degeneration on adaptive optics ophthalmoscopy:
1773 Pinnacle Study Report 8. *Eye (Lond.)* 39(6), 1211–1216. https://doi.org/10.1038/s41433-024-02877-4

1774 Harmening, W.M., Sincich, L.C., 2019. Adaptive optics for photoreceptor-targeted psychophysics. In:
1775 Bille, J. (Ed.), *High Resolution Imaging in Microscopy and Ophthalmology: New Frontiers in*
1776 *Biomedical Optics*. Springer, Cham, pp. 359–375. https://doi.org/10.1007/978-3-030-16638-0_30

1777 Harmening, W.M., Tuten, W.S., Roorda, A., Sincich, L.C., 2014. Mapping the perceptual grain of the
1778 human retina. *J. Neurosci.* 34(16), 5667–5677. https://doi.org/10.1523/JNEUROSCI.5126-13.2014

1779 Hartmann, K.I., Gomez, M.L., Bartsch, D.-U.G., Schuster, A.K., Freeman, W.R., 2012. Effect of change
1780 in drusen evolution on photoreceptor inner segment/outer segment junction. *Retina* 32(8), 1492–
1781 1499. https://doi.org/10.1097/IAE.0b013e31823f5bb1

1782 Heidelberg Engineering Inc., 2026. High Magnification Module – SPECTRALIS. https://business-
1783 lounge.heidelbergengineering.com/us/en/products/spectralis/high-magnification-module/

1784 Heier, J.S., Lad, E.M., Holz, F.G., Rosenfeld, P.J., Guymer, R.H., Boyer, D., Grossi, F., Baumal, C.R.,
1785 Korobelnik, J.-F., Slakter, J.S., Waheed, N.K., Metlapally, R., Pearce, I., Steinle, N., Francone, A.A., Hu,
1786 A., Lally, D.R., Deschatelets, P., Francois, C., … Dubska, Z., 2023. Pegcetacoplan for the treatment of
1787 geographic atrophy secondary to age-related macular degeneration (OAKS and DERBY): two
1788 multicentre, randomised, double-masked, sham-controlled, phase 3 trials. *Lancet* 402(10411), 1434–
1789 1448. https://doi.org/10.1016/S0140-6736(23)01640-9

1790 Heisler, M., Ju, M.J., Bhalla, M., Schuck, N., Athwal, A., Navajas, E.V., Beg, M.F., Sarunic, M.V., 2018.
1791 Automated identification of cone photoreceptors in adaptive optics optical coherence tomography
1792 images using transfer learning. *Biomed. Opt. Express* 9(11), 5353–5367.
1793 https://doi.org/10.1364/BOE.9.005353

1794 Heitkotter, H., Patterson, E.J., Woertz, E.N., Cava, J.A., Gaffney, M., Adhan, I., Tam, J., Cooper, R.F.,
1795 Carroll, J., 2023. Extracting spacing-derived estimates of rod density in healthy retinae. Biomed. Opt.
1796 Express 14(1), 1–17. https://doi.org/10.1364/BOE.478396

1797 Hess, K., de Silva, T., Grisso, P., Wiley, H., Thavikulwat, A.T., Keenan, T.D.L., Chew, E.Y., Cukras, C.A.,
1798 2022. Evaluation of cone- and rod-mediated parameters in dark adaptation testing as outcome

measures in age-related macular degeneration. Ophthalmol. Retin. 6(12), 1173–1184. https://doi.org/10.1016/j.oret.2022.06.011

Hillmann, D., Spahr, H., Pfäffle, C., Sudkamp, H., Franke, G., Hüttmann, G., 2016. In vivo optical imaging of physiological responses to photostimulation in human photoreceptors. Proc. Natl. Acad. Sci. U. S. A. 113(46), 13138–13143. https://doi.org/10.1073/pnas.1606426113

Hood, D.C., Zhang, X., Ramachandran, R., Talamini, C.L., Raza, A., Greenberg, J.P., Sherman, J., Tsang, S.H., Birch, D.G., 2011. The inner segment/outer segment border seen on optical coherence tomography is less intense in patients with diminished cone function. Invest. Ophthalmol. Vis. Sci. 52(13), 9703. https://doi.org/10.1167/iovs.11-8027

Hoy, S.M., 2025. Revakinagene taroretcel: First approval. Mol. Diagn. Ther. 29(4), 553–561. https://doi.org/10.1007/s40291-025-00733-3

Huang, D., Swanson, E.A., Lin, C.P., Schuman, J.S., Stinson, W.G., Chang, W., Hee, M.R., Flotte, T., Gregory, K., Puliafito, C.A., Fujimoto, J., 1991. Optical coherence tomography. Science 254(5035), 1178–1181. https://doi.org/10.1126/science.1957169

ISRCTN, 2024. ReNEW: a clinical trial investigating the efficacy and safety of elamipretide in subjects who have dry age-related macular degeneration (Dry AMD). https://www.isrctn.com/ISRCTN59733193 (accessed 16 May 2025).

Itoh, Y., Vasanji, A., Ehlers, J.P., 2016. Volumetric ellipsoid zone mapping for enhanced visualisation of outer retinal integrity with optical coherence tomography. Br. J. Ophthalmol. 100(3), 295–299. https://doi.org/10.1136/bjophthalmol-2015-307175

1819 Jiang, X., Liu, T., Pandiyan, V.P., Slezak, E., Sabesan, R., 2022. Coarse-scale optoretinography (CoORG)
1820 with extended field-of-view for normative characterization. Biomed. Opt. Express 13(11), 5989–6004.
1821 https://doi.org/10.1364/BOE.471612

1822 Jonnal, R.S., Kocaoglu, O.P., Zawadzki, R.J., Lee, S.-H., Werner, J.S., Miller, D.T., 2014. The cellular
1823 origins of the outer retinal bands in optical coherence tomography images. Invest. Ophthalmol. Vis.
1824 Sci. 55(12), 7904–7918. https://doi.org/10.1167/iovs.14-15157

1825 Kalitzeos, A., Michaelides, M., Dubra, A., 2024. Minimum intensity projection of embossed quadrant-
1826 detection images for improved photoreceptor mosaic visualisation. *Front. Ophthalmol.* 4, 1349297.
1827 https://doi.org/10.3389/fopht.2024.1349297

1828 Kalra, G., Cetin, H., Whitney, J., Yordi, S., Cakir, Y., McConville, C., Whitmore, V., Bonnay, M., Reese,
1829 J.L., Srivastava, S.K., Ehlers, J.P., 2023. Automated identification and segmentation of ellipsoid zone
1830 at-risk using deep learning on SD-OCT for predicting progression in dry AMD. *Diagnostics* 13(6), 1076.
1831 https://doi.org/10.3390/diagnostics13061076

1832 Keane, P.A., Grossi, C.M., Foster, P.J., Yang, Q., Reisman, C.A., Chan, K., Peto, T., Thomas, D., Patel, P.J.,
1833 UK Biobank Eye Vision Consortium, 2016. Optical coherence tomography in the UK Biobank study –
1834 Rapid automated analysis of retinal thickness for large population-based studies. *PLoS One* 11(10),
1835 e0164095. https://doi.org/10.1371/journal.pone.0164095

1836 Khanani, A.M., Patel, S.S., Staurenghi, G., Tadayoni, R., Danzig, C.J., Eichenbaum, D.A., Hsu, J., Wykoff,
1837 C.C., Heier, J.S., Lally, D.R., Monés, J., Nielsen, J.S., Sheth, V.S., Kaiser, P.K., Clark, J., Zhu, L., Patel, H.,
1838 Tang, J., Desai, D., … GATHER2 trial investigators, 2023. Efficacy and safety of avacincaptad pegol in
1839 patients with geographic atrophy (GATHER2): 12-month results from a randomised, double-masked,
1840 phase 3 trial. *Lancet* 402(10411), 1449–1458. https://doi.org/10.1016/S0140-6736(23)02016-0

1841 Kleerekooper, I., Verschueren, D.V., Trip, S.A., Plant, G.T., Petzold, A., 2024. Ellipsoid zone reflectivity:
1842 Exploring its potential as a novel non-invasive biomarker for assessing mitochondrial function.
1843 *Neuroophthalmology* 48(6), 417–428. https://doi.org/10.1080/01658107.2024.2345678

1844 Knudtson, M.D., Klein, R., Klein, B.E.K., 2006. Physical activity and the 15-year cumulative incidence
1845 of age-related macular degeneration: the Beaver Dam Eye Study. Br. J. Ophthalmol. 90(12), 1461–
1846 1463. https://doi.org/10.1136/bjo.2006.100438

1847 Kocaoglu, O.P., Liu, Z., Zhang, F., Kurokawa, K., Jonnal, R.S., Miller, D.T., 2016. Photoreceptor disc
1848 shedding in the living human eye. Biomed. Opt. Express 7(11), 4554–4568.
1849 https://doi.org/10.1364/BOE.7.004554

1850 Kodjikian, L., Creuzot-Garcher, C., Korobelnik, J.-F., Tadayoni, R., Delafoy, I., Leal, C., Bernard, L.,
1851 Decullier, E., Huot, L., Mathis, T., 2023. Microperimetry to predict disease progression in eyes at high
1852 risk of age-related macular degeneration disease: The PREVISION study. Acta Ophthalmol. 101(2),
1853 e135–e142. https://doi.org/10.1111/aos.15233

1854 Kolb, H., Nelson, R.F., Ahnelt, P.K., Ortuño-Lizarán, I., Cuenca, N., 2020. The architecture of the
1855 human fovea. In: Kolb, H., Fernandez, E., Jones, B., Nelson, R. (Eds.), Webvision: The Organization of
1856 the Retina and Visual System. University of Utah Health Sciences Center.
1857 https://webvision.med.utah.edu/book/part-viii-human-functional-anatomy/the-architecture-of-the-
1858 human-fovea/

1859 Konstantinou, E.K., Mendonça, L.S.M., Braun, P., Monahan, K.M., Mehta, N., Gendelman, I., Levine,
1860 E.S., Baumal, C.R., Witkin, A.J., Duker, J.S., Waheed, N.K., 2021. Retinal imaging using a confocal
1861 scanning laser ophthalmoscope-based high-magnification module. Ophthalmol. Retin. 5(5), 438–449.
1862 https://doi.org/10.1016/j.oret.2020.09.008

1863 Laforest, T., Künzi, M., Kowalczuk, L., Carpentras, D., Behar-Cohen, F., Moser, C., 2020. Transscleral
1864 optical phase imaging of the human retina. Nat. Photonics 14(7), 439–445.
1865 https://doi.org/10.1038/s41566-020-0628-y

1866 Lains, I., Han, X., Gil, J., Providencia, J., Nigalye, A., Alvarez, R., Douglas, V.P., Mendez, K., Katz, R.,
1867 Tsougranis, G., Li, J., Kelly, R.S., Kim, I.K., Lasky-Su, J., Silva, R., Miller, J.W., Liang, L., Vavvas, D., Miller,
1868 J.B., Husain, D., 2024. Plasma metabolites associated with OCT features of age-related macular
1869 degeneration. Ophthalmol. Sci. 4(1), 100570. https://doi.org/10.1016/j.xops.2024.100570

1870 Laíns, I., Miller, J.B., Park, D.H., Tsikata, E., Davoudi, S., Rahmani, S., Pierce, J., Silva, R., Chen, T.C.,
1871 Kim, I.K., Vavvas, D., Miller, J.W., Husain, D., 2017. Structural changes associated with delayed dark
1872 adaptation in age-related macular degeneration. Ophthalmology 124(9), 1340–1352.
1873 https://doi.org/10.1016/j.ophtha.2017.04.014

1874 Land, M.E., Cooper, R.F., Young, J., Berg, E., Kitchner, T., Xiang, Q., Szabo, A., Ivacic, L.C., Stepien, K.E.,
1875 Page, C.D., Carroll, J., Connor, T., Brilliant, M., 2014. Cone structure in subjects with known genetic
1876 relative risk for AMD. Optom. Vis. Sci. 91(8), 939–949.
1877 https://doi.org/10.1097/OPX.0000000000000315

1878 Landa, G., Gentile, R.C., Garcia, P.M.T., Muldoon, T.O., Rosen, R.B., 2012. External limiting membrane
1879 and visual outcome in macular hole repair: spectral domain OCT analysis. Retina 32(1), 61–69.
1880 https://doi.org/10.1097/IAE.0b013e31820c7373

1881 Landa, G., Su, E., Garcia, P.M.T., Seiple, W.H., Rosen, R.B., 2011. Inner segment-outer segment
1882 junctional layer integrity and corresponding retinal sensitivity in dry and wet forms of age-related
1883 macular degeneration. Retina 31(2), 364–370. https://doi.org/10.1097/IAE.0b013e3181e01062

1884 Lanzetta, P., Korobelnik, J.-F., Heier, J.S., Leal, S., Holz, F.G., Clark, W.L., Eichenbaum, D., Iida, T.,
1885 Xiaodong, S., Berliner, A.J., Schulze, A., Schmelter, T., Schmidt-Ott, U., Zhang, X., Vitti, R., Chu, K.W.,

1886 Reed, K., Rao, R., Bhore, R., … PULSAR Investigators, 2024. Intravitreal aflibercept 8 mg in neovascular
1887 age-related macular degeneration (PULSAR): 48-week results from a randomised, double-masked,
1888 non-inferiority, phase 3 trial. Lancet 403(10432), 1141–1152. https://doi.org/10.1016/S0140-
1889 6736(24)00109-1

1890 Larsen, P.P., Delyfer, M.-N., Schweitzer, C., Korobelnik, J.-F., Delcourt, C., 2025. Neuroretinal and
1891 retinal pigment epithelium changes and susceptibility to age-related macular degeneration: Insights
1892 from the longitudinal ALIENOR study. Ophthalmology. https://doi.org/10.1016/j.ophtha.2024.11.020

1893 Lee, B., Chen, S., Moult, E., Yu, Y., Alibhai, A., Mehta, N., Baumal, C., Waheed, N., Fujimoto, J., 2020.
1894 High-speed, ultrahigh-resolution spectral-domain OCT with extended imaging range using reference
1895 arm length matching. Transl. Vis. Sci. Technol. 9(7), 12. https://doi.org/10.1167/tvst.9.7.12

1896 Lee, J., Kang, H.G., Kim, H.R., Lee, C.S., Kim, M., Kim, S.S., Byeon, S.H., 2022. Pigmentary abnormality
1897 without significant drusen as a risk factor for late age-related macular degeneration. Sci. Rep. 12(1),
1898 1–9. https://doi.org/10.1038/s41598-022-26488-y

1899 Lee, K.E., Heitkotter, H., Carroll, J., 2021. Challenges associated with ellipsoid zone intensity
1900 measurements using optical coherence tomography. Transl. Vis. Sci. Technol. 10(12), 27.
1901 https://doi.org/10.1167/tvst.10.12.27

1902 Lee, S., Kim, K.T., Kim, D.Y., Chae, J.B., Seo, E.J., 2023. Outer nuclear layer recovery as a predictor of
1903 visual prognosis in type 1 choroidal neovascularization of neovascular age-related macular
1904 degeneration. Sci. Rep. 13(1), 1–10. https://doi.org/10.1038/s41598-023-40997-1

1905 Lek, J.J., Brassington, K.H., Luu, C.D., Chen, F.K., Arnold, J.J., Heriot, W.J., Durkin, S.R., Chakravarthy,
1906 U., Guymer, R.H., 2017. Subthreshold nanosecond laser intervention in intermediate age-related
1907 macular degeneration. Ophthalmol. Retin. 1(3), 227–239. https://doi.org/10.1016/j.oret.2016.11.001

1908 Li, J.Q., Welchowski, T., Schmid, M., Letow, J., Wolpers, C., Pascual-Camps, I., Holz, F.G., Finger, R.P.,
1909 2020. Prevalence, incidence and future projection of diabetic eye disease in Europe: A systematic
1910 review and meta-analysis. Eur. J. Epidemiol. 35(1), 11–23. https://doi.org/10.1007/s10654-019-
1911 00520-3

1912 Li, K.Y., Tiruveedhula, P., Roorda, A., 2010. Intersubject variability of foveal cone photoreceptor
1913 density in relation to eye length. Invest. Ophthalmol. Vis. Sci. 51(12), 6858–6867.
1914 https://doi.org/10.1167/iovs.10-5499

1915 Li, W., Chen, W., Zhou, X., Jiang, T., Zhang, J., Wang, M., Wu, J., Gu, J., Chang, Q., 2023. Volume-
1916 accumulated reflectivity of the outer retina (integral) on spectral domain optical coherence
1917 tomography as a predictor of cone cell density: a pilot study. BMC Ophthalmol. 23(1), 1–14.
1918 https://doi.org/10.1186/s12886-023-03022-3

1919 Liang, J., Williams, D.R., Miller, D.T., 1997. Supernormal vision and high-resolution retinal imaging
1920 through adaptive optics. J. Opt. Soc. Am. A 14(11), 2884–2892.
1921 https://doi.org/10.1364/JOSAA.14.002884

1922 Liermann, Y.N., Behning, C., Isselmann, B., Schmid, M., Dunbar, H.M.P., Luhmann, U.F.O., Finger, R.P.,
1923 Schmitz-Valckenberg, S., Holz, F.G., Pfau, M., Luu, C.D., Saßmannshausen, M., Thiele, S., Agostini, H.,
1924 Altay, L., Atia, R., Bandello, F., Basile, P.G., Behning, C., … Zakaria, N., 2025. Ellipsoid zone reflectivity
1925 as a functional imaging biomarker for age-related macular degeneration: a MACUSTAR study report.
1926 Sci. Rep. 15(1), 20093. https://doi.org/10.1038/s41598-025-20093-2

1927 Lim, S.H., Yamaguchi, T.C.N., Herrmann, R., Lee, E.K., Bae, K.H., Park, U.C., Park, K.H., Yoon, C.K., 2025.
1928 Influence of subretinal drusenoid deposit on retinal sensitivity in age-related macular degeneration.
1929 Sci. Rep. 15(1), 34952. https://doi.org/10.1038/s41598-025-34952-x

1930 Lindenberg, S., Mahmoudi, A., Oncel, D., Corradetti, G., Emamverdi, M., Almidani, L., Farahani, A.,
1931 Wakatsuki, Y., He, Y., Saju M, S., Lee, W.K., Wykoff, C.C., Sarraf, D., Freund, K.B., Sadda, S.R., 2024.
1932 Acquired Vitelliform Lesions in Intermediate Age-Related Macular Degeneration: A Cross-Sectional
1933 Study. Ophthalmol. Retin. 8(9), 854–862. https://doi.org/10.1016/j.oret.2024.05.002

1934 Lindner, M., Nadal, J., Mauschitz, M.M., Lüning, A., Czauderna, J., Pfau, M., Schmitz-Valckenberg, S.,
1935 Holz, F.G., Schmid, M., Fleckenstein, M., 2017. Combined fundus autofluorescence and near infrared
1936 reflectance as prognostic biomarkers for visual acuity in foveal-sparing geographic atrophy. Invest.
1937 Ophthalmol. Vis. Sci. 58(6), BIO61–BIO67. https://doi.org/10.1167/iovs.16-20724

1938 Litts, K.M., Messinger, J.D., Freund, K.B., Zhang, Y., Curcio, C.A., 2015. Inner segment remodeling and
1939 mitochondrial translocation in cone photoreceptors in age-related macular degeneration with outer
1940 retinal tubulation. Invest. Ophthalmol. Vis. Sci. 56(4), 2243. https://doi.org/10.1167/iovs.14-16066

1941 Litts, K.M., Zhang, Y., Freund, K.B., Curcio, C.A., 2018. Optical coherence tomography and histology of
1942 age-related macular degeneration support mitochondria as reflectivity sources. Retina 38(3), 445–
1943 461. https://doi.org/10.1097/IAE.0000000000001559

1944 Liu, Z., Aghayee, S., Soltanian-Zadeh, S., Kovalick, K., Agrawal, A., Saeedi, O., Cukras, C., Chew, E.Y.,
1945 Farsiu, S., Hammer, D.X., 2024. Quantification of human photoreceptor-retinal pigment epithelium
1946 macular topography with adaptive optics-optical coherence tomography. Diagnostics (Basel) 14(14),
1947 1501. https://doi.org/10.3390/diagnostics14101501

1948 Lombardo, M., Serrao, S., Devaney, N., Parravano, M., Lombardo, G., 2012. Adaptive optics
1949 technology for high-resolution retinal imaging. Sensors 13(1), 334–366.
1950 https://doi.org/10.3390/s130100334

1951 Lujan, B.J., Griffin, S.M., Makhijani, V.S., Antony, B.J., Chew, E.Y., Roorda, A., McDonald, H.R., 2024.
1952 Directional optical coherence tomography imaging of macular pathology. Retina 44(7), 1124–1133.
1953 https://doi.org/10.1097/IAE.0000000000003896

1954 Lujan, B., Roorda, A., Croskrey, J., Dubis, A., Cooper, R., Bayabo, J., Duncan, J., Antony, B., Carroll, J.,
1955 2015. Directional optical coherence tomography provides accurate outer nuclear layer and Henle
1956 fiber layer measurements. Retina 35(8), 1511–1520.
1957 https://doi.org/10.1097/IAE.0000000000000521

1958 Lujan, B., Roorda, A., Knighton, R., Carroll, J., 2011. Revealing Henle's fiber layer using spectral
1959 domain optical coherence tomography. Invest. Ophthalmol. Vis. Sci. 52(3), 1486–1492.
1960 https://doi.org/10.1167/iovs.10-5953

1961 Mahmoudi, A., Manafi, N., Corradetti, G., Gupta Nittala, M., Emamverdi, M., Trejo Corona, S., Wykoff,
1962 C.C., Sarraf, D., Sadda, S.R., 2024. Risk factors for development of hyper-reflective foci overlying
1963 drusen in eyes with intermediate age-related macular degeneration. Br. J. Ophthalmol. [Online ahead
1964 of print]. https://doi.org/10.1136/bjo-2023-324775

1965 Mai, J., Reiter, G.S., Riedl, S., Vogl, W.-D., Sadeghipour, A., Foos, E., McKeown, A., Bogunovic, H.,
1966 Schmidt-Erfurth, U., 2024. Quantitative comparison of automated OCT and conventional FAF-based
1967 geographic atrophy measurements in the phase 3 OAKS/DERBY trials. Sci. Rep. 14(1), 20531.
1968 https://doi.org/10.1038/s41598-024-50343-w

1969 Mai, J., Reiter, G.S., Riedl, S., Vogl, W.-D., Sadeghipour, A., McKeown, A., Foos, E., Bogunovic, H.,
1970 Schmidt-Erfurth, U., 2025. Dynamics of the EZ/RPE loss ratio on OCT over time during geographic
1971 atrophy progression and treatment with pegcetacoplan. Invest. Ophthalmol. Vis. Sci. 66(11), 48.
1972 https://doi.org/10.1167/iovs.66.11.48

1973 Mai, J., Riedl, S., Reiter, G.S., Lachinov, D., Vogl, W.D., Bogunovic, H., Schmidt-Erfurth, U., 2022.
1974 Comparison of fundus autofluorescence versus optical coherence tomography–based evaluation of
1975 the therapeutic response to pegcetacoplan in geographic atrophy. Am. J. Ophthalmol. 244, 175–182.
1976 https://doi.org/10.1016/j.ajo.2022.07.014

1977 Mantel, I., Solomos, L., Misutkova, Z., Iskandar, A., Gryczka, A., Navarro, A., Jeunet, F., Kowalczuk, L.,
1978 Dormier, R., Behar-Cohen, F., Moser, C., 2022. Transscleral optical imaging in non-neovascular age-
1979 related macular degeneration. Invest. Ophthalmol. Vis. Sci. 63(7), 392-F0430.
1980 https://iovs.arvojournals.org/article.aspx?articleid=2783833

1981 Mathew, R., Richardson, M., Sivaprasad, S., 2013. Predictive value of spectral-domain optical
1982 coherence tomography features in assessment of visual prognosis in eyes with neovascular age-
1983 related macular degeneration treated with ranibizumab. Am. J. Ophthalmol. 155(4), 720–726.e1.
1984 https://doi.org/10.1016/j.ajo.2012.10.027

1985 McGuinness, M.B., Karahalios, A., Simpson, J.A., Guymer, R.H., Robman, L.D., Hodge, A.M., Cerin, E.,
1986 Giles, G.G., Finger, R.P., 2016. Past physical activity and age-related macular degeneration: the
1987 Melbourne Collaborative Cohort Study. Br. J. Ophthalmol. 100(10), 1353–1358.
1988 https://doi.org/10.1136/bjophthalmol-2015-307438

1989 Meadway, A., Wang, X., Curcio, C.A., Zhang, Y., 2014. Microstructure of subretinal drusenoid deposits
1990 revealed by adaptive optics imaging. Biomed. Opt. Express 5(3), 713.
1991 https://doi.org/10.1364/BOE.5.000713

1992 Mendonça, L.S.M., Braun, P.X., Martin, S.M., Hüther, A., Mehta, N., Zhao, Y., Abu-Qamar, O.,
1993 Konstantinou, E.K., Regatieri, C.V.S., Witkin, A.J., Baumal, C.R., Duker, J.S., Waheed, N.K., 2020.
1994 Repeatability and reproducibility of photoreceptor density measurement in the macula using the

1995 Spectralis High Magnification Module. Ophthalmol. Retin. 4(11), 1083–1092.
1996 https://doi.org/10.1016/j.oret.2020.05.006

1997 Miller, D.T., Kurokawa, K., 2020. Cellular-scale imaging of transparent retinal structures and processes
1998 using adaptive optics optical coherence tomography. Annu. Rev. Vis. Sci. 6, 115–148.
1999 https://doi.org/10.1146/annurev-vision-091718-014650

2000 Miloudi, C., Rossant, F., Bloch, I., Chaumette, C., Leseigneur, A., Sahel, J.-A., Meimon, S., Mrejen, S.,
2001 Paques, M., 2015. The negative cone mosaic: A new manifestation of the optical Stiles-Crawford
2002 effect in normal eyes. Invest. Ophthalmol. Vis. Sci. 56(12), 7043. https://doi.org/10.1167/iovs.15-
2003 17556

2004 Mozaffari, S., Jaedicke, V., LaRocca, F., Tiruveedhula, P., Roorda, A., 2018. Versatile multi-detector
2005 scheme for adaptive optics scanning laser ophthalmoscopy. Biomed. Opt. Express 9(11), 5477–5488.
2006 https://doi.org/10.1364/BOE.9.005477

2007 Mrejen, S., Sato, T., Curcio, C.A., Spaide, R.F., 2014. Assessing the cone photoreceptor mosaic in eyes
2008 with pseudodrusen and soft drusen in vivo using adaptive optics imaging. Ophthalmology 121(2),
2009 545–551. https://doi.org/10.1016/j.ophtha.2013.09.025

2010 Muftuoglu, I.K., Mendoza, N., Gaber, R., Alam, M., You, Q., Freeman, W.R., 2017. Integrity of outer
2011 retinal layers after resolution of central involved diabetic macular edema. Retina 37(11), 2015–2024.
2012 https://doi.org/10.1097/IAE.0000000000001412

2013 Mulders, T.W.F., Klevering, B.J., Hoyng, C.B., Theelen, T., 2021. Computer-assisted photoreceptor
2014 assessment on Heidelberg Engineering Spectralis™ High Magnification Module™ images. Graefe's
2015 Arch. Clin. Exp. Ophthalmol. 259(11), 3311–3320. https://doi.org/10.1007/s00417-021-05233-7

2016 Müller, P.L., Liefers, B., Treis, T., Rodrigues, F.G., Olvera-Barrios, A., Paul, B., Dhingra, N., Lotery, A.,
2017 Bailey, C., Taylor, P., Sánchez, C.I., Tufail, A., 2021. Reliability of retinal pathology quantification in age-
2018 related macular degeneration: Implications for clinical trials and machine learning applications.
2019 Transl. Vis. Sci. Technol. 10(3), 1–11. https://doi.org/10.1167/tvst.10.3.9

2020 Murari, J., Gautier, J., Daout, J., Krafft, L., Senée, P., Mecê, P., Grieve, K., Seiple, W., Sheynikhovich, D.,
2021 Meimon, S., Paques, M., Arleo, A., 2024. Foveolar drusen decrease fixation stability in pre-
2022 symptomatic AMD. Invest. Ophthalmol. Vis. Sci. 65(8), 13. https://doi.org/10.1167/iovs.65.8.13

2023 Obata, R., & Yanagi, Y. (2014). Quantitative analysis of cone photoreceptor distribution and its
2024 relationship with axial length, age, and early age-related macular degeneration. PLoS One, 9(3),
2025 e91873. https://doi.org/10.1371/journal.pone.0091873

2026 Ogata, M., Oh, H., Nakata, A., Doi, A., Nakayama, H., Hasegawa, M., & Hirose, M. (2022).
2027 Displacement of submacular hemorrhage secondary to age-related macular degeneration with
2028 subretinal injection of air and tissue plasminogen activator. Scientific Reports, 12(1), 1–11.
2029 https://doi.org/10.1038/s41598-022-05847-1

2030 Oishi, A., Shimozono, M., Mandai, M., Hata, M., Nishida, A., & Kurimoto, Y. (2013). Recovery of
2031 photoreceptor outer segments after anti-VEGF therapy for age-related macular degeneration.
2032 Graefe's Archive for Clinical and Experimental Ophthalmology, 251(2), 435–440.
2033 https://doi.org/10.1007/s00417-012-2046-z

2034 Otani, T., Yamaguchi, Y., & Kishi, S. (2011). Improved visualization of Henle fiber layer by changing the
2035 measurement beam angle on optical coherence tomography. Retina, 31(3), 497–501.
2036 https://doi.org/10.1097/IAE.0b013e3181ef61bf

2037 Padrón-Pérez, N., Català-Mora, J., Díaz, J., Arias, L., Prat, J., & Caminal, J. M. (2018). Swept-source and
2038 optical coherence tomography angiography in patients with X-linked retinoschisis. Eye (London),
2039 32(4), 707–715. https://doi.org/10.1038/eye.2017.260

2040 Pandiyan, V. P., Maloney-Bertelli, A., Kuchenbecker, J. A., Boyle, K. C., Ling, T., Chen, Z. C., Park, B. H.,
2041 Roorda, A., Palanker, D., & Sabesan, R. (2020). The optoretinogram reveals the primary steps of
2042 phototransduction in the living human eye. *Science Advances*, 6(37), eabc1124.
2043 https://doi.org/10.1126/sciadv.abc1124

2044 Park, D., & Lujan, B. J. (2017). Normal interdigitation zone loss by motion-tracked OCT.
2045 *Ophthalmology Retina*, 1(5), 394–396. https://doi.org/10.1016/j.oret.2016.12.003

2046 Pasricha, M. V., Tai, V., Sleiman, K., Winter, K., Chiu, S. J., Farsiu, S., Stinnett, S. S., Lad, E. M., Wong, W.
2047 T., Chew, E. Y., Toth, C. A., McCall, M., Srivastava, S., Sarin, N., Schuman, S., Sevilla, M., Harrington, C.,
2048 Gunther, R., Tran-Viet, D., … Harrington, M. (2021). Local anatomic precursors to new-onset
2049 geographic atrophy in age-related macular degeneration as defined on OCT. *Ophthalmology Retina*,
2050 5(5), 396–408. https://doi.org/10.1016/j.oret.2020.09.008

2051 Patel, S. S., Lally, D. R., Hsu, J., Wykoff, C. C., Eichenbaum, D., Heier, J. S., Jaffe, G. J., Westby, K., Desai,
2052 D., Zhu, L., & Khanani, A. M. (2023). Avacincaptad pegol for geographic atrophy secondary to age-
2053 related macular degeneration: 18-month findings from the GATHER1 trial. *Eye*, 37(17), 3551–3557.
2054 https://doi.org/10.1038/s41433-023-02482-3

2055 Pauleikhoff, D., Pauleikhoff, L., & Chew, E. Y. (2022). Imaging endpoints for clinical trials in MacTel
2056 type 2. *Eye*, 36(2), 284–293. https://doi.org/10.1038/s41433-021-01657-7

2057 Pfau, M., Lindner, M., Goerdt, L., Thiele, S., Nadal, J., Schmid, M., Schmitz-Valckenberg, S., Sadda, S.
2058 R., Holz, F. G., Fleckenstein, M., & Fundus Autofluorescence in Age-Related Macular Degeneration
2059 Study Group. (2019). Prognostic value of shape-descriptive factors for the progression of geographic

atrophy secondary to age-related macular degeneration. Retina, 39(8), 1527–1540. https://doi.org/10.1097/IAE.0000000000002210

Pfau, M., Sahu, S., Rupnow, R. A., Romond, K., Millet, D., Holz, F. G., Schmitz-Valckenberg, S., Fleckenstein, M., Lim, J. I., de Sisternes, L., Leng, T., Rubin, D. L., & Hallak, J. A. (2021). Probabilistic forecasting of anti-VEGF treatment frequency in neovascular age-related macular degeneration. Translational Vision Science & Technology, 10(7), 30. https://doi.org/10.1167/tvst.10.7.30

Pfau, M., Schmitz-Valckenberg, S., Ribeiro, R., Safaei, R., McKeown, A., Fleckenstein, M., & Holz, F. G. (2022). Association of complement C3 inhibitor pegcetacoplan with reduced photoreceptor degeneration beyond areas of geographic atrophy. Scientific Reports, 12(1), 17870. https://doi.org/10.1038/s41598-022-21953-w

Pfau, M., von der Emde, L., de Sisternes, L., Hallak, J., Leng, T., Schmitz-Valckenberg, S., Holz, F., Fleckenstein, M., & Rubin, D. (2020). Progression of photoreceptor degeneration in geographic atrophy secondary to age-related macular degeneration. JAMA Ophthalmology, 138(10), 1026–1034. https://doi.org/10.1001/jamaophthalmol.2020.3057

Pfau, M., von der Emde, L., Dysli, C., Möller, P. T., Thiele, S., Lindner, M., Schmid, M., Rubin, D. L., Fleckenstein, M., Holz, F. G., & Schmitz-Valckenberg, S. (2020). Determinants of cone and rod functions in geographic atrophy: AI-based structure-function correlation. American Journal of Ophthalmology, 217, 162–173. https://doi.org/10.1016/j.ajo.2020.04.024

Pfau, M., von der Emde, L., Dysli, C., Thiele, S., Möller, P. T., Lindner, M., Nadal, J., Schmid, M., Schmitz-Valckenberg, S., Holz, F. G., & Fleckenstein, M. (2019). Light sensitivity within areas of geographic atrophy secondary to age-related macular degeneration. Investigative Ophthalmology & Visual Science, 60(12), 3992. https://doi.org/10.1167/iovs.60.12.3992

2082 Pilotto, E., Benetti, E., Convento, E., Guidolin, F., Longhin, E., Parrozzani, R., & Midena, E. (2013).
2083 Microperimetry, fundus autofluorescence, and retinal layer changes in progressing geographic
2084 atrophy. Canadian Journal of Ophthalmology, 48(5), 386–393.
2085 https://doi.org/10.1016/j.jcjo.2013.04.012

2086 Pircher, M., Kroisamer, J. S., Felberer, F., Sattmann, H., Götzinger, E., & Hitzenberger, C. K. (2010).
2087 Temporal changes of human cone photoreceptors observed in vivo with SLO/OCT. Biomedical Optics
2088 Express, 2(1), 100–112. https://doi.org/10.1364/BOE.2.000100

2089 Pircher, M., & Zawadzki, R. J. (2017). Review of adaptive optics OCT (AO-OCT): principles and
2090 applications for retinal imaging [Invited]. Biomedical Optics Express, 8(5), 2536–2562.
2091 https://doi.org/10.1364/BOE.8.002536

2092 Qin, J., Rinella, N., Zhang, Q., Zhou, H., Wong, J., Deiner, M., Roorda, A., Porco, T. C., Wang, R. K.,
2093 Schwartz, D. M., & Duncan, J. L. (2018). OCT angiography and cone photoreceptor imaging in
2094 geographic atrophy. Investigative Ophthalmology & Visual Science, 59(15), 5985.
2095 https://doi.org/10.1167/iovs.18-24804

2096 Querques, G., Kamami-Levy, C., Georges, A., Pedinielli, A., Capuano, V., Blanco-Garavito, R., Poulon,
2097 F., & Souied, E. H. (2016). Adaptive optics imaging of foveal sparing in geographic atrophy secondary
2098 to age-related macular degeneration. Retina, 36(2), 247–254.
2099 https://doi.org/10.1097/IAE.0000000000000749

2100 Querques, L., Querques, G., Forte, R., & Souied, E. (2012). Microperimetric correlations of
2101 autofluorescence and optical coherence tomography imaging in dry age-related macular
2102 degeneration. American Journal of Ophthalmology, 153(6), 1110–1115.
2103 https://doi.org/10.1016/j.ajo.2011.11.020

2104 Ramón y Cajal, S. (1892). La rétine des vertébrés. Cellule, 9, 119–257.

Ramón y Cajal, S. (1909). Histologie du système nerveux de l'homme & des vertébrés. Maloine.

Reche, J., Stocker, A., Henchoz, V., Habra, O., Escher, P., Wolf, S., & Zinkernagel, M. (2023). High-resolution optical coherence tomography in healthy individuals provides resolution at the cellular and subcellular levels. Translational Vision Science & Technology, 12(7), 12. https://doi.org/10.1167/tvst.12.7.12

Reiniger, J. L., Domdei, N., Holz, F. G., & Harmening, W. M. (2021). Human gaze is systematically offset from the center of cone topography. *Current Biology*, 31(18), 4188–4193.e3. https://doi.org/10.1016/j.cub.2021.07.006

Reumueller, A., Schmidt-Erfurth, U., Salas, M., Sacu, S., Drexler, W., Pircher, M., & Pollreisz, A. (2019). Three-dimensional adaptive optics–assisted visualization of photoreceptors in healthy and pathologically aged eyes. *Investigative Ophthalmology & Visual Science*, 60(4), 1144.

Riedl, S., Vogl, W.-D., Mai, J., Reiter, G. S., Lachinov, D., Grechenig, C., McKeown, A., Scheibler, L., Bogunović, H., & Schmidt-Erfurth, U. (2022). The effect of pegcetacoplan treatment on photoreceptor maintenance in geographic atrophy monitored by artificial intelligence–based OCT analysis. *Ophthalmology Retina*, 6(11), 1009–1018. https://doi.org/10.1016/j.oret.2022.05.005

Roorda, A., Romero-Borja, F., Donnelly III, W., Queener, H., Hebert, T., & Campbell, M. (2002). Adaptive optics scanning laser ophthalmoscopy. *Optics Express*, 10(9), 405–412. https://doi.org/10.1364/OE.10.000405

Rossi, E. A., Granger, C. E., Sharma, R., Yang, Q., Saito, K., Schwarz, C., Walters, S., Nozato, K.,Zhang, J., Kawakami, T., Fischer, W., Latchney, L. R., Hunter, J. J., Chung, M. M., & Williams, D. R. (2017). Imaging individual neurons in the retinal ganglion cell layer of the living eye. *Proceedings of the National Academy of Sciences*, 114(3), 586–591. https://doi.org/10.1073/pnas.1613445114

Rossi, E. A., Norberg, N., Eandi, C., Chaumette, C., Kapoor, S., Le, L., Snyder, V. C., Martel, J. N., Gautier, J., Gocho, K., Dansingani, K. K., Chhablani, J., Arleo, A., Mrejen, S., Sahel, J.-A., Grieve, K., & Paques, M. (2021). A new method for visualizing drusen and their progression in flood-illumination adaptive optics ophthalmoscopy. Translational Vision Science & Technology, 10(14), 19. https://doi.org/10.1167/tvst.10.14.19

Ryu, C. L., Al-Humaid, S., Rampakakis, E., Galic, I. J., & Chen, J. C. (2016). Correlation of visual acuity with fibrotic scar location in treated neovascular age-related macular degeneration eyes. Retina, 36(7), 1324–1330. https://doi.org/10.1097/IAE.0000000000000897

Sadda, S. R., Guymer, R., Holz, F. G., Schmitz-Valckenberg, S., Curcio, C. A., Bird, A. C., Blodi, B. A., Bottoni, F., Chakravarthy, U., Chew, E. Y., Csaky, K., Danis, R. P., Fleckenstein, M., Freund, K. B., Grunwald, J., Hoyng, C. B., Jaffe, G. J., Liakopoulos, S., Monés, J. M., … Staurenghi, G. (2018). Consensus definition for atrophy associated with age-related macular degeneration on OCT: Classification of Atrophy Report 3. Ophthalmology, 125(4), 537–548. https://doi.org/10.1016/j.ophtha.2017.09.028

Saeed, A., Gin, C., Hodgson, L. A. B. B., Jannaud, M., Hadoux, X., Glover, E. K., Gee, E. E., van Wijngaarden, P., Guymer, R. H., & Wu, Z. (2025). Local OCT structural correlates of deep visual sensitivity defects in early atrophic age-related macular degeneration. Ophthalmology Retina, 9(5), 412–420. https://doi.org/10.1016/j.oret.2023.09.009

Sahni, J., Dugel, P. U., Patel, S. S., Chittum, M. E., Berger, B., Del Valle Rubido, M., Sadikhov, S., Szczesny, P., Schwab, D., Nogoceke, E., Weikert, R., & Fauser, S. (2020). Safety and efficacy of different doses and regimens of faricimab vs ranibizumab in neovascular age-related macular degeneration: The AVENUE phase 2 randomized clinical trial. JAMA Ophthalmology, 138(9), 955–963. https://doi.org/10.1001/jamaophthalmol.2020.2730

Saleh, M., Flores, M., Gauthier, A. S., Elphege, E., & Delbosc, B. (2017). Quantitative analysis of photoreceptor layer reflectivity on en-face optical coherence tomography as an estimator of cone density. Graefe's Archive for Clinical and Experimental Ophthalmology, 255(11), 2119–2126. https://doi.org/10.1007/s00417-017-3759-1

Saßmannshausen, M., Ameln, J., von der Emde, L., Holz, F. G., Ach, T., & Harmening, W. M. (2024). Evaluation of retinal sensitivity in complete retinal-pigment-epithelium and outer retinal atrophy (cRORA) lesions in intermediate age-related macular degeneration (iAMD) by high-resolution microperimetry. Journal of Clinical Medicine, 13(24), Article 6171. https://doi.org/10.3390/jcm13246171

Saßmannshausen, M., Behning, C., Isselmann, B., Schmid, M., Finger, R. P., Holz, F. G., Schmitz-Valckenberg, S., Pfau, M., MACUSTAR Consortium, & Thiele, S. (2022). Relative ellipsoid zone reflectivity and its association with disease severity in age-related macular degeneration: A MACUSTAR study report. Scientific Reports, 12(1), 14933. https://doi.org/10.1038/s41598-022-18584-1

Saßmannshausen, M., Zhou, J., Pfau, M., Thiele, S., Steinberg, J., Fleckenstein, M., Holz, F. G., & Schmitz-Valckenberg, S. (2021). Longitudinal analysis of retinal thickness and retinal function in eyes with large drusen secondary to intermediate age-related macular degeneration. Ophthalmology Retina, 5(3), 241–250. https://doi.org/10.1016/j.oret.2020.06.013

Savastano, M. C., Falsini, B., Ferrara, S., Scampoli, A., Piccardi, M., Savastano, A., & Rizzo, S. (2022). Subretinal pigment epithelium illumination combined with focal electroretinogram and visual acuity for early diagnosis and prognosis of non-exudative age-related macular degeneration: New insights for personalized medicine. Translational Vision Science & Technology, 11(1), Article 3. https://doi.org/10.1167/tvst.11.1.3

2173 Sayegh, R. G., Simader, C., Scheschy, U., Montuoro, A., Kiss, C., Sacu, S., Kreil, D. P., Prünte, C., &
2174 Schmidt-Erfurth, U. (2011). A systematic comparison of spectral-domain optical coherence
2175 tomography and fundus autofluorescence in patients with geographic atrophy. Ophthalmology,
2176 118(9), 1844–1851. https://doi.org/10.1016/j.ophtha.2011.01.046

2177 Schmidt-Erfurth, U., Mai, J., Reiter, G. S., Riedl, S., Vogl, W.-D., Sadeghipour, A., McKeown, A., Foos, E.,
2178 Scheibler, L., & Bogunovic, H. (2025). Disease activity and therapeutic response to pegcetacoplan for
2179 geographic atrophy identified by deep learning-based analysis of OCT. Ophthalmology, 132(2), 181–
2180 193. https://doi.org/10.1016/j.ophtha.2023.07.015

2181 Schmitz-Valckenberg, S., Saßmannshausen, M., Braun, M., Steffen, V., Gao, S. S., Honigberg, L.,
2182 Ferrara, D., Pfau, M., & Holz, F. G. (2023). Interreader agreement and longitudinal progression of
2183 incomplete/complete retinal pigment epithelium and outer retinal atrophy in age-related macular
2184 degeneration. Ophthalmology Retina, 7(12), 1059–1068. https://doi.org/10.1016/j.oret.2023.06.006

2185 Scoles, D., Sulai, Y. N., Langlo, C. S., Fishman, G. A., Curcio, C. A., Carroll, J., & Dubra, A. (2014). In vivo
2186 imaging of human cone photoreceptor inner segments. Investigative Ophthalmology & Visual
2187 Science, 55(7), 4244–4251. https://doi.org/10.1167/iovs.14-14542

2188 Shao, L., Zhang, Q. L., Zhou, L. X., Xu, L., You, Q. S., & Wei, W. B. (2018). Using spectral-domain optical
2189 coherence tomography to evaluate the type and thickness of interdigitation zone band in adult
2190 Chinese. Scientific Reports, 8(1), 4. https://doi.org/10.1038/s41598-017-18295-4

2191 Sharma, S., Toth, C. A., Daniel, E., Grunwald, J. E., Maguire, M. G., Ying, G.-S., Huang, J., Martin, D. F.,
2192 Jaffe, G. J., & Comparison of Age-related Macular Degeneration Treatments Trials Research Group.
2193 (2016). Macular morphology and visual acuity in the second year of the Comparison of Age-Related
2194 Macular Degeneration Treatments Trials. Ophthalmology, 123(4), 865–875.
2195 https://doi.org/10.1016/j.ophtha.2015.12.014

Simader, C., Sayegh, R. G., Montuoro, A., Azhary, M., Koth, A. L., Baratsits, M., Sacu, S., Prünte, C., Kreil, D. P., & Schmidt-Erfurth, U. (2014). A longitudinal comparison of spectral-domain optical coherence tomography and fundus autofluorescence in geographic atrophy. American Journal of Ophthalmology, 158(3), 557–566.e1. https://doi.org/10.1016/j.ajo.2014.05.018

Soltanian-Zadeh, S., Liu, Z., Liu, Y., Lassoued, A., Cukras, C. A., Miller, D. T., Hammer, D. X., & Farsiu, S. (2023). Deep learning-enabled volumetric cone photoreceptor segmentation in adaptive optics optical coherence tomography images of normal and diseased eyes. Biomedical Optics Express, 14(2), 815–833. https://doi.org/10.1364/BOE.480736

Song, X., Xu, Q., Li, H., Fan, Q., Zheng, Y., Zhang, Q., Chu, C., Zhang, Z., Yuan, C., Ning, M., Bian, C., Ma, K., & Qu, Y. (2022). Automatic quantification of retinal photoreceptor integrity to predict persistent disease activity in neovascular age-related macular degeneration using deep learning. Frontiers in Neuroscience, 16, 952735. https://doi.org/10.3389/fnins.2022.952735

Spaide, R., & Curcio, C. (2011). Anatomical correlates to the bands seen in the outer retina by optical coherence tomography. Retina, 31(8), 1609–1619. https://doi.org/10.1097/IAE.0b013e

Sredar, N., Razeen, M., Kowalski, B., Carroll, J., & Dubra, A. (2021). Comparison of confocal and non-confocal split-detection cone photoreceptor imaging. Biomedical Optics Express, 12(2), 737–755. https://doi.org/10.1364/BOE.412750

Staurenghi, G., Sadda, S., Chakravarthy, U., Spaide, R. F., & International Nomenclature for Optical Coherence Tomography (IN•OCT) Panel. (2014). Proposed lexicon for anatomic landmarks in normal posterior segment spectral-domain optical coherence tomography: the IN•OCT consensus. Ophthalmology, 121(8), 1572–1578. https://doi.org/10.1016/j.ophtha.2014.02.023

Takahashi, A., Ooto, S., Yamashiro, K., Oishi, A., Tamura, H., Nakanishi, H., Ueda-Arakawa, N., Tsujikawa, A., & Yoshimura, N. (2016). Photoreceptor damage and reduction of retinal sensitivity

2219 surrounding geographic atrophy in age-related macular degeneration. American Journal of
2220 Ophthalmology, 168, 260–268. https://doi.org/10.1016/j.ajo.2016.05.014

2221 Thiele, S., Isselmann, B., Pfau, M., Holz, F. G., Schmitz-Valckenberg, S., Wu, Z., Guymer, R. H., & Luu,
2222 C. D. (2020). Validation of an automated quantification of relative ellipsoid zone reflectivity on
2223 spectral domain-optical coherence tomography images. Translational Vision Science & Technology,
2224 9(11), 1–10. https://doi.org/10.1167/tvst.9.11.8

2225 Thiele, S., Wu, Z., Isselmann, B., Pfau, M., Guymer, R. H., & Luu, C. D. (2022). Natural history of the
2226 relative ellipsoid zone reflectivity in age-related macular degeneration. Ophthalmology Retina, 6(12),
2227 1165–1172. https://doi.org/10.1016/j.oret.2022.06.003

2228 Tomita, Y., Nagai, N., Suzuki, M., Shinoda, H., Uchida, A., Mochimaru, H., Izumi-Nagai, K., Sasaki, M.,
2229 Tsubota, K., & Ozawa, Y. (2016). Functional visual acuity in age-related macular degeneration.
2230 Optometry and Vision Science, 93(1), 70–76. https://doi.org/10.1097/OPX.0000000000000755

2231 Toprak, I., Yaylalı, V., & Yildirim, C. (2017). Early deterioration in ellipsoid zone in eyes with non-
2232 neovascular age-related macular degeneration. International Ophthalmology, 37(4), 801–806.
2233 https://doi.org/10.1007/s10792-016-0140-z

2234 Trinh, M., Eshow, N., Alonso-Caneiro, D., Kalloniatis, M., & Nivison-Smith, L. (2022). Reticular
2235 pseudodrusen are associated with more advanced para-central photoreceptor degeneration in
2236 intermediate age-related macular degeneration. Investigative Ophthalmology & Visual Science,
2237 63(11), 12. https://doi.org/10.1167/iovs.63.11.12

2238 Trinh, M., Kalloniatis, M., Alonso-Caneiro, D., & Nivison-Smith, L. (2022). High-density optical
2239 coherence tomography analysis provides insights into early/intermediate age-related macular
2240 degeneration retinal layer changes. Investigative Ophthalmology & Visual Science, 63(5), 36.
2241 https://doi.org/10.1167/iovs.63.5.36

Tuten, W. S., Tiruveedhula, P., & Roorda, A. (2012). Adaptive optics scanning laser ophthalmoscope-based microperimetry. Optometry and Vision Science, 89(5), 563–574. https://doi.org/10.1097/OPX.0b013e318250c0c9

Ueda-Arakawa, N., Tsujikawa, A., Yamashiro, K., Ooto, S., Tamura, H., & Yoshimura, N. (2012). Visual prognosis of eyes with submacular hemorrhage associated with exudative age-related macular degeneration. Japanese Journal of Ophthalmology, 56(6), 589–598. https://doi.org/10.1007/s10384-012-0182-x

van Leeuwen, R., Klaver, C. C. W., Vingerling, J. R., Hofman, A., & de Jong, P. T. V. M. (2003). The risk and natural course of age-related maculopathy: follow-up at 6 1/2 years in the Rotterdam study. Archives of Ophthalmology, 121(4), 519–526. https://doi.org/10.1001/archopht.121.4.519

Vogl, W.-D., Bogunović, H., Waldstein, S. M., Riedl, S., & Schmidt-Erfurth, U. (2021). Spatio-temporal alterations in retinal and choroidal layers in the progression of age-related macular degeneration (AMD) in optical coherence tomography. Scientific Reports, 11(1), 5743. https://doi.org/10.1038/s41598-021-84630-6

Wang, X., Hoshi, S., Liu, R., Corradetti, G., Ip, M., Sarraf, D., Sadda, S. R., & Zhang, Y. (2025). Photoreceptor function and structure in retinal areas with intraretinal hyperreflective foci in age-related macular degeneration. Investigative Ophthalmology & Visual Science, 66(2), 27. https://doi.org/10.1167/iovs.66.2.27

Wang, X., Sadda, S. V. R., Ip, M. S., Sarraf, D., & Zhang, Y. (2023). In vivo longitudinal measurement of cone photoreceptor density in intermediate age-related macular degeneration. American Journal of Ophthalmology, 248, 60–75. https://doi.org/10.1016/j.ajo.2022.12.012

2263 Wang, Y., Bensaid, N., Tiruveedhula, P., Ma, J., Ravikumar, S., & Roorda, A. (2019). Human foveal cone
2264 photoreceptor topography and its dependence on eye length. eLife, 8, e47148.
2265 https://doi.org/10.7554/eLife.47148

2266 Whitmore, S. S., DeLuca, A. P., Andorf, J. L., Cheng, J. L., Mansoor, M., Fortenbach, C. R., Critser, D. B.,
2267 Russell, J. F., Stone, E. M., & Han, I. C. (2023). Modeling rod and cone photoreceptor cell survival in
2268 vivo using optical coherence tomography. Scientific Reports, 13(1), 6896.
2269 https://doi.org/10.1038/s41598-023-33378-4

2270 Wilson, J. D., Cottrell, W. J., & Foster, T. H. (2007). Index-of-refraction-dependent subcellular light
2271 scattering observed with organelle-specific dyes. Journal of Biomedical Optics, 12(1), 014010.
2272 https://doi.org/10.1117/1.2434958

2273 Wu, Z., Ayton, L. N., Guymer, R. H., & Luu, C. D. (2013a). Relationship between the second reflective
2274 band on optical coherence tomography and multifocal electroretinography in age-related macular
2275 degeneration. Investigative Ophthalmology & Visual Science, 54(4), 2800–2806.
2276 https://doi.org/10.1167/iovs.12-112

2277 Wu, Z., Ayton, L. N., Guymer, R. H., & Luu, C. D. (2013b). Second reflective band intensity in age-
2278 related macular degeneration. Ophthalmology, 120(6), 1307–1308.e1.
2279 https://doi.org/10.1016/j.ophtha.2012.11.031

2280 Wu, Z., Ayton, L. N., Luu, C. D., & Guymer, R. H. (2014). Relationship between retinal microstructures
2281 on optical coherence tomography and microperimetry in age-related macular degeneration.
2282 Ophthalmology, 121(7), 1445–1452. https://doi.org/10.1016/j.ophtha.2014.01.026

2283 Wu, Z., De Zanet, S., Blair, J. P. M., & Guymer, R. H. (2025). Loss of OCT outer retinal bands as
2284 potential clinical trial endpoints in intermediate age-related macular degeneration. Ophthalmology
2285 Science, 5(4), 100769. https://doi.org/10.1016/j.xops.2023.100769

2286 Wu, Z., Goh, K., Hodgson, L., & Guymer, R. (2023). Incomplete retinal pigment epithelial and outer
2287 retinal atrophy: Longitudinal evaluation in age-related macular degeneration. Ophthalmology, 130(2),
2288 205–212. https://doi.org/10.1016/j.ophtha.2022.08.007

2289 Wu, Z., Hodgson, L. A. B., Goh, K. L., & Guymer, R. H. (2024). Complete retinal pigment epithelial and
2290 outer retinal atrophy in age-related macular degeneration: A longitudinal evaluation. Retina, 44(7),
2291 1224–1231. https://doi.org/10.1097/IAE.0000000000003811

2292 Wu, Z., Hodgson, L. A. B., & Guymer, R. H. (2024). Targeted high-density microperimetry testing of
2293 nascent geographic atrophy in age-related macular degeneration. Ophthalmology Science, 4(2),
2294 100419. https://doi.org/10.1016/j.xops.2023.100419

2295 Wu, Z., Luu, C. D., Ayton, L. N., Goh, J. K., Lucci, L. M., Hubbard, W. C., Hageman, J. L., Hageman, G. S.,
2296 & Guymer, R. H. (2014). Optical coherence tomography-defined changes preceding the development
2297 of drusen-associated atrophy in age-related macular degeneration. Ophthalmology, 121(12), 2415–
2298 2422. https://doi.org/10.1016/j.ophtha.2014.06.031

2299 Wu, Z., Luu, C. D., Hodgson, L. A. B., Caruso, E., Tindill, N., Aung, K. Z., McGuinness, M. B., Makeyeva,
2300 G., Chen, F. K., Chakravarthy, U., Arnold, J. J., Heriot, W. J., Durkin, S. R., & Guymer, R. H. (2020).
2301 Prospective longitudinal evaluation of nascent geographic atrophy in age-related macular
2302 degeneration. Ophthalmology Retina, 4(6), 568–575. https://doi.org/10.1016/j.oret.2020.01.014

2303 Wu, Z., Luu, C. D., Hodgson, L. A. B., Caruso, E., Chen, F. K., Chakravarthy, U., Arnold, J. J., Heriot, W. J.,
2304 Runciman, J., & Guymer, R. H. (2021). Examining the added value of microperimetry and low
2305 luminance deficit for predicting progression in age-related macular degeneration. British Journal of
2306 Ophthalmology, 105(5), 711–715. https://doi.org/10.1136/bjophthalmol-2020-316264

2307 Wu, Z., Pfau, M., Blodi, B. A., Holz, F. G., Jaffe, G. J., Liakopoulos, S., Sadda, S. R., Staurenghi, G.,
2308 Bjelopera, E., Brown, T., Chang, P., Choong, J., Corradetti, G., Corvi, F., Domalpally, A., Hurtenbach, C.,

Nittala, M. G., Olson, A., Pak, J. W., … Schmitz-Valckenberg, S. (2022). OCT signs of early atrophy in age-related macular degeneration: Interreader agreement. Ophthalmology Retina, 6(1), 4–14. https://doi.org/10.1016/j.oret.2021.07.017

Wu, Z., Sadda, S. R., Ach, T., Blodi, B. A., Bottoni, F., Chakravarthy, U., Chew, E. Y., Curcio, C. A., Ferris, F. L., Fleckenstein, M., Freund, K. B., Grunwald, J. E., Holz, F. G., Jaffe, G. J., Liakopoulos, S., Lim, T. H., Monés, J. M., Pagliarini, S., Pauleikhoff, D., … Guymer, R. H. (2025). Onset of end-stage atrophic age-related macular degeneration as an endpoint—A Delphi study: Classification of Atrophy Meetings Report 7. Ophthalmology Science, 5(5), 100777. https://doi.org/10.1016/j.xops.2023.100777

Wu, Z., Terheyden, J. H., Hodgson, L. A. B., & Guymer, R. H. (2024). Choroidal signal hypertransmission on optical coherence tomography imaging: Association with development of geographic atrophy in age-related macular degeneration. Clinical & Experimental Ophthalmology, 52(4), 431–439. https://doi.org/10.1111/ceo.14293

Wynne, N., Heitkotter, H., Woertz, E. N., Cooper, R. F., & Carroll, J. (2022). Comparison of cone mosaic metrics from images acquired with the SPECTRALIS high magnification module and adaptive optics scanning light ophthalmoscopy. Translational Vision Science & Technology, 11(5), 19. https://doi.org/10.1167/tvst.11.5.19

Xu, X., Liu, X., Wang, X., Clark, M. E., McGwin, G., Owsley, C., Curcio, C. A., & Zhang, Y. (2017). Retinal pigment epithelium degeneration associated with subretinal drusenoid deposits in age-related macular degeneration. American Journal of Ophthalmology, 175, 87–98. https://doi.org/10.1016/j.ajo.2016.12.014

Xu, X., Wang, X., Sadda, S. R., & Zhang, Y. (2020). Subtype-differentiated impacts of subretinal drusenoid deposits on photoreceptors revealed by adaptive optics scanning laser ophthalmoscopy.

Graefe's Archive for Clinical and Experimental Ophthalmology, 258(9), 1931–1940. https://doi.org/10.1007/s00417-020-04741-3

Yao, H., Wu, Z., Gao, S. S., Guymer, R. H., Steffen, V., Chen, H., Hejrati, M., & Zhang, M. (2024). Deep learning approaches for detecting of nascent geographic atrophy in age-related macular degeneration. Ophthalmology Science, 4(3), 100428. https://doi.org/10.1016/j.xops.2023.100428

Yordi, S., Cakir, Y., Cetin, H., Talcott, K. E., Srivastava, S. K., Hu, J., & Ehlers, J. P. (2024). Bacillary layer detachment in neovascular age-related macular degeneration from a phase III clinical trial. Ophthalmology Retina, 8(8), 754–764. https://doi.org/10.1016/j.oret.2024.03.011

Yordi, S., Cakir, Y., Kalra, G., Cetin, H., Hu, M., Abraham, J., Reese, J., Srivastava, S. K., & Ehlers, J. P. (2024). Ellipsoid zone integrity and visual function in dry age-related macular degeneration. Journal of Personalized Medicine, 14(5), Article 428. https://doi.org/10.3390/jpm14050428

Yordi, S., Sarici, K., Cetin, H., Lunasco, L. M., Le, T. K., Sevgi, D. D., Zahid, R., Meng, X., Reese, J. L., Srivastava, S. K., & Ehlers, J. P. (2022). Bacillary detachment in neovascular age-related macular degeneration: Incidence, clinical features, and response to anti-VEGF therapy. Ophthalmology Retina, 6(11), 1061–1069. https://doi.org/10.1016/j.oret.2022.05.003

Yoshida, K., Anegondi, N., Pely, A., Zhang, M., Debraine, F., Ramesh, K., Steffen, V., Gao, S. S., Cukras, C., Rabe, C., Ferrara, D., Spaide, R. F., Sadda, S. R., Holz, F. G., & Yang, Q. (2025). Deep learning approaches to predict geographic atrophy progression using three-dimensional OCT imaging. Translational Vision Science & Technology, 14(2), 11. https://doi.org/10.1167/tvst.14.2.11

Zarbin, M. A., Hill, L., Maunz, A., Gliem, M., & Stoilov, I. (2022). Anti-VEGF-resistant subretinal fluid is associated with better vision and reduced risk of macular atrophy. British Journal of Ophthalmology, 106(11), 1561–1566. https://doi.org/10.1136/bjophthalmol-2021-320295

2353 Zayit-Soudry, S., Duncan, J. L., Syed, R., Menghini, M., & Roorda, A. J. (2013). Cone structure imaged
2354 with adaptive optics scanning laser ophthalmoscopy in eyes with nonneovascular age-related
2355 macular degeneration. Investigative Ophthalmology & Visual Science, 54(12), 7498.
2356 https://doi.org/10.1167/iovs.13-12710

2357 Zekavat, S. M., Sekimitsu, S., Ye, Y., Raghu, V., Zhao, H., Elze, T., Segrè, A. V., Wiggs, J. L., Natarajan, P.,
2358 Del Priore, L., Zebardast, N., & Wang, J. C. (2022). Photoreceptor layer thinning is an early biomarker
2359 for age-related macular degeneration: Epidemiologic and genetic evidence from UK Biobank OCT
2360 data. Ophthalmology, 129(6), 694–707. https://doi.org/10.1016/j.ophtha.2021.12.012

2361 Zhang, Y., Cense, B., Rha, J., Jonnal, R. S., Gao, W., Zawadzki, R. J., Werner, J. S., Jones, S., Olivier, S., &
2362 Miller, D. T. (2006). High-speed volumetric imaging of cone photoreceptors with adaptive optics
2363 spectral-domain optical coherence tomography. Optics Express, 14(10), 4380–4394.
2364 https://doi.org/10.1364/OE.14.004380

2365 Zhang, Y., Wang, X., Clark, M. E., Curcio, C. A., & Owsley, C. (2020). Imaging of age-related macular
2366 degeneration by adaptive optics scanning laser ophthalmoscopy in eyes with aged lenses or
2367 intraocular lenses. Translational Vision Science & Technology, 9(8), 41.
2368 https://doi.org/10.1167/tvst.9.8.41

2369 Zhang, Y., Wang, X., Rivero, E. B., Clark, M. E., Witherspoon, C. D., Spaide, R. F., Girkin, C. A., Owsley,
2370 C., & Curcio, C. A. (2014a). Photoreceptor perturbation around subretinal drusenoid deposits as
2371 revealed by adaptive optics scanning laser ophthalmoscopy. American Journal of Ophthalmology,
2372 158(3), 584–596.e1. https://doi.org/10.1016/j.ajo.2014.05.004

2373 Zhang, Y., Wang, X., Rivero, E. B., Clark, M. E., Witherspoon, C. D., Spaide, R. F., Girkin, C. A., Owsley,
2374 C., & Curcio, C. A. (2014b). Photoreceptor perturbation around subretinal drusenoid deposits as

revealed by adaptive optics scanning laser ophthalmoscopy. American Journal of Ophthalmology, 158(3), 584–596.e1. https://doi.org/10.1016/j.ajo.2014.05.004

Zhang, Y., Wang, X., Sadda, S. R., Clark, M. E., Witherspoon, C. D., Spaide, R. F., Owsley, C., & Curcio, C. A. (2020). Lifecycles of individual subretinal drusenoid deposits and evolution of outer retinal atrophy in age-related macular degeneration. Ophthalmology Retina, 4(3), 274–283. https://doi.org/10.1016/j.oret.2019.08.017

Figure 1. Organization of the human retina. (A) Schematic diagram showing the major cellular layers and their component cell types. (B) Vertical histological section of the peripheral retina highlighting cone photoreceptor morphology. (C) Histological section of the human macula immunostained with antibodies against guanine nucleotide-binding protein β3 (GNB3, green), cellular retinaldehyde-binding protein (CRALBP, red), and cytochrome-C (Cyt C, blue). This shows the morphology of the fovea and delineates the dimensions and boundaries of macular subregions. (D) Corresponding optical coherence tomography (OCT) image of the same retinal area. Note that separation of the retinal pigment epithelium from the outer retina represents post-mortem artifact, not seen on OCT. Modified from Cuenca et al. (2020). (Cuenca et al., 2020)

Figure 2. Morphological features of cones, and Müller cells across the human retina. (A) Schematic illustration and confocal images showing cone photoreceptor morphology and their cellular organization. (B) Diagram of the human fovea depicting the spatial arrangement and morphology of cones (black), bipolar cells (blue), and Müller cells (red). (C–E) Regional differences in cone morphology at the umbo (C), the parafovea (D; 1.5 mm from the foveal center), and the peripheral retina (E; 7 mm from the foveal center). (F) Schematic representation of cone morphological variations at different retinal eccentricities. Scale bars: (C–E) 20 µm. Modified from Cuenca et al. (2020). (Cuenca et al., 2020)

Figure 3. (A) Cross-section of the fovea stained with immunohistochemistry to identify specific retinal layers. Cones are labeled with guanine nucleotide-binding protein b 3 (GNB3, green), Müller cells and RPE with cellular retinaldehydebinding protein (CRALBP, red) and blood vessels with Collagen IV (blue). (B) Optical coherence tomography (OCT) image of the human fovea. The nomenclature of OCT hyperreflective bands is aligned with their corresponding histological layers as revealed in the immunostained section. (C) High magnification of the cross-section of the foveal zone immunostained with antibodies against cytochrome C (Cyt C, blue) to identity mitochondria and

GNB3, (green) and CRALBP (red). (C–E) Correlation of the outer retinal layers stained with immunohistochemistry (C) with the four hyperreflective bands observed in SD-OCT images (D) and ultrahigh-resolution OCT images (E). GCL. ganglion cell layer; INL. inner nuclear layer; IPL. internal plexiform layer; ONL. outer nuclear layer; OPL. outer plexiform layer; ELM. external limiting membrane, RPE. retinal pigment epithelium; OSIZ: outer segment interdigitation zone. Scale bar in (C) 20 mm, and (D) 100 mm. Modified from Cuenca et al. (2020)(Cuenca et al., 2020)

Figure 4: Photoreceptor and retinal pigment epithelium loss maps in a patient with non-exudative AMD. This artificial-intelligence-based image segmentation (RetinAI AG, Bern, Switzerland) shows maps of the areas of loss of the retinal pigment epithelium (RPE); myoid zone (MZ); ellipsoid zone, outer photoreceptors and interdigitation zone loss (EZ+OPR+IZ), and outer nuclear layer and henle fiber layer loss (ONL + HFL).

Figure 5. Photoreceptor degeneration and geographic atrophy progression in AMD.
Left panels: Fundus-autofluorescence (FAF) images and standardized (Z-scores, accounting for retinal location and age) outer nuclear layer (ONL), inner segment (IS), and outer segment (OS) thickness maps of three patients with geographic atrophy (GA). Black outlines mark retinal pigment epithelium (RPE) atrophy. Photoreceptor layers were segmented using a deep-learning-based method.
Right panels: En-face spectral-domain OCT mean projections of the same eyes one year later, with yellow and cyan outlines denoting baseline and year-1 GA borders, respectively. More extensive ONL thinning at baseline is associated with faster GA expansion. Modified from Pfau et al., (2020). (Pfau et al., 2020)

Figure 6: Exemplary representation of rEZR determination within a given region of interest (red box) in an OCT B-scan of a healthy eye. Please note, while native, i.e. raw OCT reflectivity data is assessed

for rEZR analyses, this figure demonstrates a logarithmic-transformed OCT image for better visualization purposes. Within the region of interest, the corresponding reflectivity profile were extracted and the peak reflectivity of the ellipsoid zone (EZ) and the external limiting membrane (ELM) automatically identified. Quantification of the EZ and ELM peak reflectivity [linear range: 0-1 arbitrary units] finally allows for rEZR assessment.

Figure 7: En face OCT projections segmented in the vitreous, retinal nerve fiber layer (RNFL) and on the photoreceptor plane (EZ). The mean gray intensity is obtained from each image and the normalized EZ reflectivity is calculated using the formula. Method described by Borrelli et al. (Borrelli et al., 2017). Images are acquired with Spectralis HRA-OCT3 (Heidelberg Engineering, Heidelberg, Germany), and extracted from an OCT angiography volumetric scan (20x20º, composed by 512 B-scans with a distance of 11μm between B-scans). The method can be reproduced using ImageJ® (National Institutes of Health, Bethesda, MD).

Figure 8. Incomplete and complete retinal pigment epithelium and outer retinal atrophy (iRORA and cRORA). A. Near infrared reflectance (NIR) image of a patient with multifocal areas of geographic atrophy (GA) associated with soft drusen and calcified soft drusen. B. Optical coherence tomography (OCT) scan showing an area of iRORA demarcated in green (magnification shown in panel C), and an area of cRORA demarcated in yellow (magnification shown in panel D). Panel C illustrates a mineralized soft drusen undergoing regression with subsidence of the outer retinal layers corresponding to an area of iRORA within the green arrowheads. Panel D pictures an area of cRORA within the yellow arrowheads. E. NIR image of a patient subretinal drusenoid deposits with pigmentary changes and mineralized drusen. F. OCT scan demonstrates an area of incomplete outer retinal atrophy (ORA) demarcated in orange (magnification shown in panel G), and an area of complete ORA demarcated in magenta (magnification shown in panel H). Panel G shows collapse of

the external limiting membrane and photoreceptor layers with preservation of the retinal pigmented epithelium (RPE) band. H. An area of cORA is demarcated within the magenta arrowheads.

Figure 9. Progression of complete retinal pigment epithelium and outer retinal atrophy (cRORA) and nascent geographic atrophy (nGA). A. Near infrared reflectance (NIR) image of a patient with multifocal areas of geographic atrophy (GA). Green arrow shows the corresponding area of optical coherence tomography (OCT) scan in panel B. The area of GA (cRORA) is demarcated by green arrowheads. Magenta arrow shows the corresponding area of OCT scan in panel C. An area of pigmentary changes is pointed with pink arrowheads. D. NIR at 8-month follow-up with green and magenta arrows demonstrating the scan position on panels E and F respectively. The area of cRORA shows enlargement (green arrowheads) whereas the area of pigmentary changes shows subsidence of the external limiting membrane and outer nuclear layer (iRORA, nascent GA). G. NIR at 12-month follow-up shows enlargement of the GA lesions pointed in green, confirmed by OCT scan on panel H. The area of nascent GA shows enlargement leading to an area of cRORA within the magenta arrowheads.

Figure 10. Near-infrared reflectance imaging (NIR) using the High Magnification Module (HMM). Panels A and B show the optical coherence tomography (OCT) scan (A) and NIR image (B) of a control subject. Yellow and magenta areas correspond to panels C and D respectively. Panels C and D show NIR using the HMM, allowing for photoreceptor pattern recognition. Panels E and F show the OCT scan (E) and NIR image (F) of a patient with intermediate AMD with small and intermediate drusen and pigmentary changes. Blue and green areas show corresponding areas for panels G and H demonstrating the HMM image.

Figure 11. High magnification module imaging across the intermediate age-related macular degeneration spectrum. Panels A and B show the optical coherence tomography (OCT) scan (A) and near infrared reflectance (NIR) image (B) of a patient with reticular pseudodrusen and geographic atrophy. The yellow area shows the correspondence of panel C, showing a NIR using the High Magnification Module (HMM). The second row show a patient with mineralized soft drusen showing two different images of HMM in the corresponding yellow and magenta areas shown in panel D. The third row illustrates a patient with drusenoid pigment epithelium detachment. The bottom row shows a patient with soft drusen and pigmentary changes.

Figure 12: Fovea-centered cone analysis using rtx1 (Imagine Eyes, Orsay, France) and its correspondence in OCT (A) and near-infrared fundus image (B). A single acquisition covers approximately 1.2x1.2mm of the retina (blue square in A, B and C). The 1º degree within fovea cannot be imaged due to the densely packed cones in this area (pink square in A, B and C). The parafoveal cone mosaic can be differentiated in good-quality images (C) and a smaller ROI can be manually selected for cone analysis (red square in C). The inbuilt software recognices the center of the cells (D) and calculates the cone density (cells/image area), inter-cell spacing (μm or minutes of arc) and regularity (% of cells with 6 neighboring cells).

Figure 13: Multimodal imaging and microperimetry of an intermediate AMD patient presenting an incomplete retinal pigment epithelium and outer retinal atrophy (iRORA) lesion. A: OCT B-scan with marked iRORA lesion (red) and eccentricity matched MP control region (blue). B: Magnification of the iRORA lesion marked by a white rectangle in A. C: Stimulus size comparison for a conventional clinical microperimetry (MP) device (MAIA) and adaptive optics scanning light ophthalmoscopy (AOSLO-MP). D: MAIA-MP estimate of retinal sensitivity at the iRORA lesion (17 dB, red) and control region (27dB, blue). The marker diameter corresponds to the MAIA-MP stimulus size on the retina. E and F: AOSLO imaging and MP at the iRORA lesion (E) and control region (F). Sensitivity thresholds

were 14 dB and 33.3 dB, respectively. Both areas show patches of normally appearing cone photoreceptors, hyperreflective aggregations and areas of hyporeflective retina. Modified from Ameln et al. (2024).(Ameln et al., 2024)

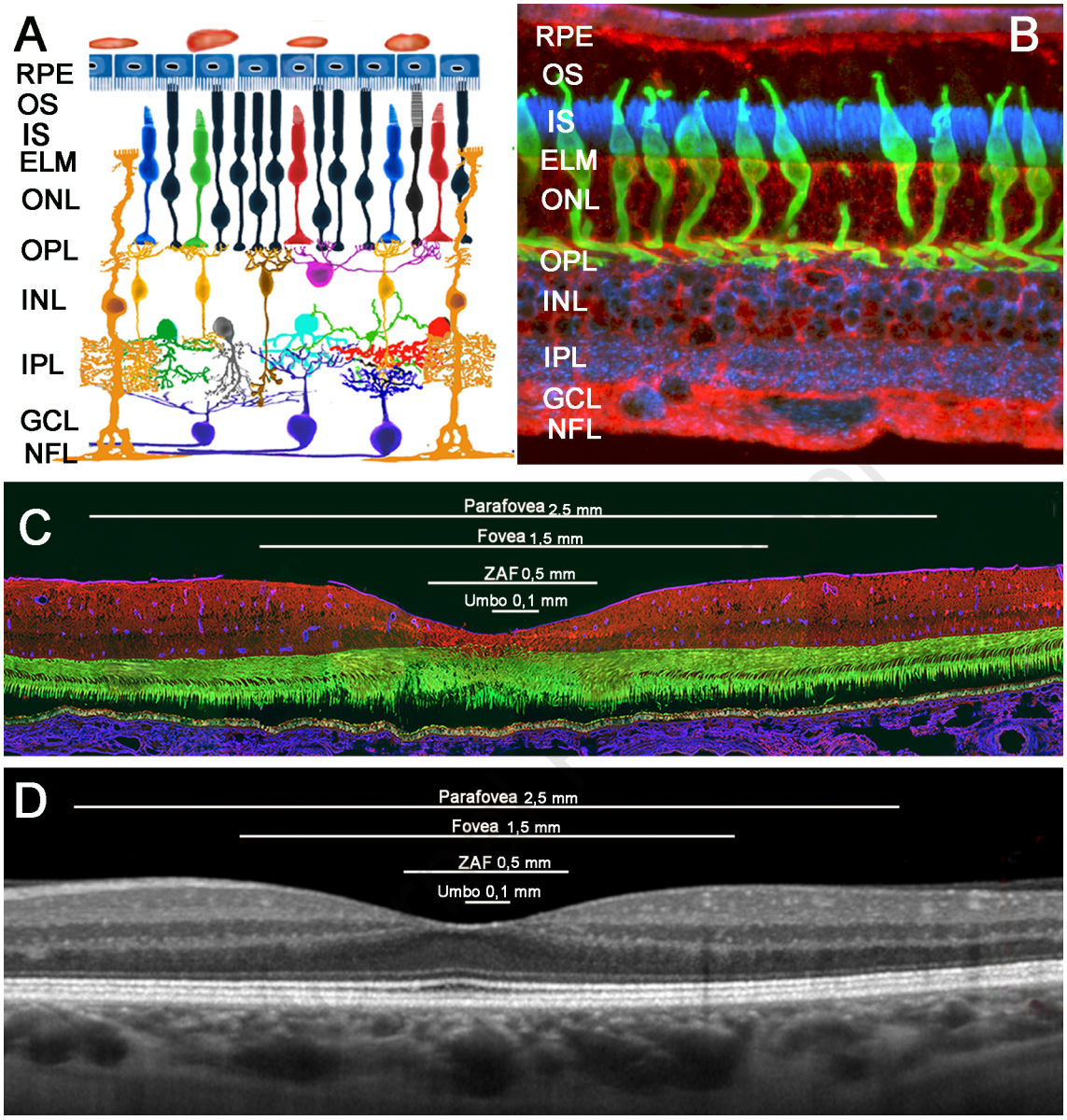
A
RPE
OS
IS
ELM
ONL
OPL
INL
IPL
GCL
NFL
B
RPE
OS
IS
ELM
ONL
OPL
INL
IPL
GCL
NFL
C
Parafovea 2,5 mm
Fovea 1,5 mm
ZAF 0,5 mm
Umbo 0,1 mm
D
Parafovea 2,5 mm
Fovea 1,5 mm
ZAF 0,5 mm
Umbo 0,1 mm

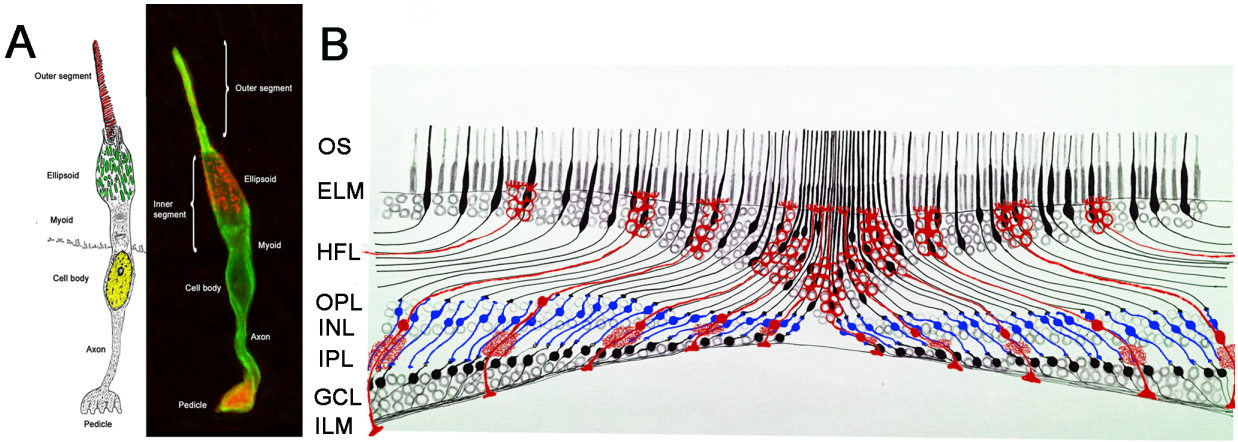
A
Outer segment
Ellipsoid
Myoid
Cell body
Axon
Pedicle
Outer segment
Inner segment
Ellipsoid
Myoid
Cell body
Axon
Pedicle
B
OS
ELM
HFL
OPL
INL
IPL
GCL
ILM

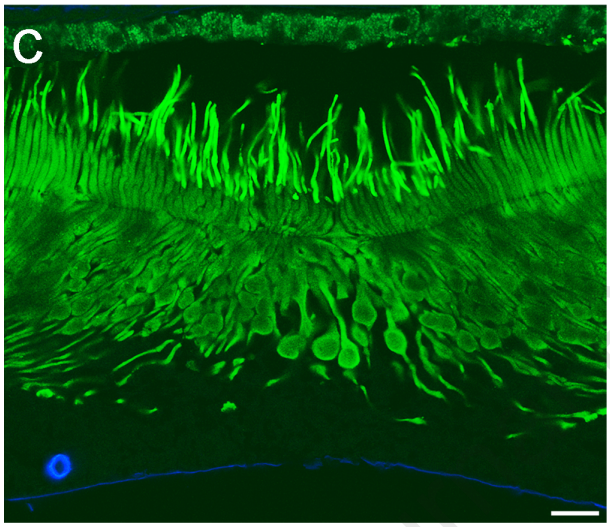
C

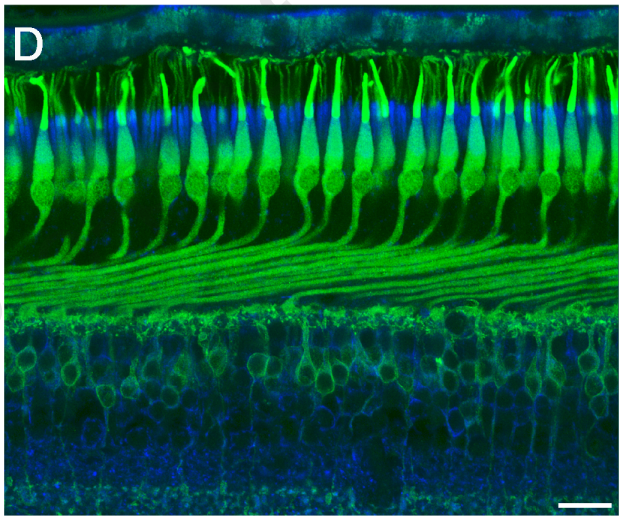
D

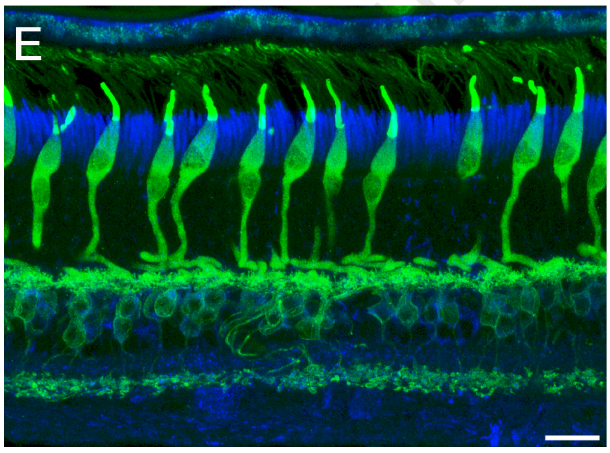
E

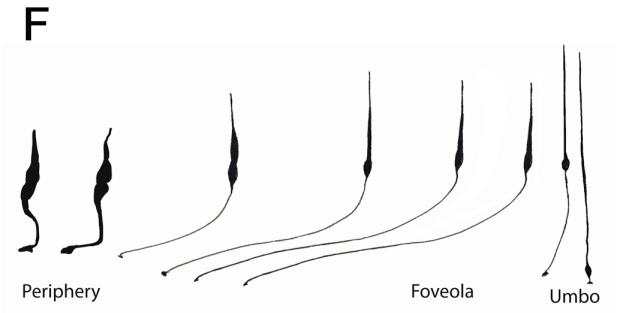
F
Periphery
Foveola
Umbo

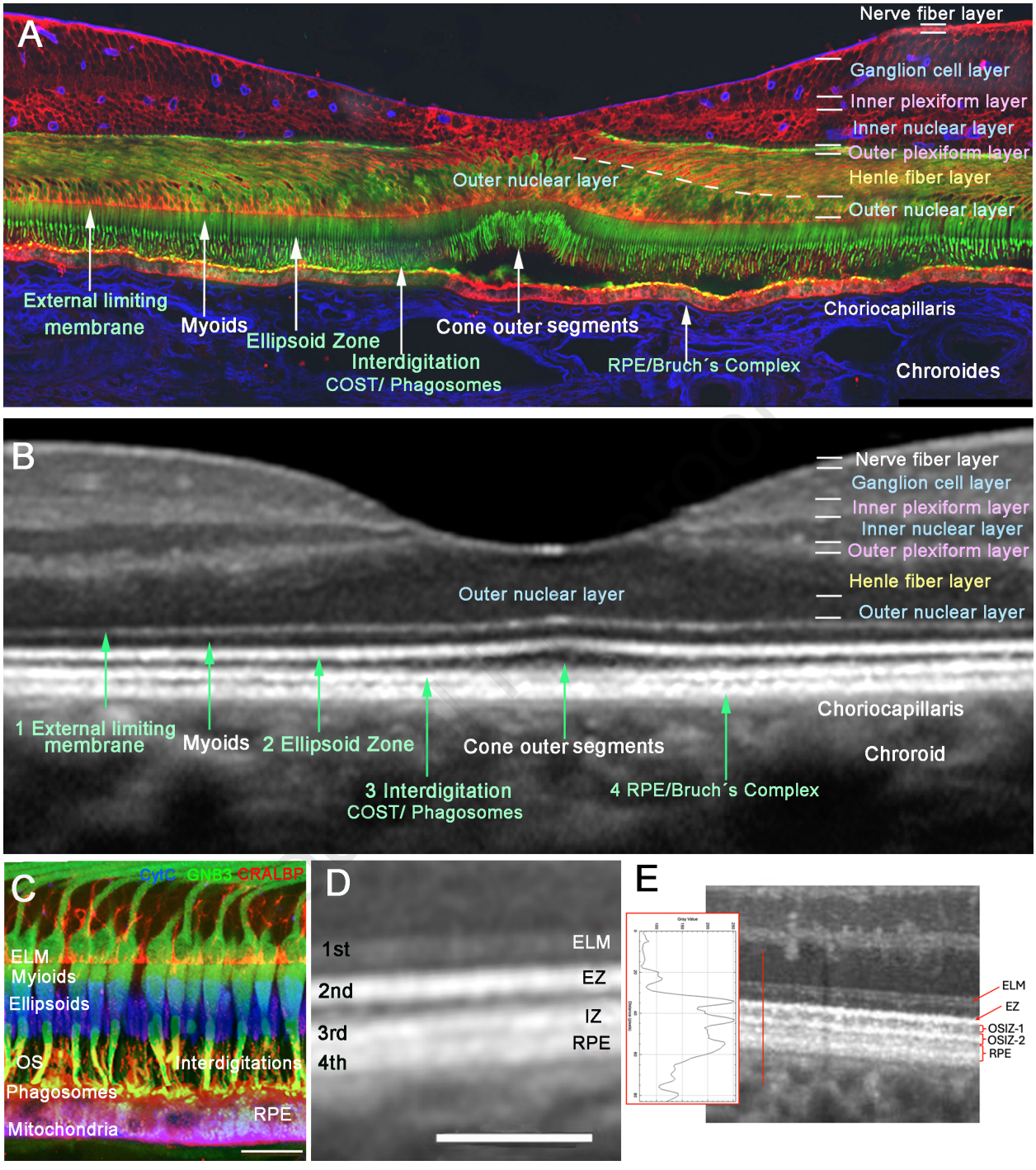
A
Nerve fiber layer
Ganglion cell layer
Inner plexiform layer
Inner nuclear layer
Outer plexiform layer
Henle fiber layer
Outer nuclear layer
Outer nuclear layer
External limiting membrane
Myoids
Ellipsoid Zone
Interdigitation
COST/ Phagosomes
Cone outer segments
RPE/Bruch´s Complex
Choriocapillaris
Chroroides
B
Nerve fiber layer
Ganglion cell layer
Inner plexiform layer
Inner nuclear layer
Outer plexiform layer
Henle fiber layer
Outer nuclear layer
Outer nuclear layer
1 External limiting membrane
Myoids
2 Ellipsoid Zone
3 Interdigitation
COST/ Phagosomes
Cone outer segments
4 RPE/Bruch´s Complex
Choriocapillaris
Chroroid
C
Cyt C GNB3 CRALBP
ELM
Myoids
Ellipsoids
OS
Interdigitations
Phagosomes
RPE
Mitochondria
D
1st
2nd
3rd
4th
ELM
EZ
IZ
RPE
E
ELM
EZ
OSIZ-1
OSIZ-2
RPE

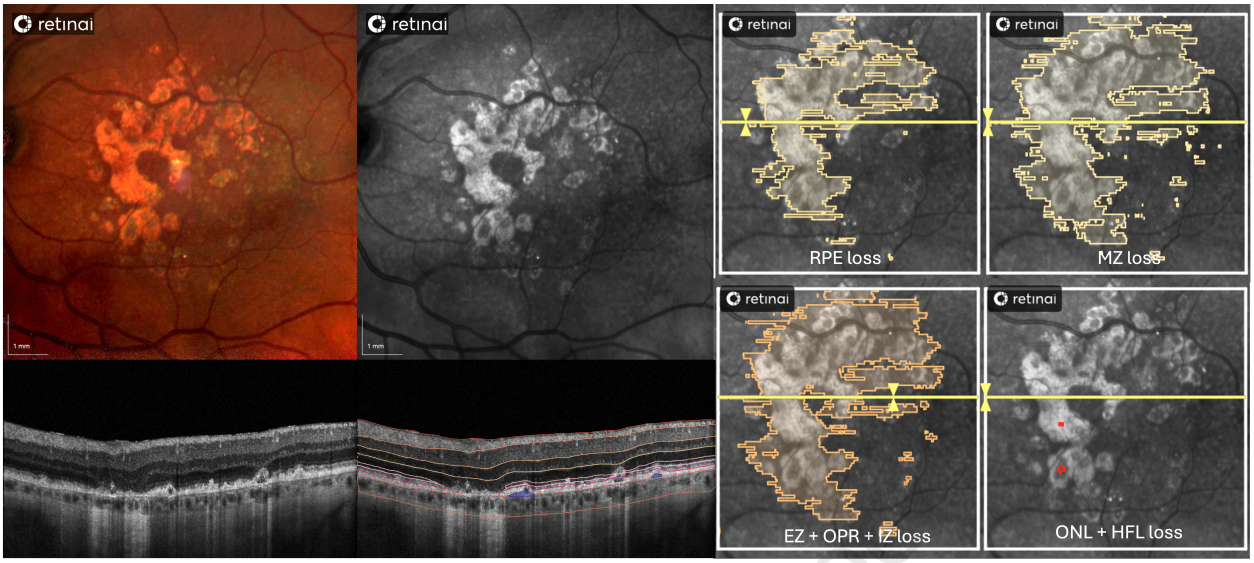

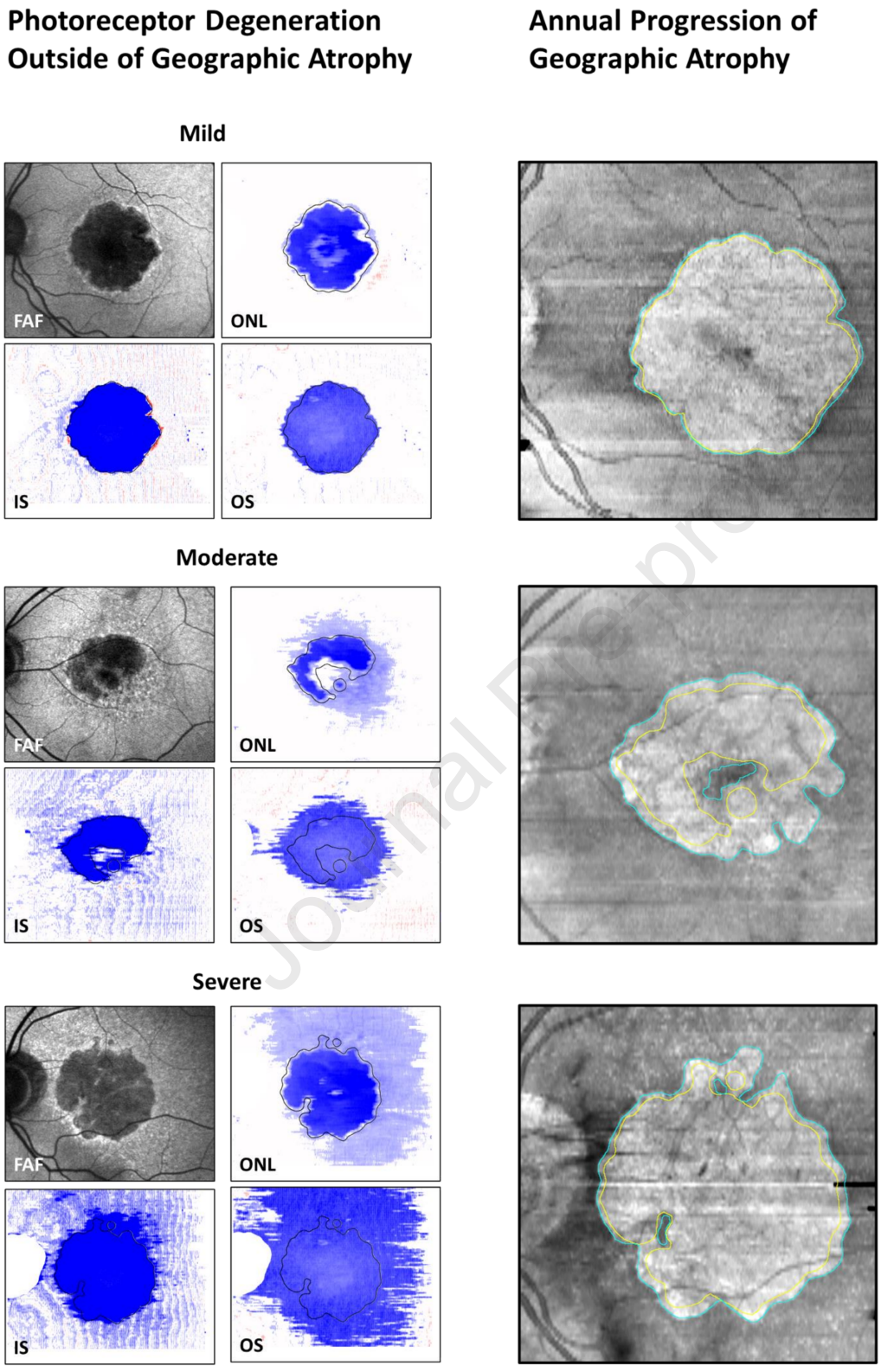

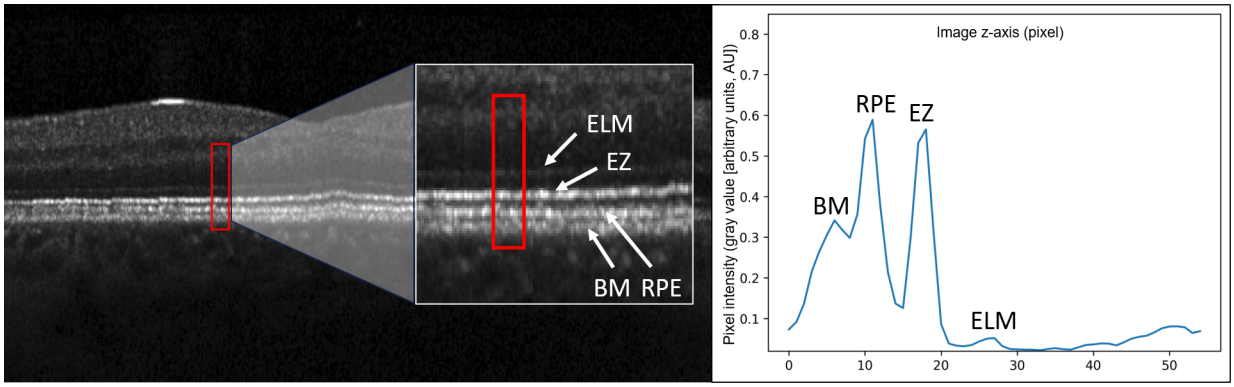

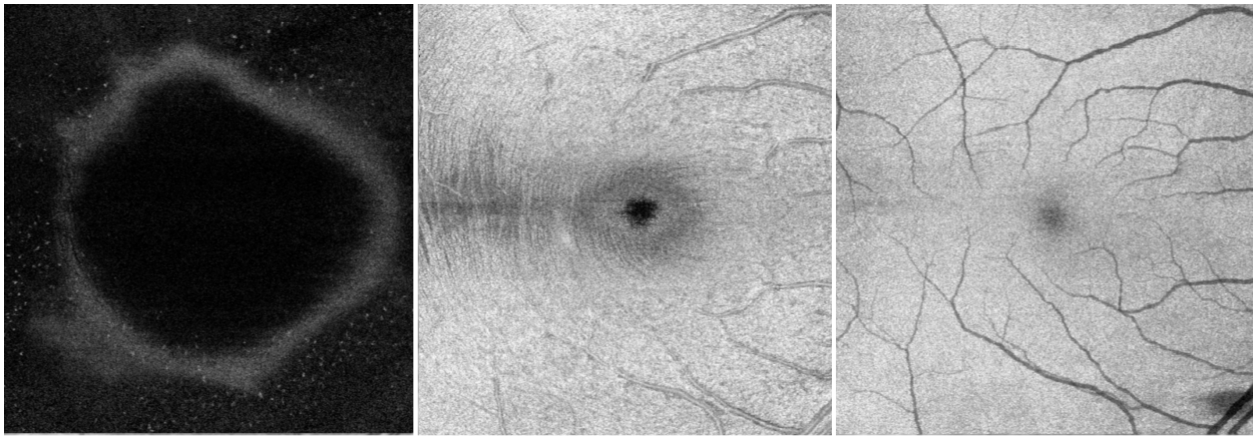

$$EZ\ normalized\ reflectivity = \frac{EZ\ mean\ brightness - vitreous\ mean\ brightness}{RNFL\ mean\ brightness}$$

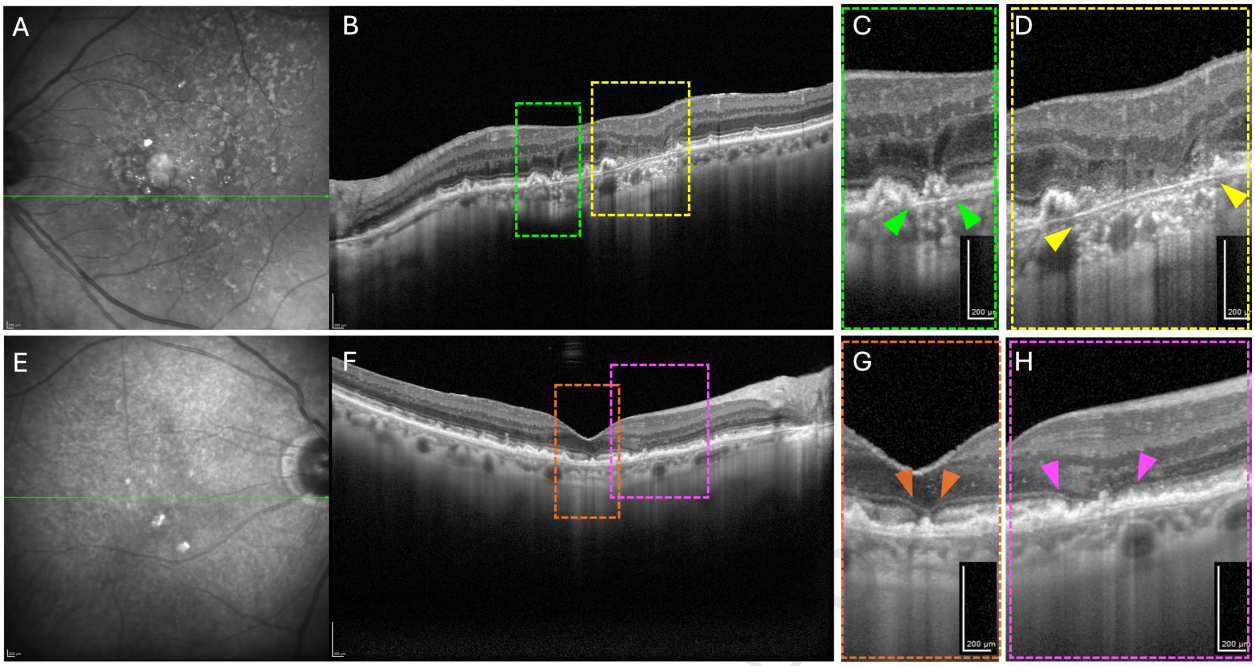

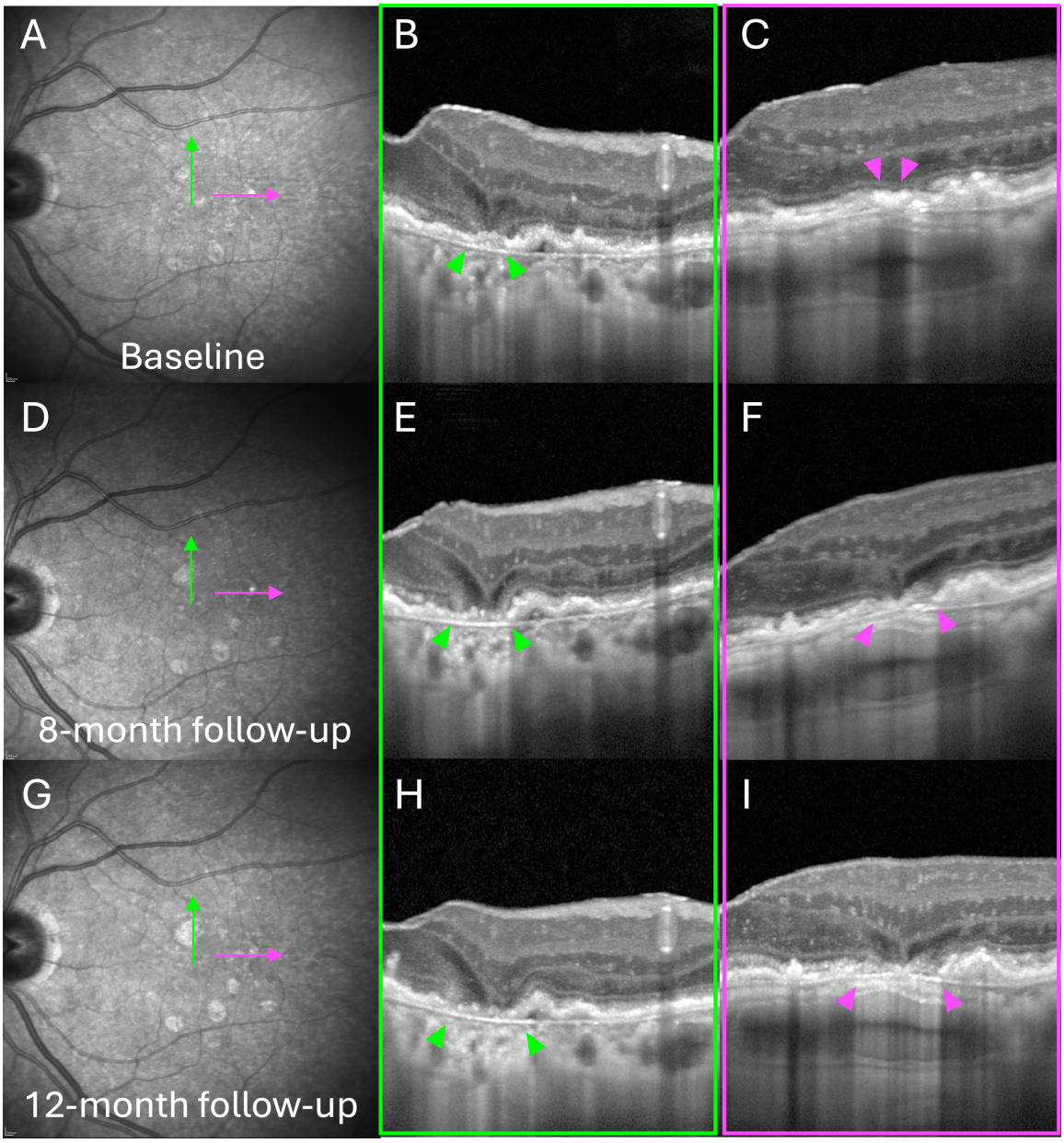
A
B
C
Baseline
D
E
F
8-month follow-up
G
H
I
12-month follow-up

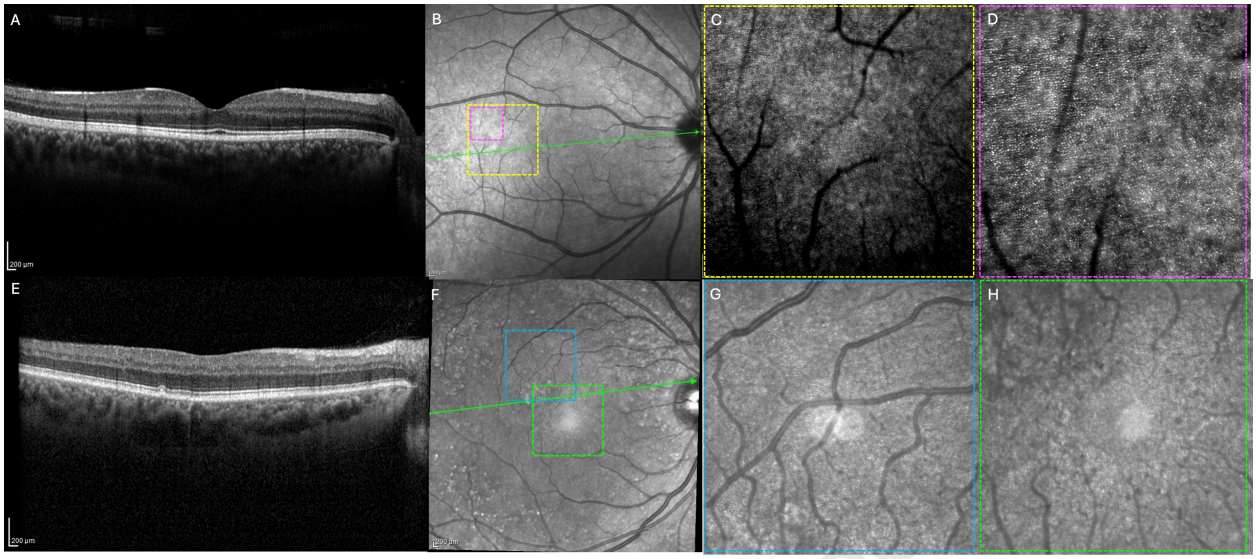

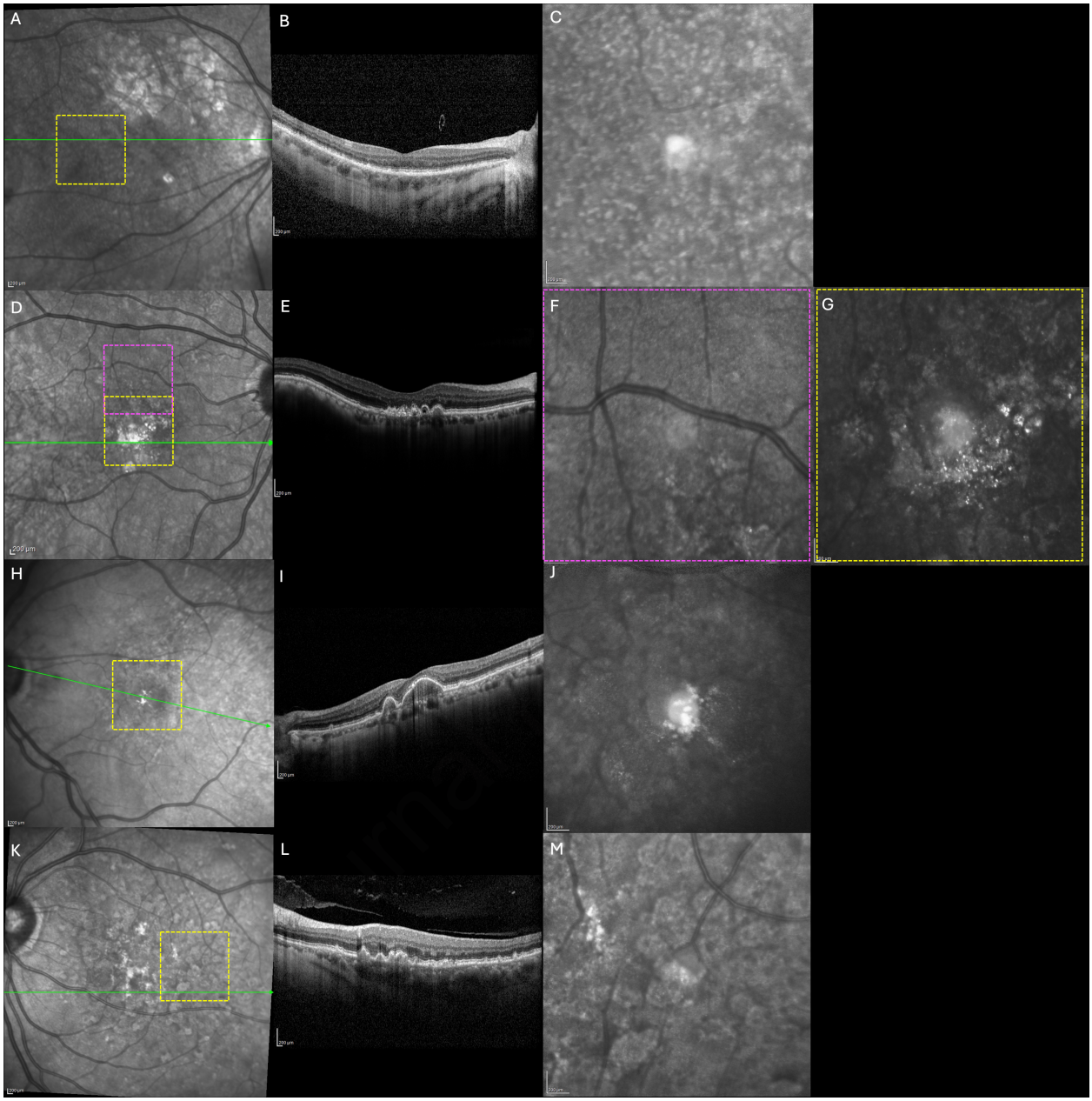
A
B
C
D
E
F
G
H
I
J
K
L
M

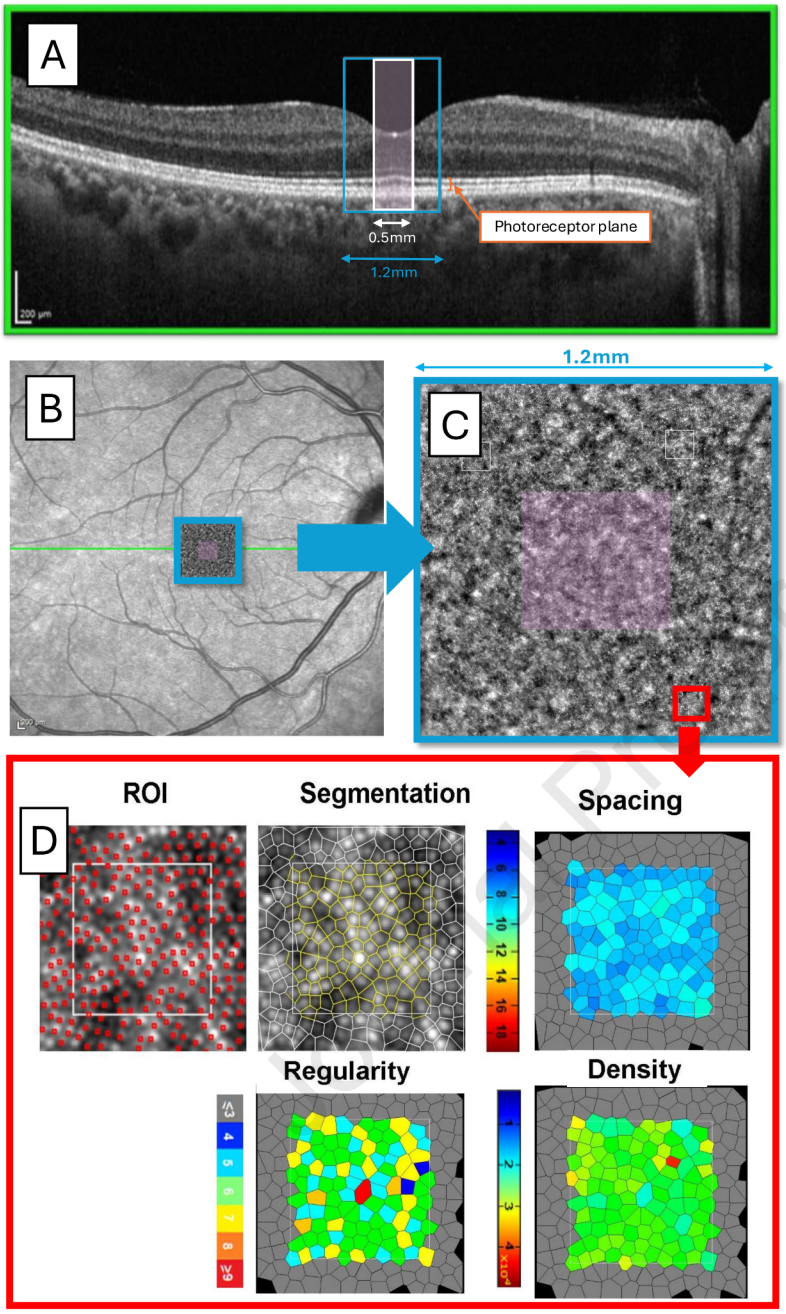
A
0.5mm
1.2mm
Photoreceptor plane
B
1.2mm
C
D
ROI
Segmentation
Spacing
Regularity
Density

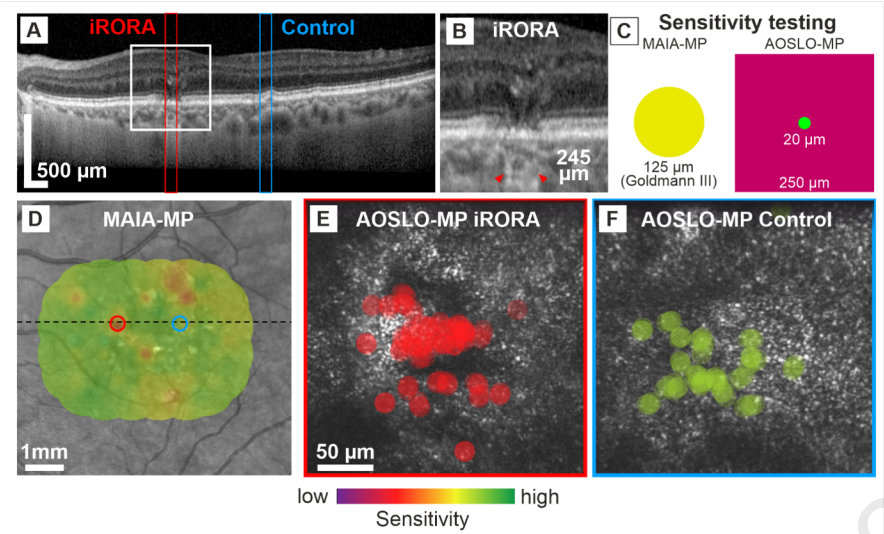

Structural photoreceptor evaluation in age-related macular degeneration. A comprehensive review of methods and clinical significance.

Declaration of interests

☐ The authors declare that they have no known competing financial interests or personal relationships that could have appeared to influence the work reported in this paper.

☒ The authors declare the following financial interests/personal relationships which may be considered as potential competing interests:

Lourdes Vidal-Oliver reports financial support was provided by Spanish Society of Retina and Vitreous. Lourdes Vidal-Oliver reports a relationship with Roche that includes: speaking and lecture fees and travel reimbursement. Lourdes Vidal-Oliver reports a relationship with Alcon Laboratories Inc that includes: speaking and lecture fees. Lourdes Vidal-Oliver reports a relationship with Bayer AG that includes: travel reimbursement. Sarah Thiele reports a relationship with Roche that includes: funding grants. Sarah Thiele reports a relationship with Bayer AG that includes: funding grants. Sarah Thiele reports a relationship with Heidelberg Engineering GmbH that includes: funding grants. Sarah Thiele reports a relationship with Novartis that includes: funding grants. Sarah Thiele reports a relationship with Allergan Irvine that includes: funding grants. Sarah Thiele reports a relationship with DORC Dutch Ophthalmic Research Center (International) BV that includes: funding grants. Wolf M Harmening reports a relationship with RhyGaze that includes: consulting or advisory. Rosa Dolz-Marco reports a relationship with Roche that includes: consulting or advisory, funding grants, and speaking and lecture fees. Rosa Dolz-Marco reports a relationship with Heidelberg Engineering GmbH that includes: consulting or advisory and speaking and lecture fees. Rosa Dolz-Marco reports a relationship with Regeneron Pharmaceuticals Inc that includes: funding grants. Rosa Dolz-Marco reports a relationship with Annexon Biosciences that includes: funding grants. Rosa Dolz-Marco reports a relationship with IVERIC bio that includes: funding grants. Rosa Dolz-Marco reports a relationship with Janssen Pharmaceuticals Inc that includes: funding grants. Rosa Dolz-Marco reports a relationship with EyePoint Pharmaceuticals Inc that includes: funding grants. Rosa Dolz-Marco reports a relationship with AbbVie Inc that includes: speaking and lecture fees. Robert P Finger reports a relationship with Biogen that includes: funding grants. Robert P Finger reports a relationship with Bayer AG that includes: funding grants. Robert P Finger reports a relationship with Apellis Pharmaceuticals, Inc that includes: funding grants. Robert P Finger reports a relationship with Alimera Sciences Inc that includes: funding grants. Robert P Finger reports a relationship with Astellas Pharma US Inc that includes: funding grants. Robert P Finger reports a relationship with Allergan Irvine that includes: funding grants. Robert P Finger reports a relationship with Caterna that includes: funding grants. Robert P Finger reports a relationship with Boehringer Ingelheim GmbH that includes: funding grants. Robert P Finger reports a relationship with Novartis that includes: funding grants. Robert P Finger reports a relationship with Ophthea that includes: funding grants. Robert P Finger reports a relationship with ODOS that includes: funding grants. Robert P Finger reports a relationship with ProGenerika that includes: funding grants. Robert P Finger reports a relationship with Roche that includes: funding grants. Robert P Finger reports a relationship with Stada Pharmaceuticals Australia Pty Limited that includes: non-financial support. Maximilian Pfau reports a relationship with Roche that includes: employment. If there are other authors, they declare that they have no known competing financial interests or personal relationships that could have appeared to influence the work reported in this paper.